CATALYSIS BY EXTREMOZYMES: COMPARING OROTIDINE 5′-MONOPHOSPHATE DECARBOXYLASES FROM PSYCHROPHILES, MESOPHILES, AND THERMOPHILES

by

Alexander C. Roy

Submitted in partial fulfilment of the requirements
for the degree of Master of Science

at

Dalhousie University
Halifax, Nova Scotia
March 2013

DALHOUSIE UNIVERSITY

DEPARTMENT OF CHEMISTRY

The undersigned hereby certify that they have read and recommend to the Faculty of Graduate Studies for acceptance a thesis entitled "CATALYSIS BY EXTREMOZYMES: COMPARING OROTIDINE 5′-MONOPHOSPHATE DECARBOXYLASES FROM PSYCHROPHILES, MESOPHILES, AND THERMOPHILES" by Alexander C. Roy in partial fulfilment of the requirements for the degree of Master of Science.

Dated: March 26, 2013

Supervisor: _____

Readers: _____

_____

_____

DALHOUSIE UNIVERSITY

DATE: March 26, 2013

AUTHOR: Alexander C. Roy

TITLE: CATALYSIS BY EXTREMOZYMES: COMPARING OROTIDINE 5′-MONOPHOSPHATE DECARBOXYLASES FROM PSYCHROPHILES, MESOPHILES, AND THERMOPHILES

DEPARTMENT OR SCHOOL: Department of Chemistry

DEGREE: MSc CONVOCATION: May YEAR: 2013

_____

Signature of Author

Table of Contents

List of Tables

List of Figures

List of Schemes

Abstract

Low temperatures impose a unique set of restrictions on the thermodynamic strategies available for enzymatic catalysis. The specific thermodynamic consequences of cold environments were determined for two psychrophile-derived variants of the highly-proficient enzyme, orotidine 5′–monophosphate decarboxylase (ODCase) — one from *Psychrobacter arcticus* 273–4 (PaODCase), and another from *Colwellia psychrerythraea* 34H (CpODCase). Determination of the kinetic parameters of these psychrozymes as a function of temperature indicated that PaODCase operates through entropy-driven ground-state-destabilisation, while CpODCase operates primarily through enthalpy-driven transition-state-stabilisation. In the context of prior studies conducted with mesozyme and thermozyme ODCase-variants, a large value of k_{cat} was found to be the most consistent hallmark of a psychrozyme. Interestingly, a low value of an enzyme's melting temperature (T_m) appeared to correlate weakly with low-temperature activity. On the whole, the trends identified herein afford greater understanding of the unique challenges to providing catalysis at low-temperatures, and how these are overcome by psychrozymes.

List of Abbreviations and Symbols Used

3D	three-dimensional
A	alanine
A_{280}	absorbed light with a wavelength of 280 nm
AGE	agarose gel electrophoresis
AMP	adenosine 5′–monophosphate
ATP	adenosine 5′–triphosphate
AU	absorbance units
b	pathlength
β	apparent compensation temperature
c	concentration
CAPS	*N*-cyclohexyl-3-aminopropanesulfonic acid
CD	circular dichroism
CHES	*N*-cyclohexyl-2-aminoethanesulfonic acid
CpODCase	ODCase variant, derived from *Colwellia psychrerythraea* 34H
$CpODCase_{-tag}$	CpODCase after removal of the prepended hexahistidine tag
$CpODCase_{+tag}$	CpODCase with a prepended hexahistidine tag
D	aspartic acid
dATP	2′–deoxyATP

dCTP	2′–deoxyCTP
ddH_2O	distilled, deionised water
$\Delta\epsilon_{279}$	difference between the extinction coefficients of OMP and UMP at 279 nm
ΔG	relative value of free-energy, or free-energy "change"
ΔG_{β}	free energy change at a temperature equal to β
$\Delta G_{<1/T>}$	free energy change at a temperature equal to T_{hm}
$\Delta G_{es}^{\ddagger}$	free energy change upon activation of ES to $\{ES\}^{\ddagger}$
$\Delta G_{e+s}^{\ddagger}$	free energy change upon activation of E + S to $\{ES\}^{\ddagger}$
ΔG_{m}	free energy change upon dissolution of ES to form E + S
$\Delta G_{non}^{\ddagger}$	free energy change upon activation of S to $\{S\}^{\ddagger}$
ΔG_{tx}	free energy change upon binding of $\{S\}^{\ddagger}$ to form $\{ES\}^{\ddagger}$
dGTP	2′–deoxyGTP
ΔH	relative value of enthalpy, or enthalpy "change"
$\Delta H_{es}^{\ddagger}$	enthalpy change upon activation of ES to $\{ES\}^{\ddagger}$
$\Delta H_{e+s}^{\ddagger}$	enthalpy change upon activation of E + S to $\{ES\}^{\ddagger}$
ΔH_{m}	enthalpy change upon dissolution of ES to form E + S
$\Delta H_{non}^{\ddagger}$	enthalpy change upon activation of S to $\{S\}^{\ddagger}$
ΔH_{tx}	enthalpy change upon binding of $\{S\}^{\ddagger}$ to form $\{ES\}^{\ddagger}$
dNTP	2′–deoxynucleoside 5′–triphosphate
ΔS	relative value of entropy , or entropy "change"
$\Delta S_{es}^{\ddagger}$	entropy change upon activation of ES to $\{ES\}^{\ddagger}$

$\Delta S_{e+s}^{\ddagger}$	entropy change upon activation of E + S to $\{ES\}^{\ddagger}$
ΔS_{m}	entropy change upon dissolution of ES to form E + S
$\Delta S_{non}^{\ddagger}$	entropy change upon activation of S to $\{S\}^{\ddagger}$
ΔS_{tx}	entropy change upon binding of $\{S\}^{\ddagger}$ to form $\{ES\}^{\ddagger}$
dsDNA	double-stranded DNA
DTT	dithiothreitol
dTTP	2′–deoxyATP
E	free enzyme; glutamic acid; folding energy
$\epsilon_{279,\,OMP}$	extinction coefficient of OMP at 279 nm
$\epsilon_{279,\,UMP}$	extinction coefficient of UMP at 279 nm
ϵ_{280}	extinction coefficient at 280 nm
EcODCase	ODCase variant derived from *Escherichia coli*
EDTA	ethylenediaminetetraacetic acid
EEO	electroendoosmosis
EGTA	ethylene glycol tetraacetic acid
EP	enzyme–product complex
E·P	loosely-bound enzyme–product complex
ES	enzyme–substrate complex
E·S	loosely-bound enzyme–substrate complex
$\{ES\}^{\ddagger}$	activated enzyme–substrate complex
ES^{n}	enzyme–substrate complex in a protonation state defined by n

$[E]_t$	concentration of all enzyme species combined
F	enzyme in a folded state
FPLC	fast performance liquid chromatography
G	glycine
g	force of gravity
$G^{\ddagger}$	free energy of an activated state
gDNA	genomic DNA
GS	ground state
h	planck constant
$H^{\ddagger}$	enthalpy of an activated state
HEPES	4- (2-hydroxyethyl)-1-piperazineethanesulfonic acid
HsODCase	ODCase variant derived from *Homo sapiens sapiens*
IC_{50}	inhibitor concentration effecting half-activity
IPTG	isopropyl β-D-1-thiogalactopyranoside
K	lysine
κ	transmission coefficient
k_1	rate constant for substrate binding
k_{-1}	rate constant for substrate release
k_2	rate constant for product formation
k_B	boltzmann constant
k_{cat}	apparent rate constant for product formation
$(k_{cat})^{max}$	maximal observed value of k_{cat}

$(k_{cat}/K_m)^{max}$	maximal observed value of k_{cat}/K_m
K_{e+s1}	equilibrium constant for deprotonation of the protonated form of E
K_{e+s2}	equilibrium constant for deprotonation of E
K_{es1}	equilibrium constant for deprotonation of the protonated form of ES
K_{es2}	equilibrium constant for deprotonation of ES
K_{d1}	dissociation constant for the deprotonated form of ES
K_{d2}	dissociation constant for the protonated form of ES
K_f	equilibrium constant for folding of E
K_m	apparent dissociation constant for ES
k_{non}	rate constant for conversion of S to P without a catalyst
K_{tx}	dissociation constant for release of $\{S\}^{\ddagger}$ from E
l	pathlength
LB	lysogeny broth
M	methionine
MES	2- (*N*-morpholino)ethanesulfonic acid
MOPS	3- (*N*-morpholino)propanesulfonic acid
MtODCase	ODCase variant derived from *Methanobacterium thermoautotrophicum* ΔH
MW	molecular weight
MWCO	molecular weight cut-off

n	Hill-coefficient
N	asparagine
ODCase	OMP decarboxylase
$ODCase_{+tag}$	ODCase variant with a prepended hexahistidine tag
OMP	orotidine 5′–triphosphate
ORF	open reading frame
P	product; proline
pI	isoelectric point
PAGE	polyacrylamide-gel electrophoresis
PaODCase	ODCase variant derived from *Psychrobacter arcticus* 273–4
$PaODCase_{-tag}$	PaODCase after removal of the prepended hexahistidine tag
$PaODCase_{+tag}$	PaODCase with a prepended hexahistidine tag
PCR	polymerase chain reaction
PIPES	piperazine-*N*,*N*′-bis (2-ethanesulfonic acid)
R	gas constant; arginine
S	substrate
$\{S\}^{\ddagger}$	activated form of S
$S^{\ddagger}$	entropy of an activated state
ScODCase	ODCase variant derived from *Saccharomyces cerevisiae*
SDS	sodium dodecylsulfate
T	threonine
T	temperature

t	time
θ	ellipticity
$[\theta]_{222}$	molar ellipticity at 222 nm
$[\theta]_{f}$	molar ellipticity of an enzyme in a folded state
$[\theta]_{u}$	molar ellipticity of an enzyme in an unfolded state
TAPS	*N*-tris (hydroxymethyl)methyl-3-aminopropanesulfonic acid
T_{hm}	harmonic mean of the experimental temperatures
T_{m}	melting temperature
T_{opt}	optimal growth-temperature
TS	transition state
U	unit of catalysis, in katals; enzyme in an unfolded state
UMP	uridine 5′–triphosphate
UV–vis	range of light including ultraviolet and visible
v_{i}	initial rate of reaction
V_{max}	maximal v_{i}
WT	wild-type

Acknowledgements

I have always been enchanted by the fundamental concept of an enzyme; the image they conjure in my mind of an incredibly-efficient, atom-scale, precision machine, operating at hundreds of actions per second, seems more in line with science-fiction than reality. The reality of enzymes is even more fantastic when you consider that these machines continue to out-perform synthetic catalysts in terms of the versatility, specificity, and efficiency of the reactions they catalyse; their nitrogen-fixing, carbon-fixing, and oxygen-producing activities are apparently capable of Terra-forming an entire planet; and that, in a human-being, a single dysfunctional enzyme can be fatal! The potential I see in enzymes – for scientific and technological advancement – drew me to the field of enzymology; a study of the mechanisms by which enzymes function.

The studies and insights that I convey in this thesis are the embodiment of my interest; however, I acknowledge that a proper thesis requires more than academic curiosity, or time spent at a lab-bench. I may never have pursued my curiosities without the support and guidance of those people in my life who wanted me to succeed, and who provided me the tools to do so. I would like to thank my mother, Beverly Joyce Clark Roy, and my father, Robert Gordon Roy, for filling my childhood with the gratification that comes from scientific discovery and elegant design. I would like to thank my grand-father, Ralph Alexander Clark, from whom I inherited – whether by nature, or by nurture – an insatiable desire to tinker with, to re-imagine, and to restore. Most of all, I would like to convey my gratitude for Professor Stephen Lewis Bearne's wise and patient mentoring, for his generous insights, and for his friendship over the six years that I've had the pleasure of knowing him. Finally, I confess I would need to write a second thesis to adequately thank the countless other friends, mentors, and muses that helped make my studies not only possible, but enjoyable, rewarding and enlightening.

Chapter 1 INTRODUCTION

Enzymes are “nature's catalysts”: they facilitate many biological processes, and through natural selection they have been developed into highly robust, proficient, selective, and versatile macromolecular machines. It is my aim to facilitate the use of enzymes as tools, by improving our practical understanding of how enzymes work. Practical understanding is enhanced by the elucidation of fundamental concepts that emerges from a rigorous investigation of controlled model systems. Orotidine 5′–monophosphate (OMP) decarboxylase (ODCase) offers a particularly good example of enzyme proficiency, and as such is my model system of choice. I hope that my work with ODCase will, in at least a small way, further the long history of enzymology, and the goal of understanding enzymatic function.

1.1 A Brief History of Enzymology

In 1897, Eduard Buchner proved that a live organism — namely yeast — was not required to drive alcoholic fermentation (Buchner, 1897). Instead, he used yeast whole cell lysate, a technique that was previously considered to be a known impossibility. The results of this experiment raised an important question: if life is not due to an intrinsic, ineffable quality, then what *is* the nature of the substance required to drive life processes? The answer came in 1926, when James B. Sumner made crystals of urease from jackbean protein, and showed convincingly that the crystals were both pure protein, and were responsible for decomposition of urea (Sumner, 1926; Sumner, 1937). This evidence made it clear that enzymes were

proteins capable of conferring reactivity to otherwise inert compounds. For his efforts, he was awarded the 1946 Nobel Prize in Chemistry.

1.1.1 Early Theories of Enzyme-Mechanism

As structure is the foundation of function, Sumner's work opened the door to a deeper investigation of the mechanism by which enzymes operate. Even before enzyme structure was understood, substrate structure was used to investigate enzyme mechanisms. Early estimations of enzyme mechanisms included the idea of a specifically-shaped substrate "key" being fitted to its corresponding enzyme "lock". The thusly-named "lock-and-key" ("Schloss-und-Schlüssel") mechanism was proposed by Emil Fischer in 1894 (Fischer, 1894). This idea was based upon experiments that showed that α–methylglucoside and *β*–methylglucoside were broken down by invertin and emulsin, respectively, but not *vice versa*. Fischer's proposed lock-and-key mechanism is both simple and robust, making it an important component of even modern mechanistic reasoning. Further, it has implications for receptor binding (*e.g.*, saccharin binding to taste bud receptors [Hamor, 1961]), and drug development (*e.g.*, design of the morphines [Gero, 1954]). These studies demonstrate that the precise 3D shape of a molecule is critical to its binding. In 1958, Koshland proposed the theory of "induced-fit" (Koshland, 1958; Koshland, 1995). This proposed mechanism was an attempt to complement the idea of a lock-and-key, with the observations that smaller analogues of substrates react less quickly, even at saturating conditions of substrate (*e.g.*, ribose 5–monophosphate is hydrolysed less

rapidly by 5′–nucleotidase than adenosine 5′–monophosphate [Heppel & Hilmoe, 1951]), and similarly α–methylglucoside is not a substrate of amylomaltase (Wiesmeyer & Cohn, 1957). Koshland argued that if the active site were of rigid design, the smaller substrate should still physically fit the larger active site. Thus, if a truncated substrate was present at saturating concentrations, one would expect that it would be bound to the same extent as the native substrate, and the rate of reaction would be the same. Because parts of a substrate molecule that are distal to the reaction site on the substrate are required for the enzyme to promote catalysis, Koshland argued that distal parts of the substrate induce a structural rearrangement in the enzyme. By rearranging its catalytic site, an enzyme is able to bind its substrate tighter, with greater selectivity, and it can orient functional groups to promote reactions between them (Koshland, 1958).

The orientation of the enzyme-substrate (ES)-complex favours substrate binding; but as Linus Pauling proposed in 1948, enzymes may ultimately bind the activated-complex, or transition state (TS), tightest of all. Similar to the idea of catalysis *via* adsorption onto a solid surface, proposed by Michael Polanyi in 1921 (Polanyi, 1921), the "Pauling paradigm" states that a catalytic site selectively stabilises the TS of a reaction in order to promote TS-formation (Pauling, 1946; Pauling, 1948; Schowen, 1978). If correct, this paradigm implies that one could design an enzyme solely on the basis of the structure of a transition state. Indeed, antibodies raised against TS-analogues (molecules that mimic the expected steric and electronic features of the TS) are capable of catalysis (Blackburn *et al*., 1989); albeit

to a lesser extent than the corresponding enzyme. The disparity between the catalytic activity of these so-called "abzymes" (or "catmabs") and enzymes may be due to a number of factors, including: TS-analogue–TS structural disparities, slow product-release, and absent cofactors. Although the latter-most of these technical hurdles has been overcome (Mahon *et al*., 1998; Nicholas *et al*., 2002; Xu *et al*., 2004), there is still a great deal of understanding about how enzyme-structure mediates function that remains elusive.

1.1.2 Modern Theories of Enzyme Mechanism

Numerous theories have been proposed to explain the magnitude of enzyme-mediated rate-enhancement, including: TS electrostatic stabilization (Warshel, 1998), ground-state (GS) destabilization and desolvation (Dewar & Storch, 1985), entropy trapping (Westheimer, 1962) (*e.g*., approximation, proximity, propinquity and togetherness [Bruice, 1976; Page & Jencks, 1971]), protein flexibility and dynamics (*e.g*., TS-promoting vibrations, dynamic enhancement of tunnelling [Cha, Murray, & Klinman, 1989; Hammes–Schiffer, 2006], and coupled fluctuation of protein-TS motions (Benkovic & Hammes–Schiffer, 2003]), pre-organisation of active sites, near attack conformations (Bruice, 2002), covalently bound TSs (Zhang & Houk, 2005), influencing dynamical TS-recrossings (Benkovic & Hammes–Schiffer, 2003; Garcia–Viloca, Gao, Karplus, & Truhlar, 2004), the "Circe effect" (Jencks, 1975), molecular orbital alignment (*i.e*., the "spatiotemporal hypothesis" [Menger & Glass, 1980]), non-covalent cooperativity and enhanced enzyme packing (Williams, Stephens, &

Zhou, 2003; Williams *et al*., 2004), and low-barrier hydrogen-bonding (Cleland & Kreevoy, 1994). Clearly, in order to understand and design enzymes, further study is required—study that could be facilitated by examining an enzyme with exaggerated characteristics, which translate to more easily measured differences in these characteristics.

1.2 Extremophiles: Lovers of Extreme Temperature

Given an enzyme of exaggerated features, how does one derive fundamental characteristics of enzyme-mediated catalysis? One possible means is by comparison of enzymes that have evolved to carry out the same reaction, by the exact same mechanism, but in varying external conditions. Thus, an obvious direction for this type of study is to use enzymes derived from extremophiles: organisms adapted to temperatures that are considered extreme from an anthropocentric point of view (Demirjian, Morís–Varas, & Cassidy, 2001; Hough & Danson, 1999). These organisms can be separated into classes based upon their requirement for, or their tolerance of, a particular environmental extreme. The enzymes that I used in the present work were derived from psychrophiles — adapted to cold, these organisms live in environments where low entropy and enthalpy are the norm.

1.2.1 A Cold Planet

The living things that most of us encounter on a routine basis live and grow under the same "moderate" conditions. These conditions may be the result of

external influences (*e.g.*, geography) or they may be internally maintained (as in endotherms). In this context, moderate conditions are defined as: pH 7.4, 21% O_2, 1 atm, salinity of 0.9–3.0%, and temperature of 37 °C. However, these conditions are not Earth's norm. In the case of temperature, its norm is much colder. It is easy to see that this is true by noting that 70% of the earth's surface is ocean, of which 90% is at a temperature of 5 °C or cooler (Cavicchioli, 2006; Methé *et al.*, 2005). Further, a large fraction of the terrestrial environment is a combination of permafrost (20%), and regions of seasonal cold (Deming & Eicken, 2007). Altogether, this means that over 75% of the earth's surface is "cold" and thus far from "moderate".

1.2.2 Cold-Adapted Organisms

Given the largely cold environment on our planet, it is not surprising that there are many organisms that are compatible with cooler temperatures. These organisms fall into a few categories: psychrophilic, psychrotolerant, and psychroactive. The term "psychrophilic" applies to an organism that absolutely requires cold temperatures (*i.e.*, it grows optimally below 15 °C, and not above 20 °C [Canganella & Wiegel, 2011]). The term "psychrotolerant", by contrast, applies to an organism that grows optimally at a higher temperature, but is also able to grow to a lesser extent at a lower one (*i.e.*, it grows optimally above 20 °C, but can also grow below 5 °C) (Canganella & Wiegel, 2011). Note that the term "psychrotroph" ("cold-nourished") has been used to mean psychrotolerant (Bowman *et al.*, 1997); however, the former has been largely supplanted by the the latter, arguably more precise, term.

Finally, the term "psychroactive" is the most intuitive moniker, meaning simply that the organism is capable of growth, to any extent, at "cold" temperatures.

In order to study the adaptions of enzyme mechanism to cold, I chose to characterise the thermodynamic parameters of the enzyme ODCase from two psychroactive species: *Psychrobacter arcticus* 273–4 and *Colwellia psychrerythraea* 34H. *P. arcticus* is a Gram-negative, rod-shaped, heterotrophic bacterium isolated from permafrost in the Kolyma region of Siberia, and was first described in 2006 under the name *Psychrobacter arcticus sp. nov.* or simply *Psychrobacter arcticus sp.* (Bakermans *et al.*, 2006). It can grow between − 10 °C and 28 °C, but grows optimally at 22 °C (Ayala–del–Río *et al.*, 2010); it is thus classified as a psychrotolerant bacterium. *C. psychrerythraea* is a γ–proteobacterium isolated from arctic marine sediments, and was first described in 2000 under the enigmatic name "strain 34H" (Huston, Krieger–Brockett, & Deming, 2000). It has an optimal growth temperature of 8 °C, a maximum growth temperature of 19 °C, and an extrapolated minimum growth temperature of − 14.5 °C — one of the lowest among bacteria (Huston, Methe, & Deming, 2004). *C. psychrerythraea* is thus an excellent example of a psychrophilic bacterium.

1.3 ODCase: a Model Enzyme

ODCase is the epitome of biological catalysts; accelerating the decarboxylation of OMP, by 10^{17}–fold over the uncatalysed reaction in water, representing a TS stabilisation of 32 kcal/mol (Radzicka & Wolfenden, 1995).

Further, it does this without any clear assistance from a metal ion or coenzyme (Begley, Appleby, & Ealick, 2000; Begley & Ealick, 2004; Gao, 2003; Miller & Wolfenden, 2002). Hence, ODCases are among the most proficient enzymes known, and have been extensively characterised.

1.4 The Biology of ODCase

ODCase is a member of the *de novo* pyrimidine biosynthesis pathway, catalysing the decarboxylation of OMP to produce uridine 5′–monophosphate (UMP), which regulates ODCase-activity through product inhibition (Shambaugh, 1979) (Figure 1.1). Inhibition of ODCase is of interest from a medical standpoint. As an enzyme that contributes to the production and maintenance of RNA, DNA, cell membranes and glycogen (Jones, 1980; Traut, 1994) it is a potential target for anti-cancer, anti-viral, or anti-microbial agents.

1.5 The Chemistry of ODCase

1.5.1 A Mechanistic Dialogue

The incredible efficiency with which ODCase completes its task, even in the absence of cofactors, has garnered interest in the precise mechanism that ODCase employs. In 1976, Beak and Siegel proposed a zwitterionic intermediate for the decarboxylation of ODCase (Beak & Siegel, 1976), this was based on the observation that the mechanism of decarboxylation of 1,3–dimethylorotic acid follows a different path at high- and low-pH. At high-pH, the pyrimidine O2 is anionic after loss of CO_2,

Figure 1.1 The Reaction Catalysed by ODCase

ODCase catalyses the decarboxylation of OMP to form UMP. UMP is implicated in product inhibition of the *de novo* pyrimidine-biosynthesis pathway, of which ODCase is a member (Shambaugh, 1979).

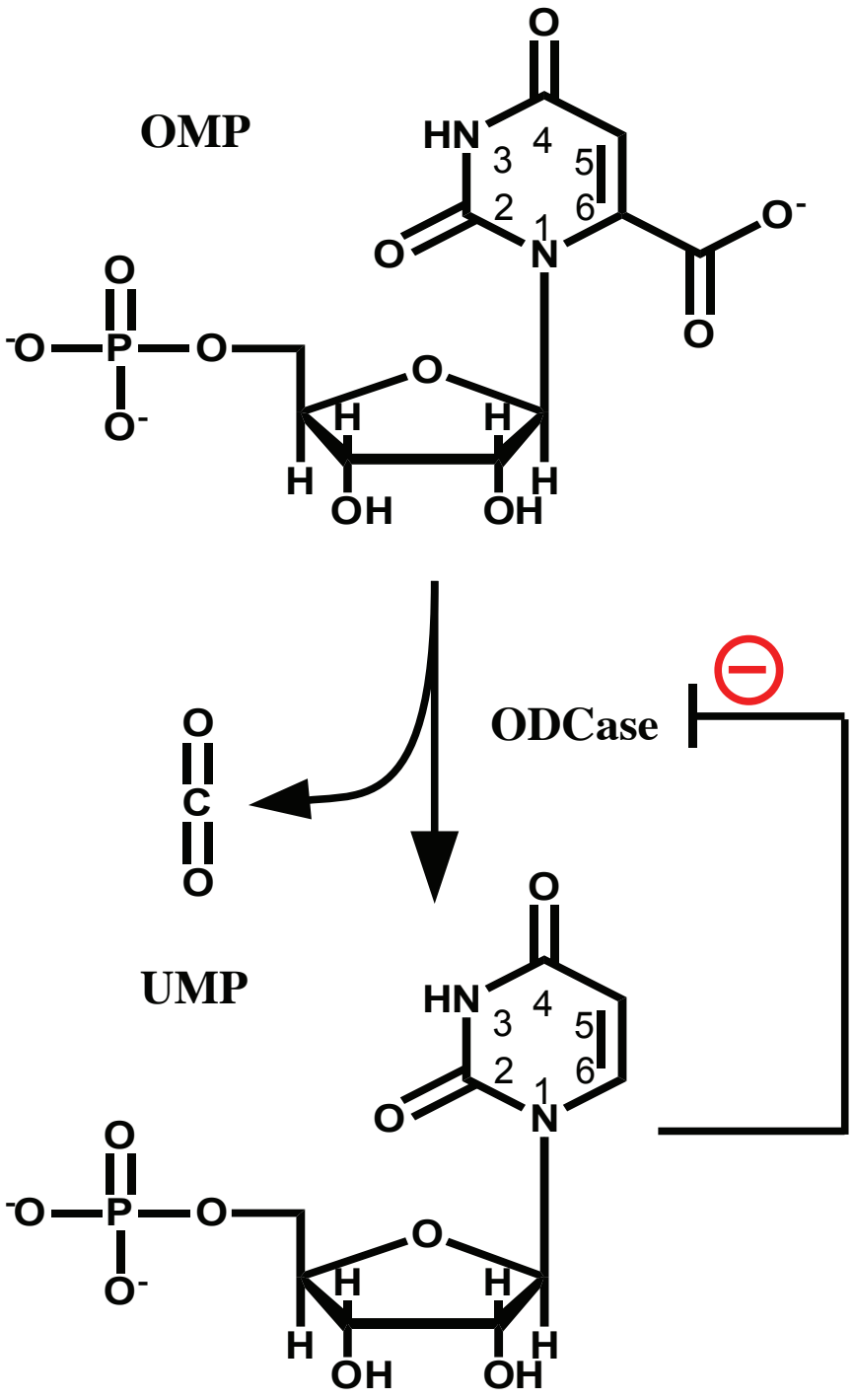

Figure 1.1

due to movement of electrons from N1 that stabilises the now-anionic C6. At low pH, O2 is protonated, and only the zwitterion between N1 and C6 remains charged.

In 1982, Silverman and Groziak proposed a covalent mechanism for ODCase, involving a Michael addition of an active-site nucleophile to C5 of OMP, and a proton to C6 (Silverman & Groziak, 1982). The tetrahedral intermediate thus formed would then expel CO_2, and the original nucleophile, to give UMP; however, later kinetic isotope experiments did not support the formation of a tetrahedral intermediate (Acheson *et al*., 1990).

In 1992, Shostack and Jones proposed a Schiff-base intermediate involving O2 of OMP (Shostak & Jones, 1992). This was based on other decarboxylases thought to use such an intermediate as an electron sink to overcome the barrier to carbanion formation. Indeed, there are enzymes known to decarboxylate other substrates using this mechanism, at a rate that competes with Schiff-base formation (Zhou *et al*., 2001). Despite these precedents, however, there was no isotope exchange observed with ^{18}O water that would support such a Schiff-base formation and this proposal was abandoned (Shostak & Jones, 1992).

In 1998, Wolfenden proposed a zinc-catalysed mechanism on the basis of atomic absorption spectroscopy that showed a pair of zinc atoms were present per active ODCase monomer (Miller, Traut, & Wolfenden, 1998). However, neither atomic nor x-ray absorption spectroscopic studies done thereafter could detect the presence of zinc in active ODCase (Cui *et al*., 1999).

1.5.2 Mutagenesis Studies

Despite all that remains to be understood about the mechanism of ODCase, some illuminating hints have been provided by mutagenesis studies. *Saccharomyces cerevisiae* ODCase (ScODCase) mutants D91A, K93A, D96A and K59A, all have 10^5-fold reduced activity, despite the latter two retaining some substrate affinity (Miller *et al*., 2001). The importance of this D–K–D–K-tetrad is further demonstrated by its structural conservation in the active sites of ScODCase, *Escherichia coli* ODCase (EcODCase), and *Methanothermobacterium thermoautotrophicum* ΔH ODCase (MtODCase), as observed using x-ray crystallography (Begley *et al*., 2000; Houk *et al*., 2001).

Mutagenesis and substrate truncation experiments have implicated binding of the phosphoribosyl group of OMP in both GS-destabilisation, and TS-stabilisation arguments for ODCase proficiency (Barnett *et al*., 2008; Miller *et al*., 2000; Miller *et al*., 2001): single-mutations of putative phosphate-binding residues attenuate ODCase-activity by up to 7,300-fold; removal of the phosphoribosyl group of OMP attenuates ODCase-activity by greater than 10^{12}-fold; and substrate-analogues of OMP that mimic the structure of OMP without its 5′–phosphate are decarboxylated 10^9-fold more slowly by ODCase, which can be largely restored by addition of phosphite (Barnett *et al*., 2008). Taken together, these studies imply that tight-binding to non-reacting components of the substrate are required to compensate for unfavourable interactions that are required for catalysis. Additional mutagenesis studies employing OMP substrate-analogues revealed that interactions with the

phosphoryl group of OMP in the GS are further enhanced in the TS, reinforcing the importance of TS-stabilisation (Barnett *et al*., 2008; Miller *et al*., 2001).

1.6 The Structure of ODCase

1.6.1 X-Ray Crystallographic Studies

The ODCase monomer is constructed around a 9-α–helix, 8-*β*–strand TIM-barrel in which the active site is housed. The barrel is capped by a loop of polypeptide that appears to close over the active site and make multiple contacts with the phosphate group of OMP: the "phosphate gripper loop" (Toth *et al*., 2009). As mentioned above, the active-site layout of Sc-, Ec-, and MtODCase are strikingly similar, each possessing a D–K–D–K-tetrad that is composed of aspartic acid and lysine residues from both subunits of the ODCase-homodimer, and positioned opposite the predicted OMP-carboxylate binding pocket (Begley *et al*., 2000; Houk *et al*., 2001) (Figure 1.2). Further, each site is observed to have multiple uncharged hydrogen bond donors predicted to contact OMP at positions O2, N3, and O4, and contraposed hydrophobic groups to contact the hydrophobic faces of the pyrimidine ring.

Structural studies of ODCase have not resolved the mechanistic debate, but have contributed some valuable insights. For instance, there are no strong acids in existing crystal structures that would promote protonation at O4 or O2 and thus stabilise a zwitterionic intermediate (Beak & Siegel, 1976; Lee & Houk, 1997; Lundberg, Blomberg, & Siegbahn, 2002), although the possibility that a

Figure 1.2 The Active-Site of EcODCase Bound to a TS-Analogue
The active-site amino acids of EcODCase are shown complexed with the TS-analogue barbituric acid ribosyl 5′–monophosphate. The catalytic D–K–D–K-tetrad, comprised of K44, D71, K73, and D76b (equivalent to ScODCase K51, D91, K93, and D96) is oriented to interact with the 6-position of the pyrimidine ring. Other interactions shown are limited to hydrogen bonds donated from weak acids, or accepted by weak bases, implying that these interactions are unlikely to be involved in protonation or deprotonation of OMP. These interactions are conserved in some form in the crystal structures of ScODCase as well as MtODCase. This figure was adapted from a review by Houk *et al*., (2004).

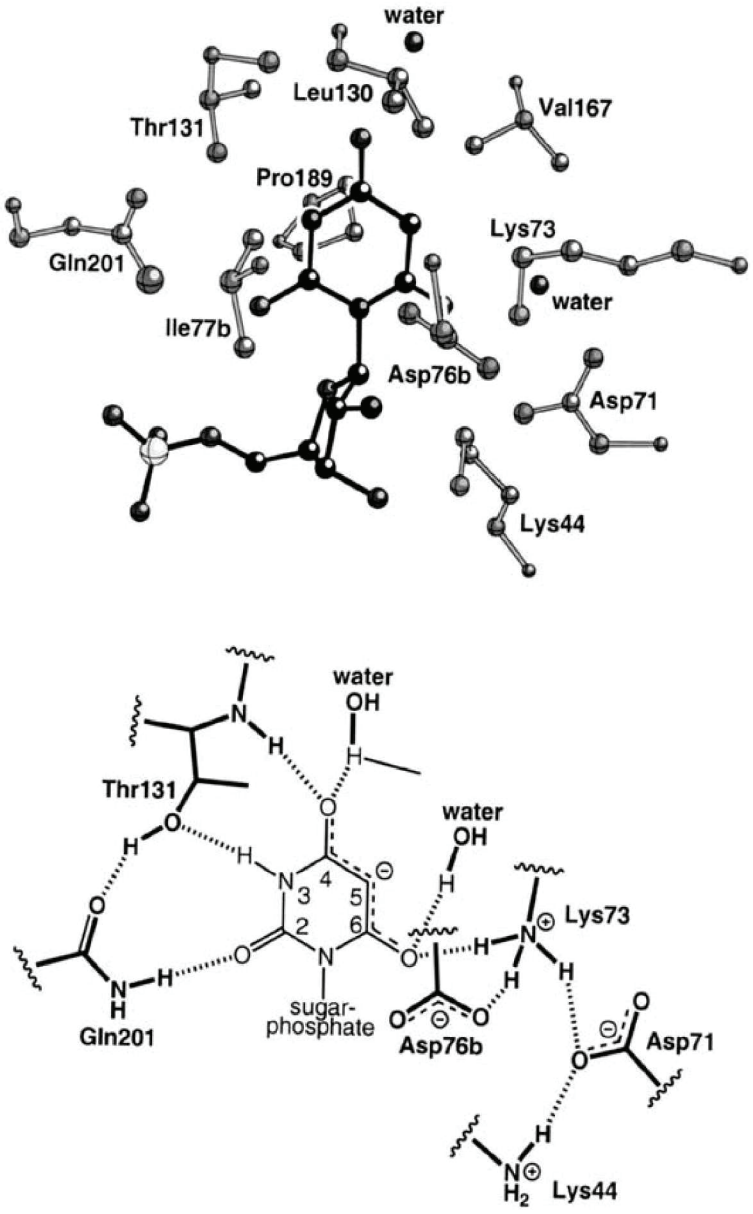
water
Leu130
Thr131
Val167
Pro189
Gln201
Lys73
water
Ile77b
Asp76b
Asp71
Lys44
water
OH
Thr131
water
OH
Lys73
Gln201
sugar-
phosphate
Asp76b
Asp71
Lys44

Figure 1.2

conformational change could produce such an interaction has not been ruled out Indeed, comparison of liganded and unliganded ODCase crystal structures imply extensive structural rearrangements occur upon substrate binding. Most significantly, the active site becomes sequestered from solvent by the phosphate gripper loop, and the active site reshapes to improve contact with the phosphoryl group and the hydrophobic faces of the pyrimidine ring (Houk *et al*., 2004).

1.6.2 Structures of ODCase Mutants

Mutagenesis studies have been coupled with crystallography to further implicate residues in the D–K–D–K-tetrad with catalysis (Wu, Gillon, & Pai, 2002). MtODCase mutants D70A and K72A (analogous to ScODCase mutants D91A and K93A) were crystallized in the presence of OMP, but the crystal structures revealed a UMP in the active-site, implying that some decarboxylase activity remained. Interestingly, in these structures the carboxyl group of D70 was replaced by a chloride ion, and the amino group of K72 was replaced by a water. Similar phenomena were observed for MtODCase mutants D75N and K42A (analogous to ScODCase mutants D95A and K59A) crystallised in the presence of the ODCase TS-analogue, 6–azaUMP. Furthermore, the MtODCase double mutant D70A/K72A crystallised with a bound OMP in the same configuration as 6–azaUMP, but with the 6-carboxyl group of OMP replacing the sidechain of D70, and a water replacing the amino group of K72; an observation the authors used to argue in favour of GS-destabilisation (Wu *et al*., 2002).

1.6.3 Key Structural Components of ODCase-Activity

Despite the lack of resolution amid the mechanistic debate, the mechanistic and structural studies described above clearly indicate the importance of a few ODCase components: a phosphate gripper loop that closes over the active site is needed to sequester the active site from water and contact the phosphoryl group of OMP; contacts with the phosphoribosyl group are required to promote formation of $\{ES\}^{\ddagger}$; and a catalytically-required D–K–D–K-tetrad of alternating aspartic acid and lysine residues is nearly superposed with the carboxyl moiety of OMP. These components are at least part of what makes ODCase an incredibly proficient enzyme, and a fascinating platform for exploring fundamental enzymology.

1.7 Enzyme Thermodynamics

Fundamental enzymology is largely comprised of two disciplines: chemical kinetics, and thermodynamics. By understanding and applying concepts from both, one can begin to unravel the mechanism of an enzyme-catalysed reaction. In this section I provide a brief review of these concepts, with an emphasis on those necessary for understanding my investigation of ODCase-variants.

1.7.1 Thermodynamic Model of ODCase-Activity

A generic enzymatic reaction can be divided into three broadly-defined stages, as diagrammed in Scheme 1.1, each with associated kinetic and thermodynamic parameters. The first of these stages involves binding of substrate (S) to the active site of an enzyme (E), to form a loosely-associated enzyme-substrate complex (E·S),

Scheme 1.1 A Generic Reaction-Coordinate-Diagram for an Enzyme-Catalysed Reaction

The relationships between the key kinetic, equilibrium, and thermodynamic constants under study are depicted here. The directionality of each ΔG is defined by the corresponding arrow (*i.e.*, ΔG_{tx} describes a binding-equilibrium, whereas ΔG_{m} describes a dissociating-equilibrium, and $\Delta G_{es}^{\ddagger}$ and $\Delta G_{e+s}^{\ddagger}$ describe activations). The convention of subscripts used here is consistently applied throughout this thesis to connect related concepts (*e.g.* the enthalpy change associated with substrate release is designated "ΔH_{m}", and the entropy change associated with overcoming the activation barrier of the uncatalysed reaction is designated "$\Delta S_{non}^{\ddagger}$"). It is relevant to note that the subscript "m" is often reserved for an apparent Michaelis constant that is determined under steady-state conditions, whereas I employ rapid equilibrium assumptions throughout. From rapid equilibrium assumptions, it follows that the thermodynamics of substrate release can be ascertained from K_{m} and the canonical relationships that completely describe a system's thermodynamics using only its equilibria. For this reason I consider appropriate the use of the apparent Michaelis constant and the subscript "m" to define the equilibrium thermodynamic constants, ΔG_{m}, ΔH_{m}, and ΔS_{m}.

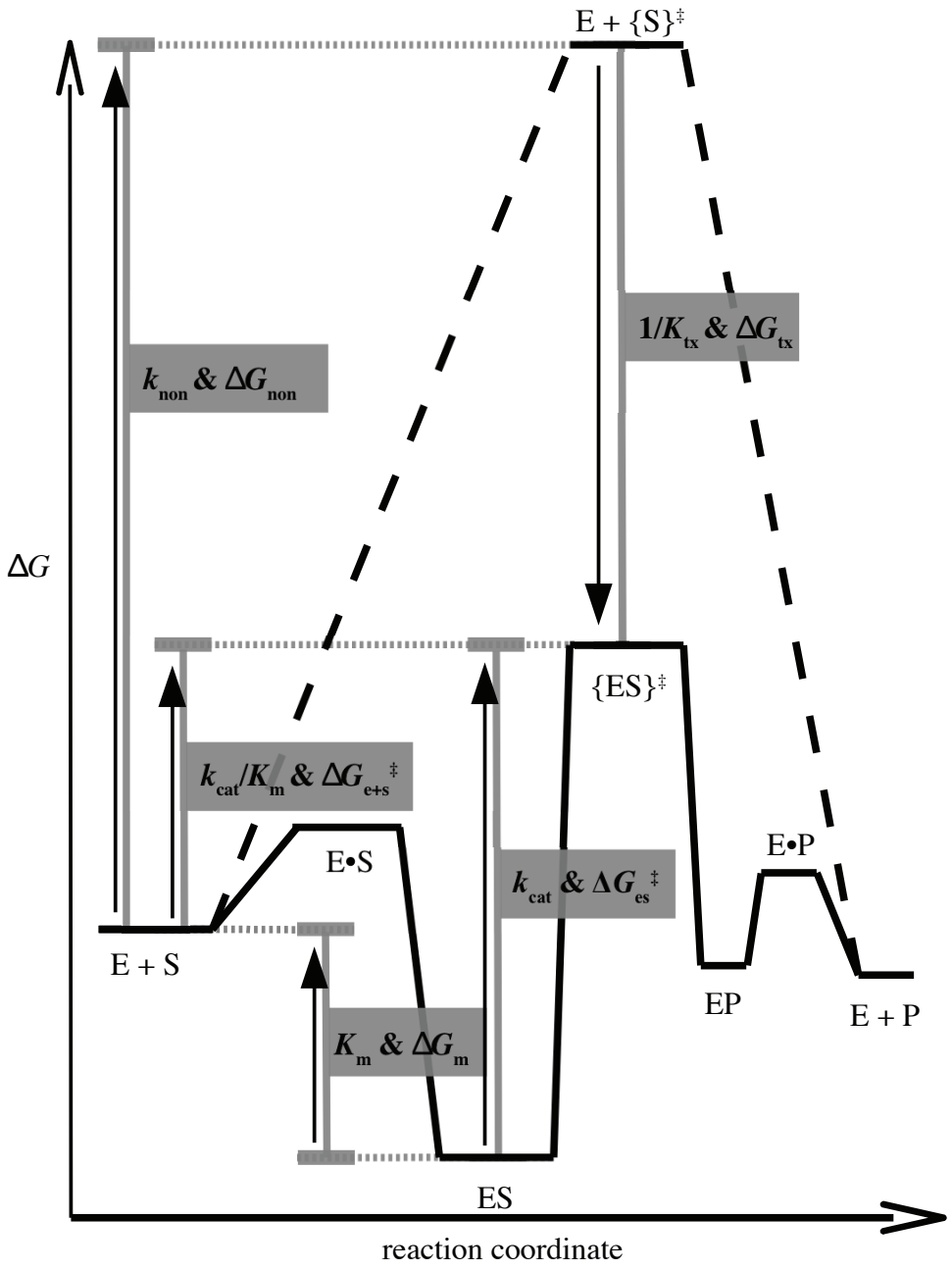

Scheme 1.1 A generic reaction coordinate diagram for an enzyme-catalysed reaction.

that collapses into a more stable ES-complex. This process subsumes any concomitant conformational changes or "Circe effects" (as described by Jencks [1975]). In a system where "rapid equilibrium" is assumed between the bound and unbound forms, this process can be abstracted as a two-stage model with the apparent dissociation constant (or apparent Michaelis constant), K_m, defined by eqn. 1.1 (Segel, 1975). These assumptions are corroborated by investigations of ScODCase (Porter & Short, 2000) and MtODCase (Wood *et al*., 2009) which revealed that both of these enzymes are limited by the rate of product formation, and not by substrate binding The rapid equilibrium assumptions also permit application of the canonical thermodynamic expressions of chemical equilibria to K_m. Thus the Gibbs free energy change associated with the equilibrium between free and enzyme-bound substrate (ΔG_m) can be defined by eqn. 1.2, where R is the gas constant, and T is the temperature at which K_m was determined.

$$K_m \approx [E][S]/[ES] \tag{1.1}$$

$$\Delta G_m = -RT \cdot \ln K_m \tag{1.2}$$

The second stage involves activation of the ES-complex to form the TS-complex ($\{ES\}^{\ddagger}$) that leads to product formation (EP). The rate of conversion from ES to EP is defined by the apparent turnover number, k_{cat}. k_{cat} is related to the free energy of activation corresponding to the rate determining step, $\Delta G_{es}^{\ddagger}$, using the

canonical transition state theory approach (Segel, 1975). The result is eqn. 1.3, wherein κ is a transmission coefficient that subsumes reflections or recrossings of the activation barrier and is generally close to unity, k_B is the Boltzmann constant, and h is Planck's constant. This equation applies equally well evaluation of the barrier to the uncatalysed reaction in solution ($\Delta G_{non}^{\ddagger}$) from the associated rate constant, k_{non}.

$$k_{cat} = \kappa(k_B T/h)\cdot e^{-(\Delta G_{es}^{\ddagger}/RT)} \tag{1.3}$$

Formation of $\{ES\}^{\ddagger}$ can alternatively be thought of as an equilibrium between the TS formed during the uncatalysed reaction in solution ($\{S\}^{\ddagger}$) and E, as described by Richard Wolfenden (Miller & Wolfenden, 2002; Radzicka & Wolfenden, 1995; Wolfenden, 2003). Wolfenden defines the affinity of the enzyme for its putative TS as the "proficiency" of the enzyme, which for historical reasons is expressed as the reciprocal of the virtual dissociation constant, K_{tx}, given in eqn. 1.4. As with K_m, K_{tx} is related to the equilibrium of a dissociation. However, in contrast to K_m, which describes the equilibrium formed by dissociation of the GS ES-complex, K_{tx} describes the virtual equilibrium resulting from dissociation of the TS ES-complex. In order to facilitate discussion of TS-stabilisation, I hereafter exclusively consider the free energy change upon association of the enzyme with its substrate in the TS (*i.e.*, E + $\{S\}^{\ddagger} \rightarrow \{ES\}^{\ddagger}$), characterised by the proficiency, $1/K_{tx}$, and the associated free energy change described by eqn. 1.4 and 1.5, respectively.

$$\text{proficiency} = 1/K_{tx} = (k_{cat}/K_m)/k_{non} \quad (1.4)$$

$$\Delta G_{tx} = -RT\cdot\ln(1/K_{tx}) \quad (1.5)$$

The third stage involves release of the product (P) from E, potentially through a loosely-associated enzyme-product complex (E·P). If the affinity of E for P is great enough, then product-inhibition results (Segel, 1975).

The efficiency afforded by the enzyme to overall turnover of E + S to E + P is exemplified by the particular case of limited substrate relative to the apparent dissociation constant, K_m (the [S] << K_m regime), in which case the reaction may resemble a bimolecular reaction between enzyme and substrate with a second-order rate constant, k_{cat}/K_m, and an overall reaction barrier, $\Delta G_{e+s}^{\ddagger}$ (defined in eqn. 1.6 and 1.7, respectively), that is significantly less energetically 'steep' than the barrier to the uncatalysed reaction, $\Delta G_{non}^{\ddagger}$. Alternatively, when substrate is abundant relative to the apparent dissociation constant, K_m (the [S] >> K_m regime), the [ES] approaches the total concentration of enzyme ($[E]_t$), and the observed rate constant for turnover approaches V_{max}, a zero-order apparent rate constant, which is defined in eqn. 1.8. Regardless of the specific reaction in question, the overall effect is the same: the substrate surmounts a reaction barrier that the enzyme attenuated in some manner, and the kinetics of the reaction under conditions of saturating [S] and rapid-equilibrium are consistent with the Henri–Michaelis–Menten equation (eqn. 1.9).

$$\text{Rate of P-formation} = (k_{cat}/K_m)\cdot[E][S] \tag{1.6}$$

$$k_{cat}/K_m = \kappa(k_B T/h)\cdot e^{-(\Delta G_{e\text{-}s}^{\ddagger}/RT)}; \text{ assuming constant [E]} \tag{1.7}$$

$$\text{Rate of P-formation} = k_{cat}[E]_t = V_{max} \tag{1.8}$$

$$\text{Rate of P-formation} = V_{max}\cdot[S] / (K_m + [S]) \tag{1.9}$$

1.7.2 The Contribution of Entropy and Enthalpy to ODCase-Activity

The free energy changes described above can be divided into associated changes in the entropy (ΔS), or enthalpy (ΔH) of the E–S system. The relationship between ΔG, ΔH, and ΔS, in the context of the transitions depicted in Scheme 1.1, is defined by eqn. 1.10, where T is the temperature at which the transition is taking place. Experimentally, this relationship is used in concert with eqn. 1.2, 1.3, 1.5, or 1.7, to derive the corresponding van't Hoff equations (Tellinghuisen, 2006), eqn. 1.11 and 1.12, or Eyring–Polanyi equations (Evans & Polanyi, 1935; Eyring, 1935), eqn. 1.13 and 1.14, which define ΔH, and ΔS as unique components of a linear function of temperature.

$$\Delta G = \Delta H - T\cdot\Delta S \tag{1.10}$$

$$\ln K_m = -(\Delta H_m / R)\cdot(1/T) + (\Delta S_m / R) \tag{1.11}$$

$$\ln(1 / K_{tx}) = -(\Delta H_{tx} / \mathrm{R}) \cdot (1/T) + (\Delta S_{tx} / \mathrm{R}) \quad (1.12)$$

$$\ln(k_{cat} / T) = -(\Delta H_{es} / \mathrm{R}) \cdot (1/T) + (\Delta S_{es} / \mathrm{R}) + \ln(k_B/h) \quad (1.13)$$

$$\ln[(k_{cat} / K_m) / T] = -(\Delta H_{e+s} / \mathrm{R}) \cdot (1/T) + (\Delta S_{e+s} / \mathrm{R}) + \ln(k_B/h) \quad (1.14)$$

1.7.3 Interrelations of the Thermodynamic Parameters of Enzymatic and Non-Enzymatic Decarboxylation of OMP

The thermodynamic parameters that characterise TS-binding and stabilisation, ΔG_{tx}, ΔH_{tx}, and ΔS_{tx}, are related to the corresponding parameters for formation of the non-enzymatic TS ($\Delta G_{non}^{\ddagger}$, $\Delta H_{non}^{\ddagger}$, and $\Delta S_{non}^{\ddagger}$), for the equilibrium pertinent to dissociation of the ES-complex (ΔG_m, ΔH_m, and ΔS_m), and for activation of the ES-complex to the TS ($\Delta G_{es}^{\ddagger}$, $\Delta H_{es}^{\ddagger}$, and $\Delta S_{es}^{\ddagger}$) by eqn. 1.15, 1.16, and 1.17, respectively.

$$\Delta G_{tx} = \Delta G_{es}^{\ddagger} - (\Delta G_{non}^{\ddagger} + \Delta G_m) \quad (1.15)$$

$$\Delta H_{tx} = \Delta H_{es}^{\ddagger} - (\Delta H_{non}^{\ddagger} + \Delta H_m) \quad (1.16)$$

$$\Delta S_{tx} = \Delta S_{es}^{\ddagger} - (\Delta S_{non}^{\ddagger} + \Delta S_m) \quad (1.17)$$

These equations, together with eqn. 1.10, are a mathematical representation of the

challenges involved in enzyme design: thermodynamic tuning through these parameters cannot be done in isolation; a change in one requires compensatory changes from the others. How enzymes ultimately do this differs from variant to variant, and is the topic of the next section.

1.8 Enzymes from Extremophiles

In the previous sections I described the structural and mechanistic components of ODCase, why I believe they make ODCase a fascinating topic of study, and the nature of the thermodynamic framework that enzymes like ODCase operate within. In this section, I expound on the larger field of "extremozymes"; in particular, the structural and mechanistic components of enzymes optimised for extremes of heat and cold. To facilitate such discussion, I use the following classifications throughout the remainder of this thesis (inspired by Hough & Danson [1999]): "thermozymes" are enzymes optimised for catalysis under high-temperature conditions, and are comparatively thermostable (a melting temperature, T_m, > 60 °C); by extension, "mesozymes" are enzymes optimised for catalysis under moderate conditions (60 °C > T_m > 37 °C) and "psychrozymes" for low-temperature conditions (37 °C > T_m). If thermal stability is unknown, then a provisional definition is used on the basis of the organism from which the enzyme was isolated (*i.e.*, thermozymes from thermophiles, psychrozymes from psychrophiles, *etc.*). Although the individual enzymes within these classes vary extensively amongst themselves in terms of the specific interactions and mechanisms used to promote reactions, a comparison of the

thermodynamic differences between the classes reveals some reliable trends.

1.8.1 Structural Distinctions

There are a number of notable structural features that are consistently used by each of the aforementioned classes of enzymes, as elucidated by comparative analyses (Gianese, Bossa, & Pascarella, 2002; Imanaka, 2011; Kumar & Nussinov, 2004; Russell, 2000; Smalas *et al*., 2000). Compared to mesozymes, thermozymes tend towards more disulfide-bonds, H-bonds, and proline residues, as well as tighter packing and greater contact between hydrophobic residues (Imanaka, 2011), which ultimately results in greater structural rigidity (D'Amico *et al*., 2003). By contrast, psychrozymes tend towards fewer proline residues and disulfide bonds, and a higher occurrence of glycine-clusters, which contribute to greater structural flexibilty (D'Amico *et al*., 2003; Feller, 2003; Lonhienne, Gerday, & Feller, 2000; Russell, 2000). Interestingly, both thermozymes and psychrozymes tend towards more ion-pairs relative to their mesozyme counterparts (Kumar & Nussinov, 2004; Smalas *et al*., 2000).

1.8.1.1 Structural Distinctions from Mutagenesis Studies

A general approach for positively identifying primary sequence differences that bestow thermal-stability or -lability has emerged from numerous investigations, and has been used to great effect (Rahman *et al*., 1998; Imanaka, Shibazaki, & Takagi, 1986). Typically, this approach involves a pair of enzymes that possess high

amino acid sequence similarity, but differing stability or activity at a particular temperature. Divergent amino acids are identified, and then substitutions are made to create intermediate-sequence variants with properties that are a balance, or even a combination of the original pair. The properties of one variant bestowed upon the other implicate the associated primary structure elements.

The first example I present of the aforementioned experimental approach is the application of an ion-pair network in glutamate dehydrogenase from *Pyrococcus furiosus,* to a less heat-stable variant from *Thermococcus kodakarensis* (Rahman *et al*., 1998). The authors made a single T138E substitution in the *T. kodakarensis* glutamate dehydrogenase, on the basis of sequence homology, resulting in improved thermostability, and a higher optimal temperature of activity. In another example, the authors sought to study the effect of increased internal hydrophobicity on thermostability of the neutral protease from *Bacillus stearothermophilus* (Imanaka, Shibazaki, & Takagi, 1986). In this case, a G144A substitution was made based on the thermostable thermolysin from *Bacillus thermoproteolyticus*. Despite the arguably minor steric difference between these two residues, their substitution doubled the proteolytic activity remaining after a 30 min incubation at 75 °C from 25% to 50%.

1.8.1.2 Structural Distinctions from Bioinformatics

Rather than conducting mutational analyses, many comparative studies use the tools of bioinformatics. Typically this involves alignment of primary structures,

accounting numbers and types of amino acids, and possibly correlating these counts with regions of 3D structures. The studies that follow exemplify this approach.

The implementations of ion-pairs in the structures of psychro-, meso-, and thermozymes are particularly diverse, and often more complex than was initially anticipated. For example, in a study comparing the primary structure of an *E. coli* mesozyme, O^6–methylguanine methyltransferase, to the thermostable *T. kodakarensis* variant, a mere 6% increase in ion-pairs was observed (Hashimoto *et al*., 1999). One might initially have expected a much larger disparity would be required to effect the large difference in stability observed between these enzymes. However, closer examination of the distribution of these ion-pairs revealed that the thermostable variant had 50% more charged residues in the solvent-accessible surface area, and 50% more hydrophobic residues, particularly aromatic ones, otherwise (Hashimoto *et al*., 1999). Similar findings were observed in a 3D structural comparison of 28 psychro-, meso-, and thermozyme variants (Gianese *et al*., 2002).

A structural comparison of citrate synthase from *P. furiosus*, *Arthobacter* Ds2–3R, and chicken revealed similar packing, burial of non-polar surface area, and main-chain hydrogen bonding in the respective thermozyme, psychrozyme, and mesozyme variants (Kumar & Nussinov, 2004). However, more charged residues were observed in the primary structure of both the psychrozyme and thermozyme. Calculations revealed that the psychrozyme had a greater variability in the contribution of each ion-pair to stability (*e.g*., destabilising in the active-site, but stabilising at the enzyme's surface) than those of the thermozyme. Furthermore, the

ion-pairs of the thermozyme were found to be clustered in the active-site and at the dimer interface, while those of the psychrozyme were dispersed. Overall, the thermozyme appeared to use salt bridges for countering disorder at the active-site or dimer interface, while the psychrozyme used salt bridges for improving solvation and active-site flexibility (Kumar & Nussinov, 2004).

1.8.1.3 Lessons from Structural Distinctions

It is uncommon to find all of the strategies presented above in a single enzyme, or even to find them used in the same way by enzymes adapted to the same temperature. Rather, these strategies should be thought of as precision tools that are employed to overcome situation-dependent structural or mechanistic deficits.

1.8.2 Thermodynamic Distinctions

1.8.2.1 Thermodynamic Links between Structure and Function

Although gross structural distinctions are rarely found, the thermodynamic-underpinnings of these structural distinctions reveals some reliable rules. A molecular-dynamics study of uracil DNA glycosylase from atlantic cod (a cold-active enzyme), and from humans, revealed that the Leu_{272} loop of these enzymes is an important structural feature for DNA-recognition and binding. Calculations revealed that this loop is also the most flexible part of the psychrozyme-variant. By contrast, the Leu_{272} loop of the human variant has been deemed much less flexible (Olufsen *et al*., 2005). The computationally-determined flexibility of this loop

correlates well with experimental k_{cat}/K_m values, consistent with the idea that flexibility plays a central role in adaptation to cold environments (Olufsen *et al*., 2005). Indeed, mechanistic studies of ribonuclease, aspartate aminotransferase, and dihydrofolate reductase, using stopped-flow and temperature-jump methods, nuclear magnetic resonance, and single-molecule fluorescence techniques revealed that flexibility, and conformational diversity and cooperativity, are fundamental pillars of catalysis by enzymes (Hammes, Benkovic, & Hammes–Schiffer, 2011).

1.8.2.2 A Theory of Activity from the Thermodynamics of Folding

By combining the data and insights of multiple studies, a broader picture begins to emerge. One such gathering of multiple data sets involved psychrophilic, mesophilic, and thermophilic α–amylases, which were examined on the basis of conformational stability, heat-inactivation, irreversible unfolding, activation parameters of catalysis, properties of the enzyme–TS-analogue-complex, and structural permeability, described by D'Amico *et al*., (2003). The synthesis of these data allowed the authors to develop a model of the folding funnels for psychrozymes and thermozymes, shown in Figure 1.3. The model is based, in-part, on the observation that psychrozymes tend to unfold cooperatively and without intermediates (D'Amico, Gerday, & Feller, 2001; Feller, d'Amico, & Gerday, 1999) (Figure 1.3 left; purple arrows), whereas thermozymes require a higher temperature to overcome the intermediate folding barriers (D'Amico *et al*., 2001; Feller *et al*., 1999; Rahman *et al*., 1998) (Figure 1.3, right; purple arrows). The shapes of the bottoms of

these proposed folding funnels (*i.e.*, the catalytically-active GS-conformations) have implications for activation-barrier height, and the ES-complexes propensity towards TS-formation, in cases where the thermozyme and psychrozyme have similar activated-complexes, with similar entropies and enthalpies (*e.g.*, enzymes that catalyse the same chemical transformation *via* the same mechanism). According to this model, psychrozymes have a broad, high-diversity ensemble of active conformations that are accessible with very little energetic input (Figure 1.3 left; blue lines). These characteristics indicate a larger drop in entropy will be required upon ES-activation; consequently, $\Delta S_{es}^{\ddagger}$ will be more negative, and TS-formation less entropically favourable. However, they also indicate a smaller rise in enthalpy upon ES-activation (*i.e.*, $\Delta H_{es}^{\ddagger}$ is less positive, more enthalpically favourable). By capitalising on the attenuated impact of $\Delta S_{es}^{\ddagger}$ at low T, this strategy ultimate leads to larger values of k_{cat} at reduced temperatures. This theory is thus effectively an argument for the use of GS-destabilisation by psychrozymes: raising the GS-enthalpy closer to the TS-enthalpy. By contrast, rigid thermozymes are predicted to require a comparatively greater amount of energy to overcome the barriers into or between their narrowly-defined catalytically-active conformations (Figure 1.3 left; blue lines); characteristics that indicate smaller drops (or possibly gains) in entropy, upon formation of the activated-complex, $\Delta S_{es}^{\ddagger}$, larger values of $\Delta H_{es}^{\ddagger}$, and smaller values of k_{cat} at low temperatures. Indeed, these predictions are largely supported by experimental evidence (Kumar *et al.*, 2000; Ma *et al.*, 2000; Tsai, Ma, & Nussinov, 1999).

Figure 1.3 Proposed Folding Funnels of Psychrozyme and Thermozyme

The folding funnels proposed for a psychrozyme (left) and a thermozyme (right) as a function of folding energy (E_{fold}). In this model an unfolded psychrozyme folds in a single, highly-cooperative transition, whereas a thermozyme folds in stages, with intermediate barriers to continued folding (magenta arrows). The inactive conformation (red mark) is promoted into one of the active conformations (blue lines) by an event, such as substrate binding, and is then poised for catalytic turnover. This figure was adapted from the work of D'Amico *et al*. (2003).

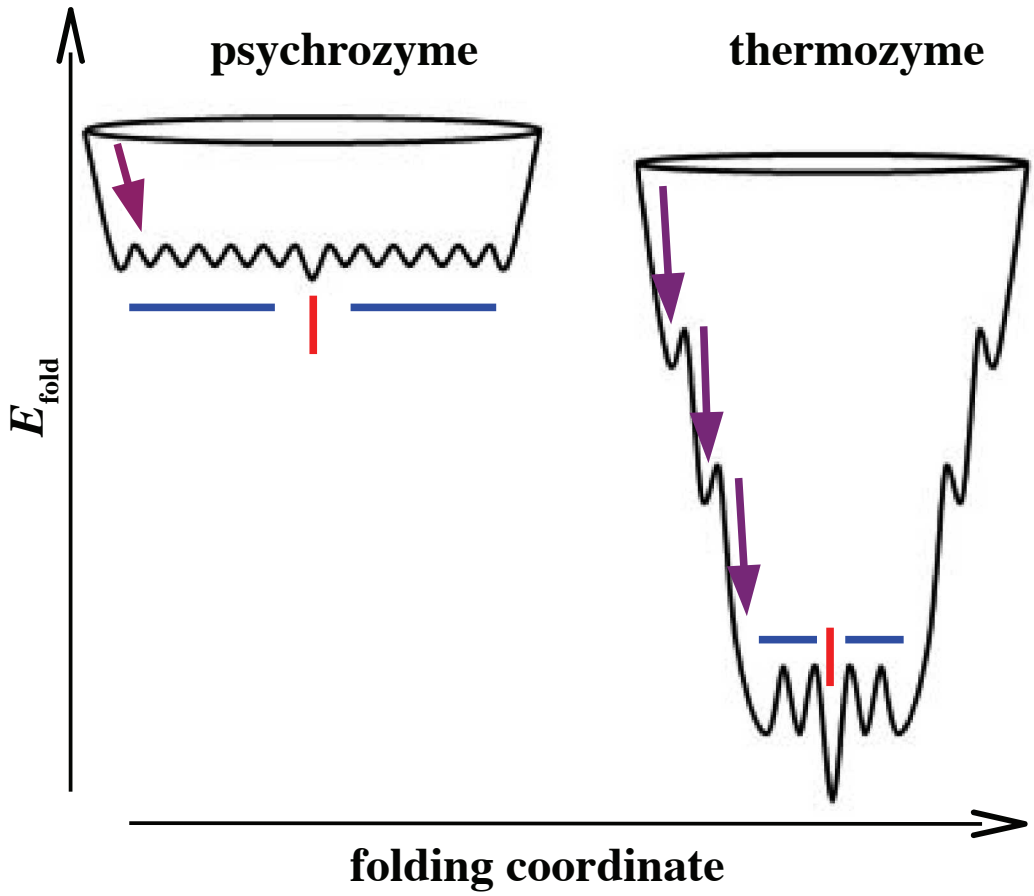

Figure 1.3

The rule-proving exception to the model presented above is the case of multi-domain psychrozymes. The strategy used by these psychrozymes is described below, and in the context of a related theory of psychrozyme-structure, proposed by Lonhienne *et al*. (2000). Lonhienne *et al*. propose that these psychrozymes segregate flexibility to active-site domains, and rigidity to structural domains, the latter guiding the former between clusters of active conformations, ultimately increasing the accessibility of diverse, catalytically-active conformations, without compromising the stability of the active site, or k_{cat}. The altered folding funnel proposed for such an enzyme may resemble that depicted in Figure 1.4. The structure of the enzyme that gives rise to the folding funnel depicted in Figure 1.4 would be predicted to have distinct thermal transitions, despite having a single diverse ensemble of catalytically-active conformations. Indeed, microcalorimetric investigations of phosphoglycerate kinase, which can be divided into heat-stable and heat-labile domains, and which relies on gross structural changes at a "hinge" to reach its active conformation, does segregate in this fashion, and is observed to make two distinct, individually-cooperative melting transitions (Bentahir *et al*., 2000). By contrast, the cold-active α–amylase variant from *Alteromonas haloplanctis*, which reaches its active conformation through delocalised structural changes, unfolds in a highly cooperative fashion (Feller *et al*., 1999). Regardless of how it is manifest, increased flexibility is the major unifying characteristic responsible for reducing $\Delta H_{es}^{\ddagger}$ and $\Delta S_{es}^{\ddagger}$, and ultimately increasing k_{cat} at low temperatures (D'Amico *et al*., 2003; Lonhienne *et al*., 2000).

Figure 1.4 Proposed Folding-Funnels of Psychrozymes with Thermodynamically Segregated, or Cooperative, Structural Domains
The folding funnels proposed for a psychrozyme with thermodynamically segregated (left) or thermodynamically cooperative (right) stuctural domains, as a function of folding energy (E_{fold}) are shown above an illustration of their corresponding mechanisms. A psychrozyme that must possess a high k_{cat} and a low K_m, faces an inherent conflict between raising $\Delta S_{es}^{\ddagger}$ and lowering $\Delta H_{es}^{\ddagger}$, while concomitantly lowering ΔS_m and raising $\Delta H_m^{\ddagger}$. The mechanism proposed by Lonhienne *et al*. (2000) outlines a possible solution. Both the segregated and cooperative psychrozyme (red and blue circle, and magenta circle, respectively) fold in a single, highly cooperative transition (magenta arrows), and reach a well of catalytically-inactive conformations (red lines and mark) bordered by a broad plateau of catalytically-active conformations; however, the transition onto this plateau is distinct. The segregated psychrozyme has a rigid, low entropy domain (red semicircle), which moves only at the hinge region (black dot), and a flexible, high-entropy, active-site domain (blue semicircle), which may freely sample the catalytically-inactive conformations. When the segregated psychrozyme binds its substrate (orange shape, and arrow), a conformational change in the rigid domain leads to tight-binding. Once bound, the substrate-flexible-domain complex is free to sample the catalytically-active conformations, In this way, the thermodynamically segregated psychrozyme maintains most of the rate-enhancement associated with the cooperative psychrozyme, but with a bias towards conformations that include the substrate. This figure was adapted from a report by D'Amico *et al*. (2003) to illustrate the concepts described by Lonhienne *et al*. (2000).

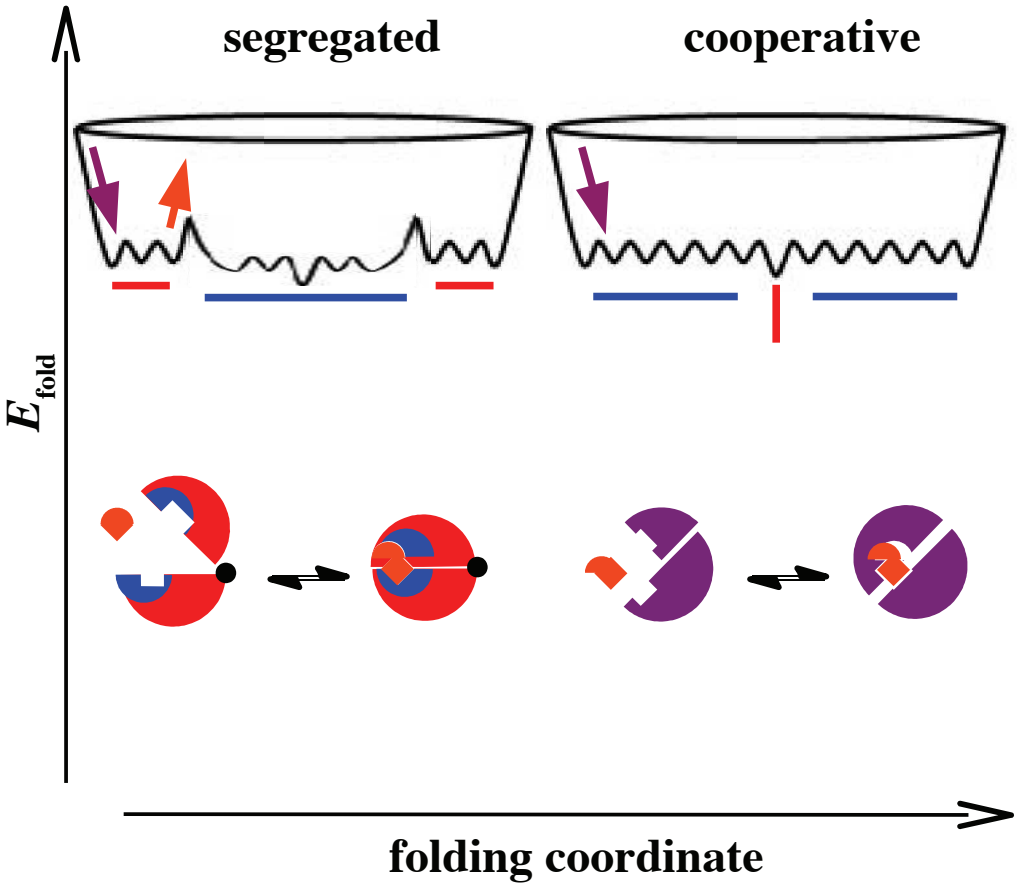

Figure 1.4

The other aspect of the theory proposed by D'Amico *et al*. (2003) is how it relates to the K_m of psychrozymes. In order to maintain a K_m value that is sufficiently low to be compatible with low native concentrations of a particular metabolite, some psychrozymes effect changes in the thermodynamic parameters of substrate release, ΔS_m and ΔH_m, that oppose the aforementioned changes in $\Delta S_{es}^{\ddagger}$ and $\Delta H_{es}^{\ddagger}$. Put another way, these psychrozymes make ΔS_m and ΔH_m less negative and/or more positive, to effect a reduction in K_m that ultimately shifts the GS equilibrium away from free substrate, and toward the ES-complex. Indeed, the aforementioned approach of phosphoglycerate kinase also attends to these outcomes. Through a gross structural transition distal to the active-site, and in response to substrate-binding, it transforms into a structure that presents a diverse ensemble of active conformations. Thus, structural components of the enzyme that mediate substrate release are effectively decoupled from those required for formation of the TS. Consequently, thermodynamic parameters that define substrate release, ΔS_m and ΔH_m, can be modulated *via* changes in local structure without affecting the thermodynamic parameters associated with activation, $\Delta S_{es}^{\ddagger}$ and $\Delta H_{es}^{\ddagger}$ (Bentahir *et al*., 2000; Lonhienne *et al*., 2000). By contrast, the psychrozyme-variant of α–amylase (described above) can afford to use a cooperative folding path (and concomitantly coupled k_{cat} and K_m values), because its environment is ostensibly rich in substrate (D'Amico *et al*., 2003; Feller *et al*., 1999). One of the experimental implications of this model is that measuring thermal stability by loss of activity may obscure the existence of more stable domains, which would be detected using biophysical

methods (*e.g.*, CD-spectroscopy) that measure structural changes directly (Lonhienne *et al.*, 2000).

The models proposed by D'Amico *et al.*, (2003) and Lonhienne *et al.* (2000), describe two regions of folding-funnels, and how they are altered to facilitate enzyme-activity at extremes of temperature. The first region is comprised of catalytically-capable ground states and is found at the bottom of the folding funnel. This region is either broad, flat, and shallow, to favour conformational promiscuity and stuctural flexibility in conditions of low ambient thermal energy (*i.e.*, the typical environment of a psychrozyme), or it is narrow, jagged, and deep, to favour conformational selection and structural rigidity in the face of forceful thermal "jostling" (*i.e.*, in the typical environment of a thermozyme). The second region borders the first, and provides a smooth path of approach to support cooperative folding of psychrozymes, or a recalcitrant path of approach, requiring multiple distinct folding transitions, each with an associated energetic barrier, of thermozymes. The caveat to this description is that some psychrozymes may require an intermediate region between the two described above, which allows these enzymes to segregate their structures into a flexible, catalytically-active domain, and a rigid, susbtrate-trapping domain. Ultimately, the concepts underlying the description above, may provide a rational basis for understanding the stability-activity relationship observed for psychro-, meso-, and thermozymes.

1.8.2.3 Mechanistic-Lessons from the Thermodynamics of Extremozyme-Structure

With a few caveats, the investigations outlined in the preceding subsections predict that I should have observed the following characteristics in Pa-, and CpODCase: reduced values of ΔH and ΔS for substrate release and activation of the GS-complex to the TS-complex, and a correspondingly reduced thermal stability (*i.e.*, reduced T_m), increased turnover (*i.e.*, increased k_{cat}), and increased dissociation of substrate from ES (*i.e.*, increased K_m).

1.9 Relevance and Scope

My goal in this thesis was to determine how the thermodynamic aspects of enzyme catalysed reactions are modified to cope with the unique challenges of a cold environment; challenges that have been overcome by all of the aforementioned varieties of cold-adapted organisms. Consequently, I chose to study two variants of the incredibly proficient enzyme, ODCase—one from *P. arcticus* 273–4, and another from *C. psychrerythraea* 34H—to learn the molecular mechanisms by which these enzymes were adapted to the cold. These mechanisms are of direct relevance to biocatalysis at low temperatures (Antranikian, Vorgias, & Bertoldo, 2005; Sellek & Chaudhuri, 1999), and the products that rely upon it, such as pharmaceuticals, detergents, biodiesel fuels, agrochemicals, and foods such as cheese and yogurt (Aguilar, Ingemansson, & Magnien, 1998; Salameh & Wiegel, 2007). Understanding biocatalysis is also critical for the development of emerging technologies, such as biosensors (Aguilar *et al.*, 1998).

My hope is that by furthering efforts to determine a set of empirically derived

fundamentals, I will contribute to the ultimate goal of enzymology: a conceptual and practical understanding of exactly what makes enzymes such incredible catalysts. With this goal in mind, I sought to reveal distinctions that are directly related to the fundamental properties of enzyme-mediated catalysis, by careful comparison of ODCase-variants.

The next two chapters recount my observations concerning the activity and stability of PaODCase (Chapter 2) and CpODCase (Chapter 3), as functions of temperature and pH. The fourth chapter expounds upon the observations of the prior two by integrating previously-collected data describing Sc-, Ec-, and MtODCases, and ultimately discussing the implications of these combined data for ODCase structure and function. The fifth chapter summarises this body of work, and describes how I imagine the investigation will proceed from here. The methods are described in Chapter 6, and additional results, as well as the references, are left to appendices found on the last pages of this thesis.

Chapter 2 RESULTS: PaODCase

2.1 Isolation and Kinetic Assessment of PaODCase$_{+tag}$ and PaODCase$_{-tag}$

An *E. coli* BL21(DE3) cell line was created by Brandi Mahaney (Bearne lab, Department of Biochemistry & Molecular Biology, Dalhousie University, Halifax, NS) that hosted the plasmid pET-15b-PaODC (see § 5.1). I isolated the fusion protein, PaODCase$_{+tag}$, from these *E. coli* cells using standard procedures (see § 5.2.9), as can be seen from Figure 2.1 (Panel A). PaODCase$_{+tag}$ is a fusion of WT-PaODCase with an N-terminal polypeptide that incorporates six histidine residues and an intervening thrombin cleavage site (Figure 2.2). The anticipated cleavage product is nearly identical to the wild-type sequence, but for three residues prepended to the N-terminus: glycine, serine, and histidine. Biotinylated-thrombin was used to remove the N-terminal hexahistidine tag and yield PaODCase$_{-tag}$. Comparison of the specific activity of these two recombinant enzymes as a function of varying substrate concentration (Figure 2.1, Panel B) revealed no significant changes in catalytic-activity resulting from the thrombin-catalysed cleavage-reaction. It was my aim to use the ODCase-variant that best represented the wild-type, and so in light of the similar catalytic activity, and greater sequence authenticity afforded by removal of the N-terminal tag, I opted to use PaODCase$_{-tag}$ for all further investigations. Hereafter, the delimiting subscript is dropped, and PaODCase$_{-tag}$ is referred to as PaODCase.

Figure 2.1. Initial Characterisation of PaODCase$_{+tag}$ and PaODCase$_{-tag}$
Thrombin-catalysed cleavage of the N-terminal hexahistidine tag from PaODC$_{+tag}$ (predicted MW of 27.1 kDa), to yield PaODC$_{-tag}$ (predicted MW of 25.0 kDa), proceeds to completion with no apparent byproducts seen after SDS-PAGE (Panel A). A comparison of the activity of PaODCase$_{+tag}$ and PaODCase$_{-tag}$ (both 40 nM) is shown in Panel B. Assays were conducted in MOPS buffer (10 mM, pH 8.0) containing NaCl (100 mM) and OMP (3.66, 7.32, 11.0, 14.6, 29.3, 58.5, and 117 μM). v_i is the initial rate determined by fitting the corresponding progress curve with a parabolic function. Initial rate kinetic data were fit to eqn. 1.9 by non-linear regression analysis using *KaleidaGraph* v.3.5 (Synergy Software, Reading, PA) to determine the values of V_{max} and K_m. Plotting the initial rates as a function of OMP concentration revealed that PaODC$_{-tag}$ (□) and PaODC$_{+tag}$ (○) have indistinguishable K_m values (9.8 ± 1.3 μM vs.10.7 ± 0.7 μM, respectively), and that PaODC$_{-tag}$ has an approximately 6% greater V_{max} (0.71 ± 0.29 μM/s), as compared to PaODC$_{+tag}$ (0.67 ± 0.13 μM/s, Panel B). Experimental details are described in § 5.2.17.

A

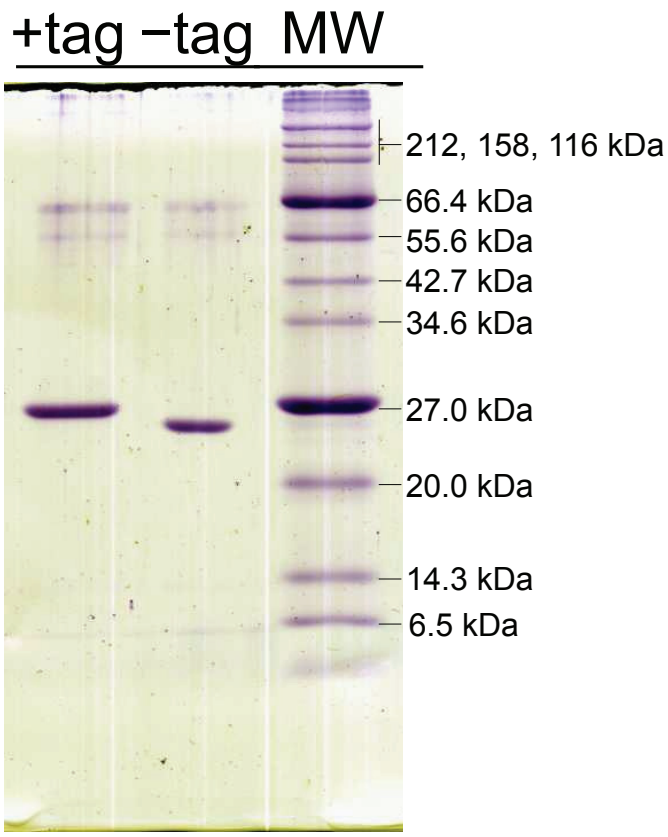

Figure 2.1 (page 1 of 2)

B

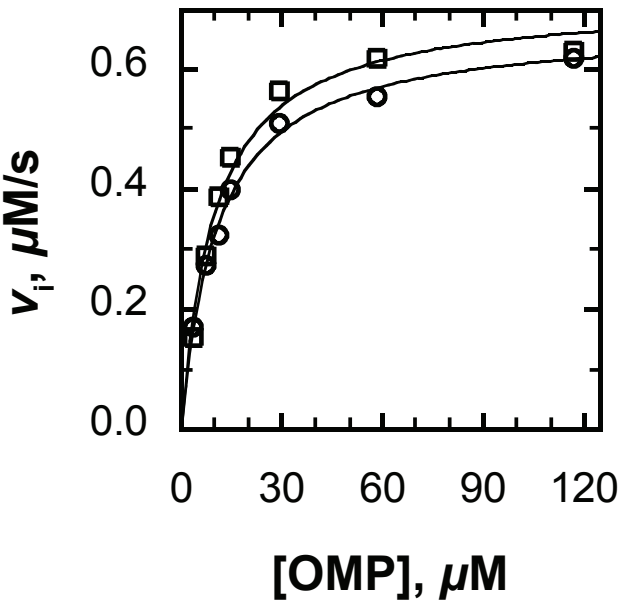

Figure 2.1 (page 2 of 2)

Figure 2.2 Primary Structure of PaODCase$_{+tag}$

PaODCase$_{+tag}$ is a recombinant enzyme composed of: the WT PaODCase sequence (from M to the C–terminus), a Ni^{2+}–chelating hexahistidine sequence (in **bold**), and an intervening thrombin cleavage site (outlined; scissile bond labelled with a '▼'). Digestion with thrombin generates PaODCase$_{-tag}$, which differs from the WT sequence by three N–terminal residues in the order: glycine, serine, and histidine (in *italics*).

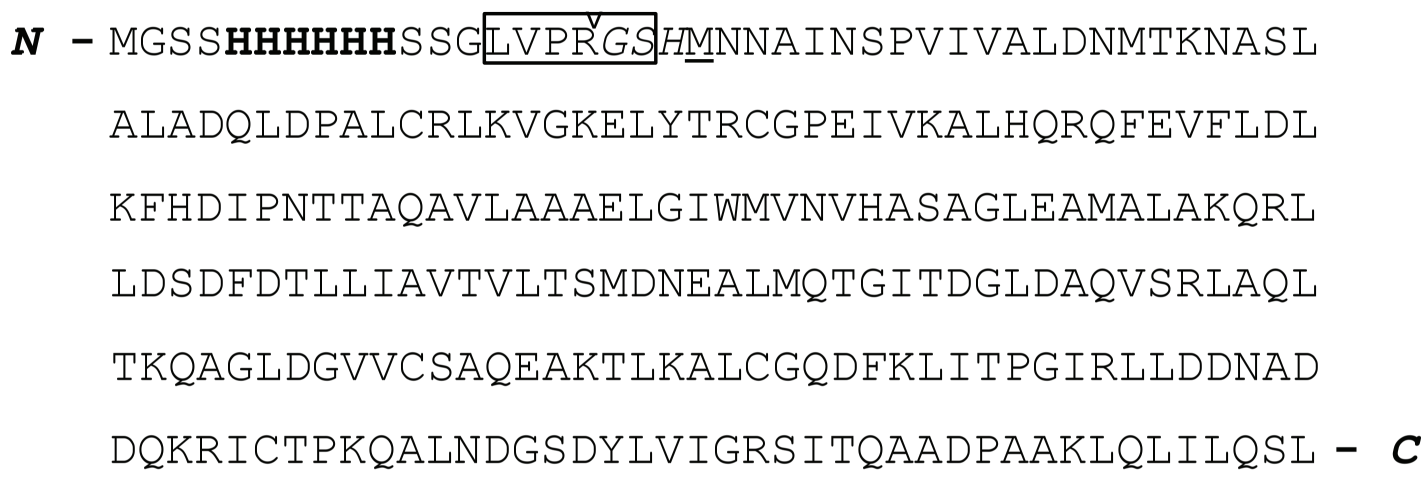
N - MGSSHHHHHHSSGLVPRGSHMNNAINSPVIVALDNMTKNASL
ALADQLDPALCRLKVGKELYTRCGPEIVKALHQRQFEVFLDL
KFHDIPNTTAQAVLAAAELGIWMVNVHASAGLEAMALAKQRL
LDSDFDTLLIAVTVLTSMDNEALMQTGITDGLDAQVSRLAQL
TKQAGLDGVVCSAQEAKTLKALCGQDFKLITPGIRLLDDNAD
DQKRICTPKQALNDGSDYLVIGRSITQAADPAAKLQLILQSL - C

Figure 2.2

2.2 The effect of pH on the Kinetic Parameters of PaODCase

Kinetic assays generally suffer less from random error due to signal-noise if the observed rates are greater in magnitude (*i.e.*, the relative error is diminished). The maximum rate of an enzyme-catalysed reaction occurs at its pH-optimum; hence, I assayed the activity of PaODCase over a range of pH values (6.0–9.5) to determine the optimal pH for PaODCase-mediated catalysis. The resulting activity profiles (Figure 2.3) and kinetic constants (Table 2.1) revealed that maximal activity of PaODCase is observed at pH 8.0.

Scheme 2.1 depicts a general mechanism by which changes in pH can effect changes in enzyme activity. In this model, equilibration of the noncovalent complex, ES^n, is assumed to be rapid compared to catalytic turnover (*via* k_2). Further, ES^n is the only enzyme-substrate complex capable of product formation. The superscripts n + 1 and n − 1 represent a higher- or lower-order protonation state, respectively. K_{e+s1} and K_{e+s2} are the acid-dissociation constants corresponding to the free enzyme and substrate in solution (E + S); K_{es1} and K_{es2} are the acid-dissociation constants for interconversion between the productive ES-complex, $(ES)^n$, and the non-productive ES-complexes ($(ES)^{n+1}$ and $(ES)^{n-1}$), while K_{d1}, and K_{d2}, are the substrate-dissociation constants for the non-productive complexes. For this model, the rapid-equilibrium assumption is applied such that $K_m = k_{-1}/k_1$ and $k_{cat} = k_2$, giving rise to the pH-dependencies described by eqn. 2.1 and 2.2 (Segel, 1975), where $(k_{cat})^{max}$ and $(k_{cat}/K_m)^{max}$ are the maximum values of the corresponding parameters. Changes in the value of log (k_{cat}) as a function of pH are understood to reflect the protonation state of

Figure 2.3 pH Profiles of PaODCase-Activity

pH profiles were constructed from apparent logk_{cat} (Panel A) and log(k_{cat}/K_m) (Panel B) values obtained from assays of PaODCase activity as a function of pH. The buffers used in these assays were : MES (pH 6.0–6.5, ▲), PIPES (pH 6.5–7.5, ○), HEPES (pH 7.5–8.5, ◆), TAPS (pH 8.5–9.0, □), and CHES (pH 9.0–9.5, ▼). The curves shown were obtained by taking the log of the values listed in Table 2.1, potting the logarithms as a function of pH and fitting with eqn. 2.2 (Panel A) and 2.1 (Panel B) by non-linear regression analysis using *KaleidaGraph* v.3.5 (Synergy Software, Reading, PA). The acid-dissociation constants corresponding to ES (Panel A), or E + S (Panel B), are listed in Table 2.2. The experimental procedure is described in detail in § 5.2.17 and 5.2.18.

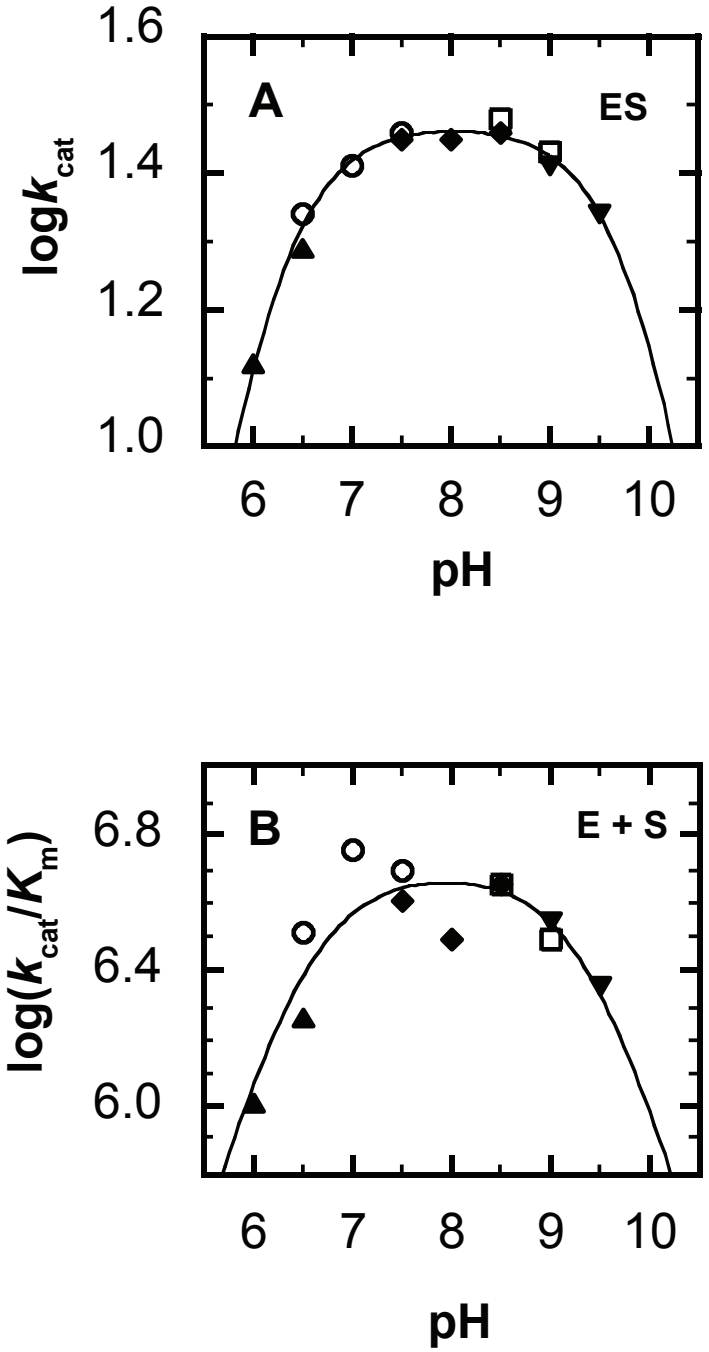
A
ES
logk_{cat}
1.6
1.4
1.2
1.0
6
7
8
9
10
pH
B
E + S
log(k_{cat}/K_m)
6.8
6.4
6.0
6
7
8
9
10
pH

Figure 2.3

Table 2.1

Apparent Kinetic and Equilibrium Constants for PaODCase-Mediated Decarboxyation of OMP as a Function of pH

buffer and pH	PaODCase		
	k_{cat}, s^{-1}	K_m, μM	k_{cat}/K_m, $M^{-1} \cdot s^{-1}$
MES			
6.0	13.2 ± 1.1	12.9 ± 2.9	1.02 ± 0.26
6.5	19.7 ± 1.7	10.8 ± 2.3	1.82 ± 0.45
PIPES			
6.5	22.00 ± 0.62	6.83 ± 0.52	3.22 ± 0.29
7.0	25.5 ± 1.2	4.53 ± 0.66	5.62 ± 0.97
7.5	28.9 ± 2.0	5.9 ± 1.2	4.9 ± 1.2
HEPES			
7.5	28.2 ± 1.3	7.06 ± 0.88	4.00 ± 0.54
8.0	28.1 ± 2.0	9.1 ± 1.5	3.10 ± 0.56
8.5	38.0 ± 2.5	7.9 ± 1.3	4.79 ± 0.94
TAPS			
8.5	30.0 ± 1.4	6.63 ± 0.86	66.3 ± 6.9
9.0	26.7 ± 1.4	8.6 ± 1.1	60.3 ± 1.7
CHES			
9.0	25.5 ± 1.4	7.4 ± 1.0	67.8 ± 2.3
9.5	22.1 ± 1.1	9.8 ± 1.2	68.0 ± 6.9

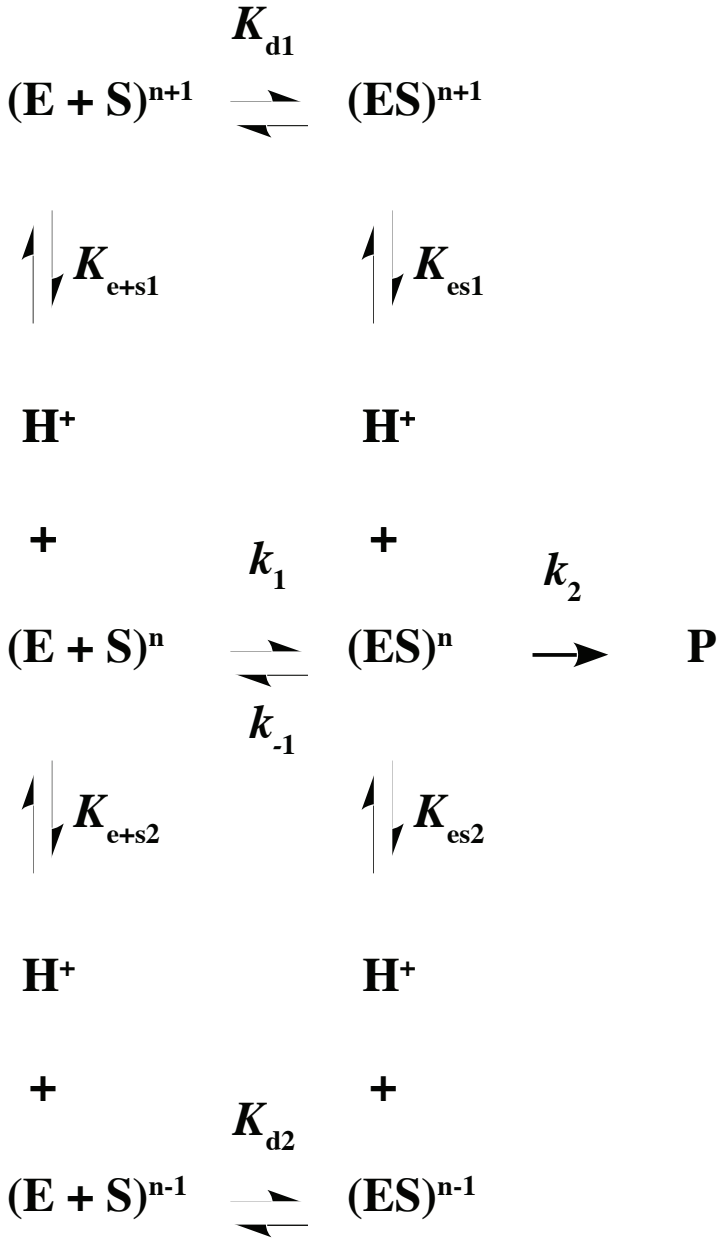

Scheme 2.1 General kinetic mechanism describing the effect of pH on ODCase-activity (adapted from Segel [1975]).

the ES-complex, while changes in the value of log (k_{cat}/K_m) reflect the protonation state of free E + S in solution.

$$\log_{10}(k_{cat}/K_m) = \log_{10}(k_{cat}/K_m)^{max} - \log_{10}\left(1 + \frac{[H^+]}{K_{e+s1}} + \frac{K_{e+s2}}{[H^+]}\right) \quad (2.1)$$

$$\log_{10}(k_{cat}) = \log_{10}(k_{cat})^{max} - \log_{10}\left(1 + \frac{[H^+]}{K_{es1}} + \frac{K_{es2}}{[H^+]}\right) \quad (2.2)$$

Because ΔG_m for PaODCase-mediated decarboxylation of OMP is significantly smaller than $\Delta G_{es}^{\ddagger}$ (see § 2.6), it is reasonable to make rapid-equilibrium assumptions. Thus, I fit the equilibrium and kinetic constants with eqn. 2.1 and 2.2 (Figure 2.3) to obtain the ionisation constants listed in Table 2.2. The lower pK values (6.1 and 6.5 for ES and E + S, respectively) may arise from the ionisation of the substrate phosphoryl group, or one of the aspartic acid residues at position 10, 60, or 65. The higher pK values (10.0 and 9.4 for ES and E + S, respectively) may correspond to one of the lysines at position-36 or -62. Based on a report from Smiley & Saleh (1999), the EP-complex is strengthened at alkaline pH, raising the possibility that the loss of activity is due in part to increased product inhibition.

2.3 Consistency of Active-PaODCase in Kinetic Assays

To avoid confounding effects that might occur from changes in quaternary

Table 2.2

pK_a Values of Species Involved in PaODCase-Mediated Decarboxylation of OMP and Kinetic Constants at pH-Optima[a]

ES	
log $(k_{cat})^{max}$	1.4716 ± 0.0076[c]
$(k_{cat})^{max}$, s^{-1}	29.62 ± 0.51[c]
pK_{es1}[b]	6.112 ± 0.031
pK_{es2}[b]	9.950 ± 0.073
E + S	
log $(k_{cat}/K_m)^{max}$	6.686 ± 0.055[c]
$(k_{cat}/K_m)^{max}$, $\times 10^6$ $M^{-1}\cdot s^{-1}$	4.85 ± 0.61[c]
pK_{e+s1}[b]	6.50 ± 0.15
pK_{e+s2}[b]	9.39 ± 0.22

[a] Values and their associated errors are derived from non-linear regression analysis of Figure 2.3

[b] As defined in Scheme 2.1

[c] Corresponds to the optimum pH for PaODCase-activity

structure of PaODCase, all assays were conducted using similar concentrations of PaODCase (20–30 nM). Further, the rate of decarboxylation was determined to be directly proportional to the concentration of active enzyme, assuming a constant proportion of active enzyme, over the full range of temperatures (10–65 °C), and OMP concentrations (4.6–223 μM) used (Figure 2.4).

2.4 Inhibition of PaODCase by UMP

It has been previously reported that other variants of ODCase are inhibited by the product of OMP-decarboxylation, UMP (Shambaugh, 1979; Smiley & Saleh, 1999)—likely in a competitive manner (Wu, Gillon, & Pai, 2002). To assess the impact of product-inhibition on my velocity measurements, I determined the IC_{50}-value due to UMP-inhibition. Fitting the kinetic data in Figure 2.5 with eqn. 5.8 revealed that the IC_{50} is 35.8-fold greater than the K_m for OMP (716 ± 25 μM, as compared with 20.0 ± 8.96 μM, respectively) under similar conditions, indicating that product release is strongly favoured. The large Hill-coefficient, n, for UMP-mediated inhibition (4.90 ± 0.95), indicates that that the active form of PaODCase has multiple UMP binding-sites. This is consistent with prior observations that each of the two potential active-sites in an ODCase-homodimer is comprised of amino acids from both monomers, and that both of these sites can bind UMP (Begley *et al*., 2000; Houk *et al*., 2001; Wu, Gillon, & Pai, 2002).

Figure 2.4 Correlation between PaODCase-Activity and Concentration
PaODCase-activity was assessed in the presence of OMP (223 μM [Panel A] and 4.6 μM [Panel B]), at 10 °C (□ and ■), 25 °C (○ and ●), and 65 °C (△ and ▲) over a range of enzyme concentrations (6.99, 14.0, 21.0, 27.9, 34.9, 41.9, 48.8, 55.9 nM [Panel A] or 4.44, 8.88, 13.3, 17.8, 22.2, 26.6, 31.1, and 35.5 nM [Panel B] at 10 °C; 7.36, 14.7, 22.1, 29.4, 36.8, 44.2, 51.5, and 58.9 nM [Panel A] or 4.12, 8.24, 12.4, 16.5, 20.6, 24.7, 28.8, and 33.0 nM [Panel B] at 25 °C; and 10.4, 20.8, 31.2, 41.6, 52.0, 62.5, 72.9, and 83.3 nM [Panel A] or 4.43, 8.85, 13.3, 17.7, 22.1, 26.6, 31.0, and 35.4 nM [Panel B] at 65 °C). Initial-rate kinetic data were plotted as a function of enzyme concentration and fit by linear regression analysis using *KaleidaGraph* v.3.5 (Synergy Software, Reading, PA) to determine the goodness of fit. Error bars represent the first standard deviation from the mean of triplicate assays. Panel A shows the correlation between PaODCase-activity and concentration in the presence of 223 μM OMP. At 10 °C (□) and 25 °C (○), PaODCase-activity was observed to be linearly dependent on its concentration. At 65 °C, linear dependence is observed from 10.4 to 41.6 nM (△), but does not continue from 52.0 to 83.3 nM (▲). Panel B shows the correlation between PaODCase-activity and concentration in the presence of 4.6 μM OMP. At 10 and 25 °C, PaODCase-activity was observed to be linearly dependent on its concentration up to 28.8 (□) or 31.1 nM (○), but deviated thereafter (■ and ●). At 65 °C, linear dependence is observed from 4.43 to 26.6 nM (△), but does not continue from 31.0 to 35.4 nM (▲). Detailed methods are described in § 5.2.17 and 5.2.21.

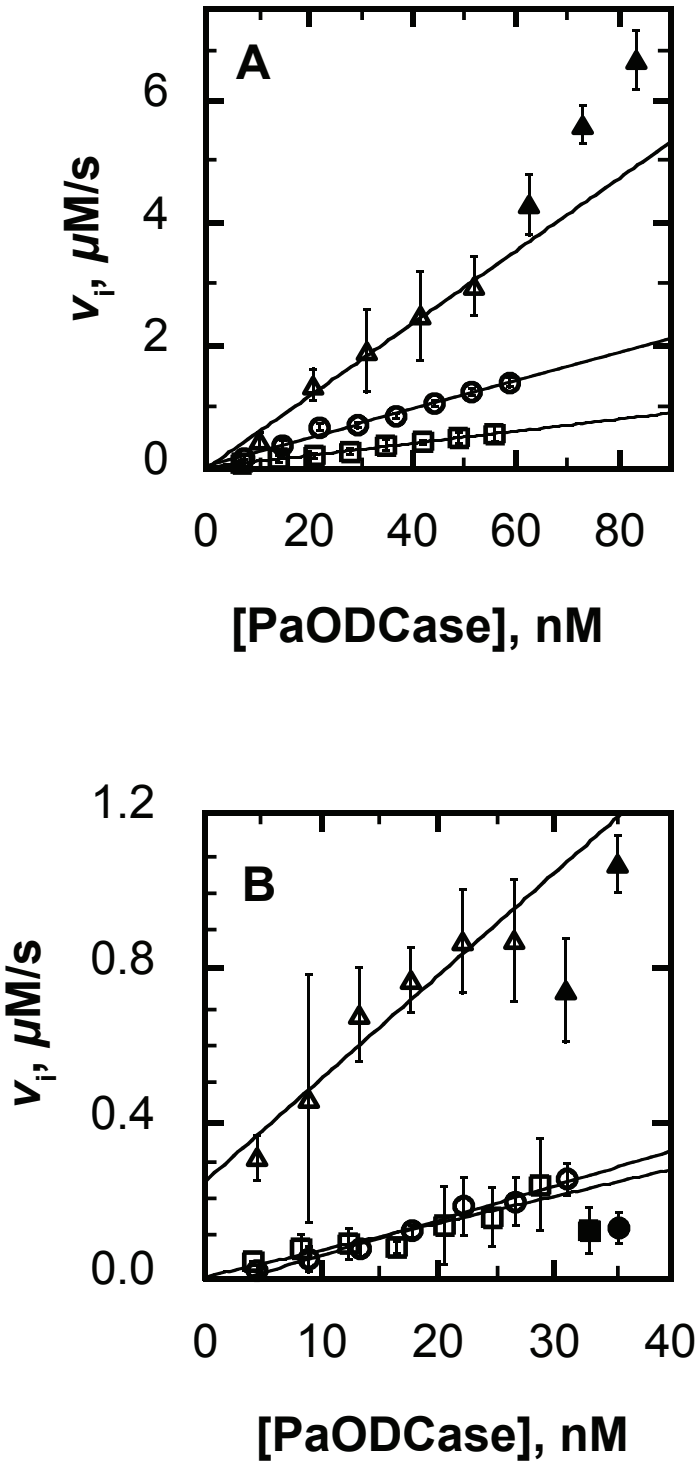
A
6
4
2
0
v_i, μM/s
0
20
40
60
80
[PaODCase], nM
B
1.2
0.8
0.4
0.0
v_i, μM/s
0
10
20
30
40
[PaODCase], nM

Figure 2.4

Figure 2.5 Inhibition of PaODCase-Activity by UMP.
Inhibition of PaODCase (15 nM) by UMP (227, 283, 340, 397, 453, 510, 567, 623, 680, and 736 μM), at 25 °C, is shown. In addition to PaODCase and UMP, reactions contained MOPS buffer (10 mM, pH 8.0) NaCl (100 mM) and OMP (44 μM). Assays containing greater than 736-μM UMP were impractical because their absorption exceeded the UV-vis detection-limit. Initial-rate kinetic data were plotted as a function of UMP concentration and fit to eqn. 5.8 by non-linear regression analysis using *KaleidaGraph* v.3.5 (Synergy Software, Reading, PA). Error bars represent the first standard deviation from the mean of triplicate assays. The IC_{50} value for UMP is 716 ± 25 μM, and the Hill-coefficient (n) is 4.90 ± 0.95. Detailed methods are described in § 5.2.17 and 5.2.19.

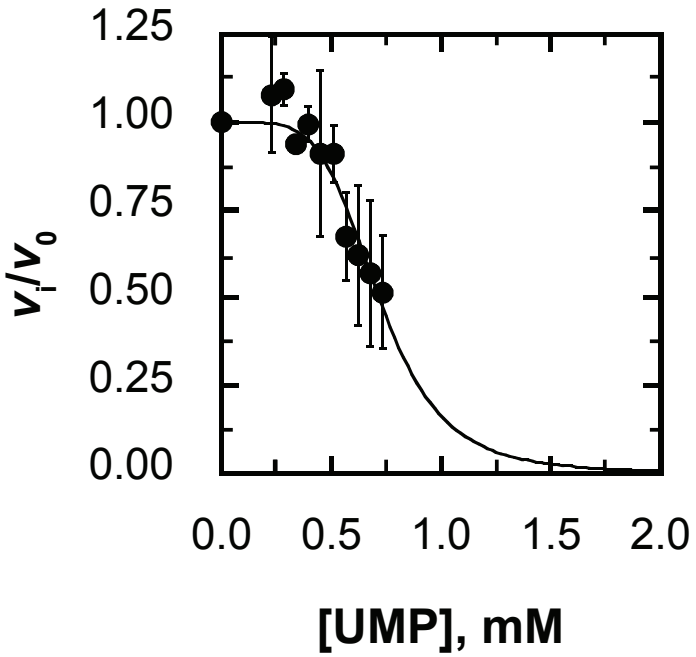

Figure 2.5

2.5 Thermal Stability of PaODCase

Because I intended to study the temperature dependence of the PaODCase-mediated decarboxylation reaction, I conducted a series of experiments to estimate the thermal stability of PaODCase. In particular, I determined the extent of α–helical content by measuring the enzyme's molar ellipticity at 222 nm ($[\theta]_{222}$). In this context, I define the melting temperature of an enzyme (T_m) as the temperature at which $[\theta]_{222}$ is the average of the $[\theta]_{222}$ corresponding to the folded and unfolded states ($[\theta]_f$ and $[\theta]_u$, respectively). Non-linear regression fitting of the data to eqn. 5.3 revealed that $[\theta]_{222}$ of the folded and unfolded states is -0.454 ± 0.041, and $-0.088 \pm 0.067 \times 10^3$ deg·cm^2·dmol^{-1}, respectively, and the T_m is 25.9 ± 3.7 °C (Figure 2.6, Panel B). CD spectra corresponding to each temperature examined are shown in Figure 2.6, Panel A.

2.6 Thermodynamic Parameters of PaODCase-Activity

In order to better understand the distinctions between PaODCase, and other ODCase-variants, I determined the thermodynamic parameters of PaODCase-mediated decarboxylation of OMP; specifically, those described in Scheme 1.1. In this context, the reaction coordinate may be described by five constants: three apparent kinetic constants, k_{cat}, k_{cat}/K_m, and k_{non}, an apparent dissociation constant, K_m, and a virtual association constant, $1/K_{tx}$. Each step along the reaction coordinate is accompanied by a ΔS and ΔH; I was able to calculate the values of ΔH and ΔS corresponding to the equilibrium constants using the method of van't Hoff, and the

Figure 2.6 Temperature Profile of PaODCase α–Helical Character

The CD-spectra of PaODCase, as a function of temperature, are shown in Panel A. The ellipticity of each enzyme sample over the range 190–260 nm was corrected for concentration of enzyme (35 [■], 57 [◆], 36 [▼], 12 [●], and 9.8 μM [▲]) and pathlength of sample (0.1 cm), to give the molar ellipticity. Each trace is the average of six individual spectra recorded at 4 (■), 10 (◆), 20 (▼), 30 (●), or 50 °C (▲). The extent of α–helical character was estimated from the molar ellipticity at 222 nm ($[\theta]_{222}$), and used to define the melting point (T_m) of PaODCase. T_m is the temperature at which $[\theta]_{222}$ is the average of the $[\theta]_{222}$ of the folded and unfolded states. $[\theta]_{222}$ is plotted as a function of temperature in Panel B. Error bars represent the first standard deviation from the mean of the molar ellipticities obtained from the six spectra. The data were fit to eqn. 5.3 by non-linear regression analysis using *KaleidaGraph* v.3.5 (Synergy Software, Reading, PA). The thus-calculated $[\theta]_{222}$ of the folded and unfolded states are -0.454 ± 0.041, and $-0.088 \pm 0.067 \times 10^3$ deg·cm^2·dmol^{-1}, respectively, and the T_m is 25.9 ± 3.7 °C. Detailed methods are described in § 5.2.16

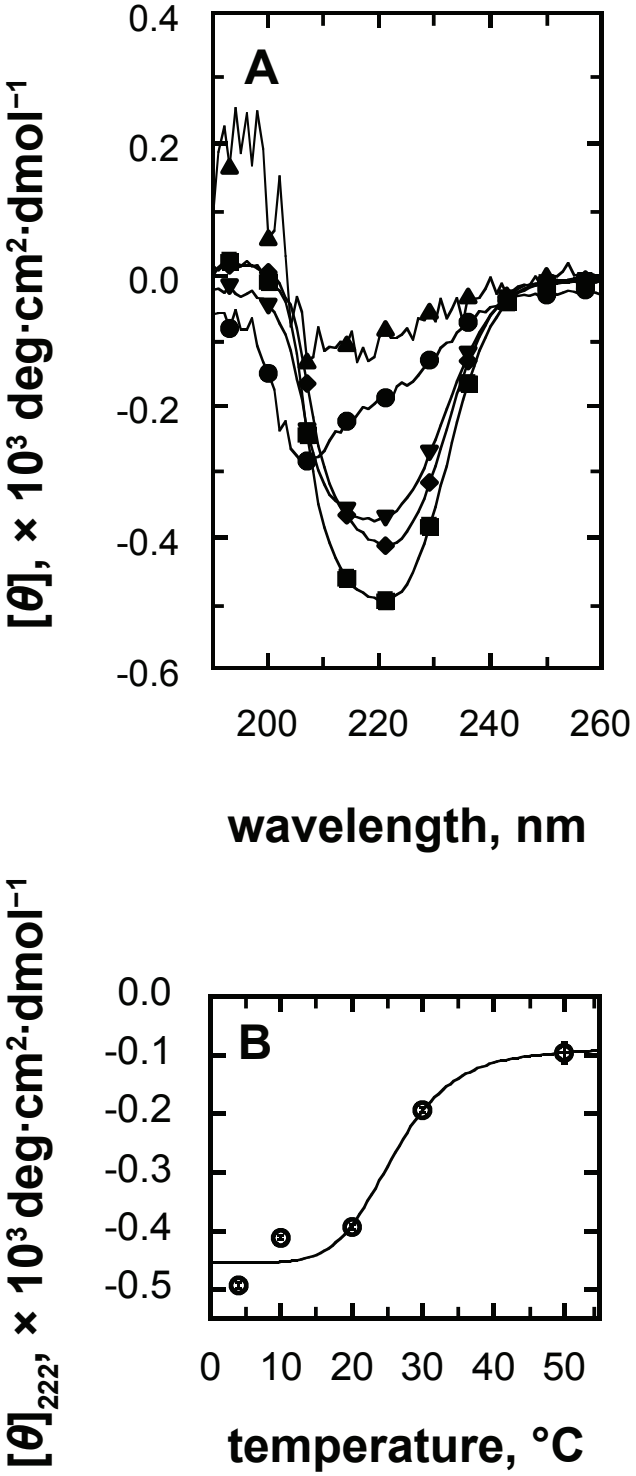
A
0.4
0.2
0.0
-0.2
-0.4
-0.6
200
220
240
260
[θ], × 10³ deg·cm²·dmol⁻¹
wavelength, nm
B
0.0
-0.1
-0.2
-0.3
-0.4
-0.5
0
10
20
30
40
50
[θ]222, × 10³ deg·cm²·dmol⁻¹
temperature, °C

Figure 2.6

values of $\Delta H^{\ddagger}$ and $\Delta S^{\ddagger}$ corresponding to the kinetic constants using the method of Eyring and Polanyi (see § 1.7.1); Figure 2.7 displays the plots constructed by these methods. Using eqn 1.10, the corresponding values of ΔG were evaluated for catalytic turnover at 25 °C. These thermodynamic parameters are collected in Table 2.3.

The van't Hoff plots reveal that TS-binding, as indicated by $1/K_{tx}$, and GS-complex dissociation, as indicated by K_m, are both attenuated with increasing temperature (Figure 2.7, Panel A and B, respectively). However, the Eyring–Polanyi plot of k_{cat} reveals that this effect is counterbalanced by the rate of product formation by the ES-complex, which is exponentially augmented by the increases in temperature (Panel C). The net result is revealed by Panel D: a pseudo second-order rate constant k_{cat}/K_m that is significantly less dependent on the temperature.

Figure 2.7 van't Hoff and Eyring–Polanyi Plots of PaODCase-Activity
Comparison of the kinetic and equilibrium constants at varying temperature revealed the extent to which ΔH and ΔS, contributed to the overall energetics of the chemical transitions investigated herein. The activity of PaODCase was assayed as a function of OMP concentration at 10, 15, 25, 30, 35, 40, 45, 50, 55, and 65 °C to derive K_m, k_{cat}, and k_{cat}/K_m at each of these temperatures. From these values, and with the known correlation between k_{non} and temperature (predicted by Radzicka & Wolfenden [1995] using the decarboxylation of 1–methylorotic acid as a model), K_{tx} was calculated using eqn. 1.4. Van't Hoff plots of $1/K_{tx}$ and K_m, as functions of temperature, are shown in Panels A and B, respectively. Eyring–Polanyi plots of k_{cat} and k_{cat}/K_m as functions of temperature, are shown in Panels C and D, respectively. Error bars represent the estimated error in the prediction of the kinetic and equilibrium constants from non-linear regression using eqn. 1.9. Each of the plots was fit to eqn. 1.11–1.14 (Panel A–D) by linear regression analysis using *KaleidaGraph* v.3.5 (Synergy Software, Reading, PA), to elucidate the ΔH and ΔS of the associated chemical transitions. The estimated values of ΔH and ΔS are listed in Table 2.3. Detailed methods are described in § 1.7.1, 5.2.17, and 5.2.20.

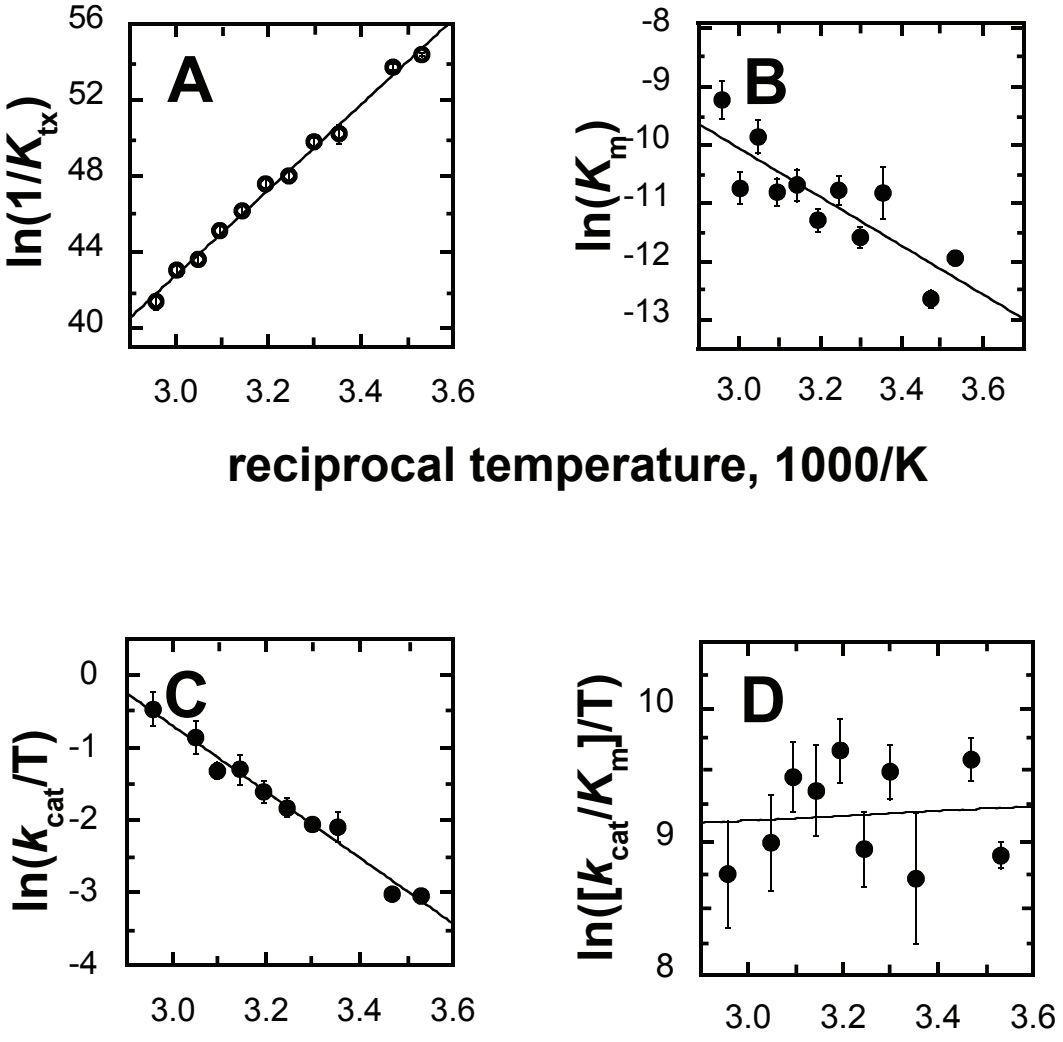
A
B
C
D
ln(1/K_tx)
ln(K_m)
ln(k_cat/T)
ln([k_cat/K_m]/T)
reciprocal temperature, 1000/K
reciprocal temperature, 1000/K

Figure 2.7

Table 2.3

Individual Contributions of Enthalpy and Entropy Changes to the Energetics of PaODCase-Catalysed Decarboxylation of OMP[a]

$E + \{S\}^{\ddagger} \rightleftharpoons \{ES\}^{\ddagger}$		
ΔG_{tx},[b] kcal/mol	ΔH_{tx}, kcal/mol	ΔS_{tx}, cal/mol·K
− 30.1 ± 2.3	− 44.7 ± 1.2	− 49.2 ± 4.0
$ES \rightleftharpoons E + S$		
ΔG_{m},[b] kcal/mol	ΔH_{m}, kcal/mol	ΔS_{m}, cal/mol·K
6.9 ± 3.5	8.3 ± 1.7	5.0 ± 5.7
$ES \rightarrow \{ES\}^{\ddagger}$		
$\Delta G_{es}^{\ddagger}$,[b] kcal/mol	$\Delta H_{es}^{\ddagger}$, kcal/mol	$\Delta S_{es}^{\ddagger}$, cal/mol·K
8.6 ± 3.8	− 0.2 ± 1.4	− 30.1 ± 8.1
$E + S \rightarrow \{ES\}^{\ddagger}$		
$\Delta G_{e+s}^{\ddagger}$,[b] kcal/mol	$\Delta H_{e+s}^{\ddagger}$, kcal/mol	$\Delta S_{e+s}^{\ddagger}$, cal/mol·K
15.43 ± 0.83	9.01 ± 0.45	− 21.5 ± 1.2

[a] As outlined in Scheme 1.1

[b] Calculated for 25 °C using eqn. 1.10

Chapter 3 RESULTS: CpODCase

3.1 Plasmid Construction and Transformation of *E. coli* BL21(DE3) Cells

To further explore the relationship between catalytic strategy and optimal growth temperature, I identified another potential source of cold-adapted enzymes: *C. psychrerythraea* 34H. The ORF corresponding to CpODCase (0.7 kb) was identified using the previously isolated and annotated genome of *C. psychrerythraea* 34H. PCR amplification of the CpODCase-ORF from genomic DNA was followed by digestion of the PCR product by the endonucleases *Bam*HI and *Nde*I, and insertion of the DNA fragment into a pET–15b vector (5.7 kb) to create the novel plasmid, pET–15b–CpODCase (6.4 kb). This plasmid was cloned in *E. coli* DH5α cells, purified, and the ORF was sequenced to confirm sequence-fidelity. The purified plasmid was then used to transform *E. coli* BL21(DE3) cells, for protein expression.

3.2 Isolation and Kinetic Assessment of CpODCase$_{+tag}$ and CpODCase$_{-tag}$

I isolated the fusion protein, CpODCase$_{+tag}$, using Ni^{2+}-affinity chromatography, but subsequent thrombin-catalysed cleavage of the hexahistidine-tag produced a contaminating byproduct (~10 kDa), in addition to CpODCase$_{-tag}$ (Figure 3.1, Panel A). Using anion-exchange FPLC I was able to isolate CpODCase$_{-tag}$ to >99%-purity (Figure 3.1, Panel B). I compared the activity CpODCase$_{+tag}$ and CpODCase$_{-tag}$ as a function of varying substrate concentration (Figure 3.1, Panel C), and determined that removal of the hexahistidine tag (for the primary structure, see Figure 3.2) effects no

Figure 3.1. Initial Characterisation of CpODCase$_{+tag}$ and CpODCase$_{-tag}$

Thrombin–catalysed cleavage of the N–terminal hexahistidine tag from CpODCase$_{+tag}$ (predicted MW of 27.2 kDa; Panel A, lane '0'), to yield CpODCase$_{-tag}$ (predicted MW of 25.0 kDa; Panel B, shown following SDS-PAGE at a 5:1 ratio of protein–concentrations in the lanes labelled "5" and "1", respectively), proceeds with simultaneous production of a secondary byproduct of approximately 10 kDa (Panel A). The byproduct appears to accumulate in concert with the cleavage reaction at each time point assessed (0, 30, 60, 120, 240, and 480 min). After overnight cleavage, and purification using anion–exchange FPLC, CpODCase$_{-tag}$ is purified to >99%. Molecular weight markers, (lanes labelled "M") are provided as a visual reference. A comparison of the activity of CpODCase$_{+tag}$ and CpODCase$_{-tag}$ (both 17 nM) is shown in Panel C. Assays were conducted in MOPS buffer (10 mM, pH 8.0) containing NaCl (100 mM) and OMP (2.3, 4.6, 6.9, 9.2, 11.5, 13.8, 16.1, 18.4, 20.7, 23, 34.5, 46, and 92 μM for CpODCase$_{+tag}$; 0.985, 1.17, 1.95, 3.28, 3.66, 4.00, 7.35, 7.74, 8.37, 10.8, 11.0, 11.9, 14.7, 15.7, 16.2, 18.3, 18.9, 19.6, 37.4, 37.9, 38.2, 83.6, 85.3, 86.6, 165, 166, and 169 μM for CpODCase$_{-tag}$). v_i is the initial rate determined by fitting the corresponding progress curve with a parabolic function. Initial rate kinetic data were fit to eqn. 1.9 by non–linear regression analysis using *KaleidaGraph* v.3.5 (Synergy Software, Reading, PA) to determine the values of V_{max} and K_m. Plotting the initial rates as a function of OMP concentration revealed that CpODC$_{-tag}$ (■) has a nearly 3–fold lower K_m (3.38 ± 0.73 μM *vs*. 9.0 ± 1.1 μM), and that CpODC$_{+tag}$ (●) has an approximately 9% greater V_{max} (1.104 ± 0.046 μM/s vs.1.012 ± 0.043 μM/s). Experimental details are elaborated upon in § 5.2.17.

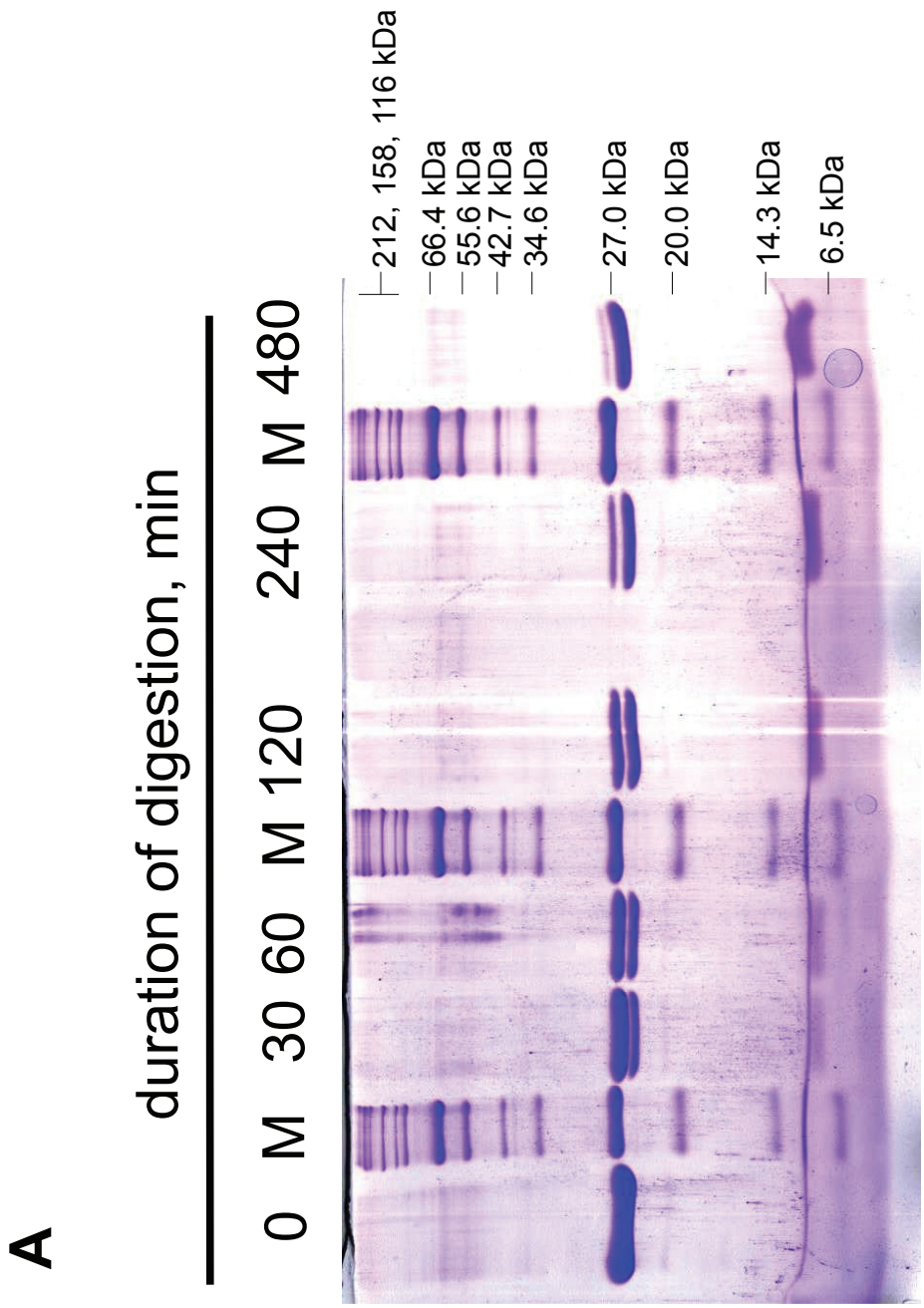

Figure 3.1 (page 1 of 3)

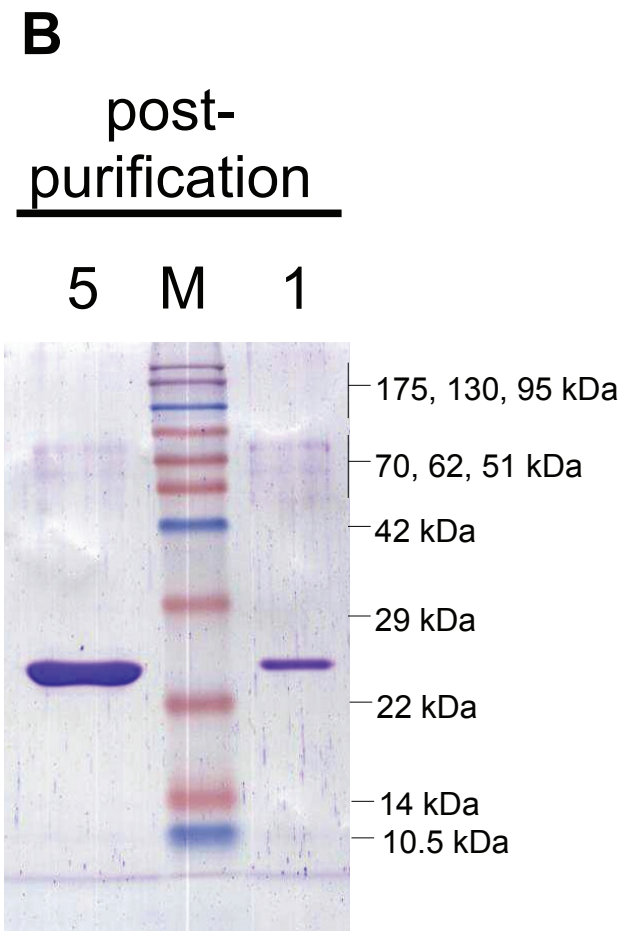

Figure 3.1 (page 2 of 3)

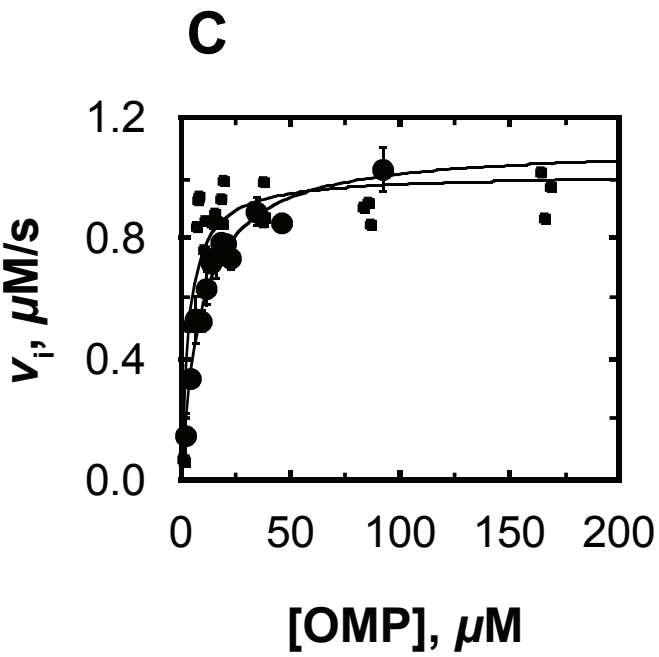

Figure 3.1 (page 3 of 3)

significant change in catalytic activity. It was my aim to use the ODCase-variant that best represented the wild type, and so in light of the similar catalytic activity, and greater sequence authenticity afforded by removal of the N-terminal tag, I opted to use CpODCase$_{-tag}$ for all further investigations. Hereafter, the delimiting subscript is dropped, and CpODCase$_{-tag}$ is referred to as CpODCase.

3.3 The Effect of pH on the Kinetic Parameters of CpODCase

To minimise random error in my kinetic assays of CpODCase-mediated decarboxylation of OMP, I determined the pH that afforded maximal CpODCase-activity. The resulting activity profiles (Figure 3.3) and kinetic constants (Table 3.1) revealed that maximal activity of CpODCase is observed at pH 8.0.

In order to characterise the pH-dependence of CpODCase-activity, I fit the data plotted in Figure 3.3 with eqn. 2.1 and 2.2, and obtained the ionisation constants listed in Table 3.2. The lower pK values (5.4 and 8.0 for ES and E + S, respectively) may arise from the ionisation of the substrate phosphoryl group, or one of the active-site aspartic acid residues at positions 14, 63, and 68. The higher pK values (10.0 and 9.4 for ES and E + S, respectively) may correspond to one of the active site lysine residues at positions 39 and 65. Loss of activity at alkaline pH could also be due, in part, to increased product-inhibition — a consequence of increased affinity for UMP (Smiley & Saleh, 1999).

Figure 3.2 Primary Structure of CpODCase$_{+tag}$

CpODCase$_{+tag}$ is a recombinant enzyme composed of: the WT CpODCase sequence (from M to the C-terminus), a Ni^{2+}-chelating hexahistidine sequence (in **bold**), and an intervening thrombin cleavage site (outlined; scissile bond labelled with a 'v'). Digestion with thrombin generates CpODCase$_{-tag}$, which differs from the WT sequence by three N-terminal residues in the order: glycine, serine, and histidine (in *italics*).

N **–** MGSS**HHHHHH**SSGLVPR*GS**H***MNDPKVVVALDFDRKQDALSFV

DKIQPTDARLKVGKEMFTYFGPEFVKQLTGKGFDVFLDLKFH

DIPNTVAKAVTAAADLGVWMVNVHASGGSQMMTKAKQALDNY

GNDAPLLIAVTVLTSMGQEDLHGLGINKTPAEQVNFLANLTK

QSGLDGVVCSAWEAEQLKADLGKEFKLITPGIRPAGSAQDDQ

QRIMTPKQAIDVGVDYLVIGRPITKAVDPQLVLQQINGTIR **–** ***C***

Figure 3.2

Figure 3.3 pH Profiles of CpODCase-Activity

pH profiles were constructed from apparent logk_{cat} (Panel A) and log(k_{cat}/K_m) (Panel B) values obtained from assays of CpODCase activity as a function of pH. The buffers used in these assays were : PIPES (pH 6.5–7.5, ○), HEPES (pH 7.5–8.5, ◆), TAPS (pH 8.5–9.0, □), CHES (pH 9.0–9.5, ▼) and CAPS (pH 10.0–11.0, ◊). The log of the values listed in Table 3.1 were potted as a function of pH, and fit with eqn. 2.2 (Panel A) or 2.1 (Panel B) by non-linear regression analysis, using *KaleidaGraph* v.3.5 (Synergy Software, Reading, PA). The acid-dissociation constants corresponding to ES (Panel A), or E + S (Panel B), are listed in Table 3.2. The experimental procedure is described in detail in § 5.2.17 and 5.2.18.

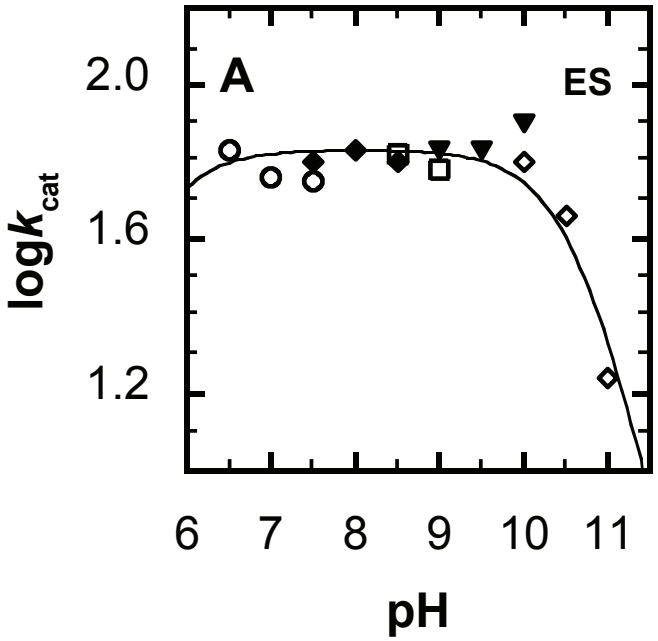
A
ES
2.0
1.6
1.2
logk_{cat}
6
7
8
9
10
11
pH

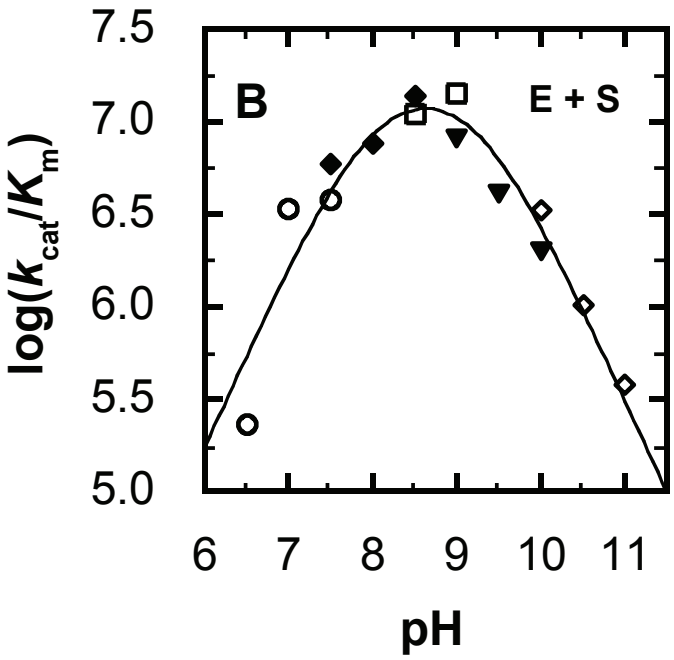
B
E + S
7.5
7.0
6.5
6.0
5.5
5.0
log(k_{cat}/K_m)
6
7
8
9
10
11
pH

Figure 3.3

Table 3.1

Apparent Kinetic and Equilibrium Constants for CpODCase-Mediated Decarboxyation of OMP as a Function of pH

buffer and pH	CpODCase		
	k_{cat}, s^{-1}	K_m, μM	k_{cat}/K_m, $M^{-1} \cdot s^{-1}$
PIPES			
6.5	68 ± 30	290 ± 220	0.23 ± 0.20
7.0	58.1 ± 2.9	17.1 ± 2.4	3.38 ± 0.47
7.5	56.2 ± 2.6	14.8 ± 1.9	3.79 ± 0.53
HEPES			
7.5	62.4 ± 3.1	10.5 ± 1.7	5.9 ± 1.0
8.0	68.0 ± 2.8	9.04 ± 1.1	7.5 ± 1.0
8.5	63.7 ± 4.4	4.6 ± 1.5	13.8 ± 5.2
TAPS			
8.5	66.3 ± 6.9	5.9 ± 2.6	11.0 ± 5.8
9.0	60.3 ± 1.7	4.24 ± 0.61	14.2 ± 2.2
CHES			
9.0	67.8 ± 2.3	8.2 ± 1.1	8.2 ± 1.1
9.5	68.0 ± 6.9	16.8 ± 5.8	4.04 ± 1.5
10.0	79.9 ± 7.2	40.3 ± 8.3	1.98 ± 0.45
CAPS			
10.0	63.4 ± 2.3	18.9 ± 2.3	3.34 ± 0.46
10.5	46.1 ± 5.8	44 ± 13	1.03 ± 0.33
11.0	17.3 ± 2.6	45 ± 17	0.38 ± 0.15

Table 3.2

pK_a Values of Species Involved in CpODCase-Mediated Decarboxylation of OMP and Kinetic Constants at pH-Optima[a]

ES	
log $(k_{cat})^{max}$	1.831 ± 0.024[c]
$(k_{cat})^{max}$, s^{-1}	67.83 ± 0.89[c]
pK_{es1}[b]	5.40 ± 0.99
pK_{es2}[b]	10.661 ± 0.098
E + S	
log $(k_{cat}/K_m)^{max}$	7.23 ± 0.14[c]
$(k_{cat}/K_m)^{max}$, $\times 10^6$ $M^{-1}\cdot s^{-1}$	17.21 ± 0.35[c]
pK_{e+s1}[b]	7.98 ± 0.22
pK_{e+s2}[b]	9.26 ± 0.21

[a] Values and their associated errors are derived from non- linear regression analysis of Figure 3.3

[b] As defined in Scheme 2.1

[c] Corresponds to the optimum pH for CpODCase-activity

3.4 Consistency of Active-CpODCase in Kinetic Assays

To avoid confounding effects that might occur from changes in quaternary structure of CpODCase, all assays were conducted using similar concentrations of CpODCase (10–20 nM). Further, the rate of decarboxylation was determined to be directly proportional to the concentration of active enzyme, assuming a constant proportion of active enzyme, over the full range of temperatures (10–60 °C) and OMP-concentrations (1.5–150 μM) used (Figure 3.4).

3.5 Inhibition of CpODCase by UMP

To assess the impact of product inhibition on my velocity measurements, I determined the IC_{50}-value due to UMP-inhibition. Fitting the kinetic data in Figure 3.5 with eqn. 5.8 revealed that the IC_{50} is 150-fold greater than the K_m for OMP (506 ± 12 μM, as compared with 3.38 ± 0.73 μM) under similar conditions, indicating that product release is strongly favoured. The large Hill-coefficient, n (5.11 ± 0.96), for UMP-mediated inhibition, indicates that the active form of CpODCase has multiple UMP binding-sites. Note that the same result was observed for inhibition of PaODCase, presumably due to formation of homodimeric structures (Begley *et al.*, 2000; Houk *et al.*, 2001; Wu, Gillon, & Pai, 2002). These results indicate that both Pa-, and CpODCase are active as homodimers, or oligomers thereof.

Figure 3.4 Correlation Between CpODCase-Activity and Concentration
CpODCase-activity was assessed, at 10 °C (□ and ■) and 60 °C (●) in the presence of OMP (1.5 and 92 μM at 10 °C; 15 and 142 μM at 60 °C), over a range of enzyme concentrations (14.0, 28.1, 56.3, 112 nM at 10 °C; 3.52, 7.04, 14.09, and 28.1 nM at 60 °C) Initial-rate kinetic data were plotted as a function of enzyme concentration and fit by linear regression analysis using *KaleidaGraph* v.3.5 (Synergy Software, Reading, PA) to determine the goodness of fit. Error bars represent the first standard deviation from the mean of triplicate assays. At 10 °C and 60 °C, CpODCase-activity was observed to be linearly dependent on its concentration in the presence of all concentrations of OMP assessed. Detailed methods are described in § 5.2.17 and 5.2.21.

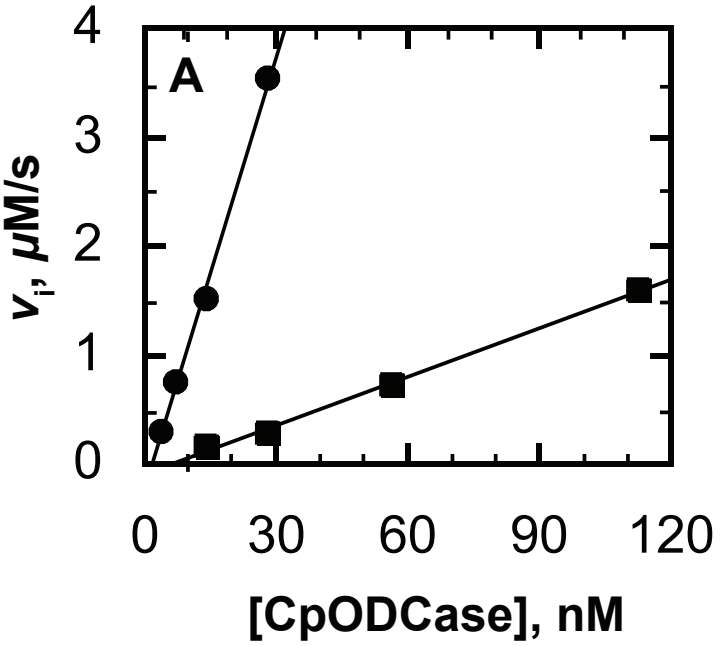
A
v_i, μM/s
0
1
2
3
4
0
30
60
90
120
[CpODCase], nM

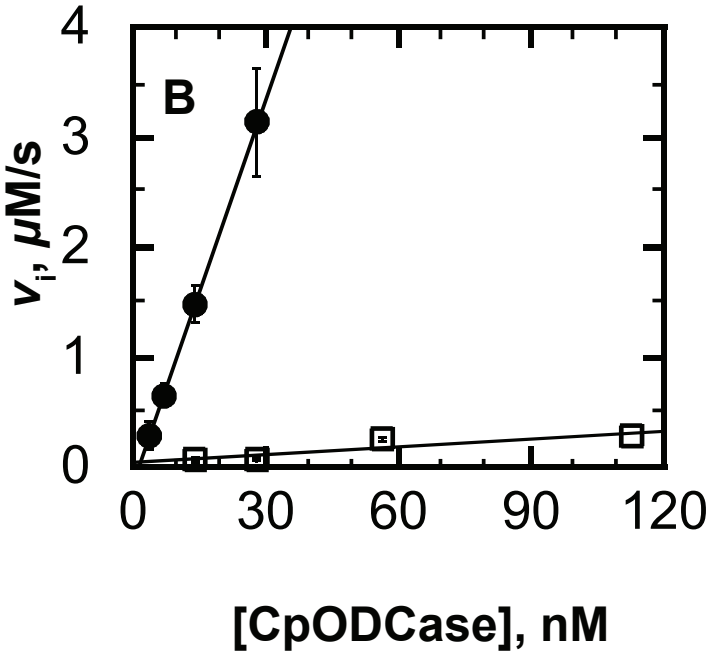
B
v_i, μM/s
0
1
2
3
4
0
30
60
90
120
[CpODCase], nM

Figure 3.4

Figure 3.5 Inhibition of CpODCase-Activity by UMP

Inhibition of CpODCase (29 nM) by UMP (185, 278, 371, 464, 510, and 557 μM), at 25 °C, is shown. In addition to CpODCase and UMP, reactions contained MOPS buffer (10 mM, pH 8.0) NaCl (100 mM) and OMP (28 μM). Assays containing greater than 557-μM UMP were impractical because their absorption exceeded the UV-vis detection-limit. Initial-rate kinetic data were plotted as a function of UMP concentration and fit to eqn. 5.8 by non-linear regression analysis using *KaleidaGraph* v.3.5 (Synergy Software, Reading, PA). Error bars represent the first standard deviation from the mean of triplicate assays. The IC_{50} value for UMP is 506 ± 12 μM, and the Hill-coefficient (n) is 5.11 ± 0.96. Detailed methods are described in § 5.2.17 and 5.2.19.

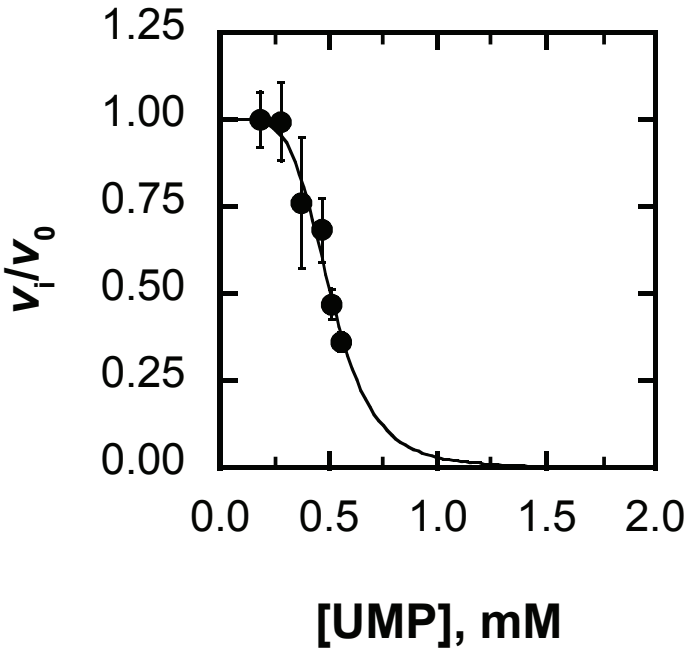

Figure 3.5

3.6 Thermal Stability of CpODCase

To better understand the thermal stability of psychrozymes in the context of their other characteristics, I conducted a series of assays to evaluate the thermal stability of CpODCase. By measuring the CD-spectra of CpODCase as a function of temperature (Figure 3.6, Panel A), I was able to construct the corresponding plot of molar ellipticity at 222 nm ($[\theta]_{222}$), displayed in Figure 3.6, Panel B. A non-linear regression fit of eqn. 5.3 to these data revealed that the T_m of CpODCase is 33.7 ± 1.0 °C.

3.7 Thermodynamic Parameters of CpODCase-Activity

Using a similar approach to the one described in § 2.6, I calculated the values of ΔH and ΔS, corresponding to the equilibrium constants K_m and K_{tx}, and the values of $\Delta H^{\ddagger}$ and $\Delta S^{\ddagger}$, corresponding to the kinetic constants k_{cat} and k_{cat}/K_m; Figure 3.7 displays the plots constructed by these methods. Using eqn 1.10, the corresponding values of ΔG were evaluated for catalytic turnover at 25 °C. These thermodynamic parameters are collected in Table 3.3.

Figure 3.7 reveals that TS-binding, as indicated by K_{tx}, and substrate-binding, as indicated by K_m, were both attenuated with increasing temperature (Panel A and B, respectively). However, the effect of this attenuation on the overall turnover is outweighed by the increased rate of product formation by the ES-complex. Ultimately, both k_{cat} and k_{cat}/K_m are exponentially augmented by increases in temperature (Panel C and D).

Figure 3.6 Temperature Profile of CpODCase α–Helical Character
The CD-spectra of CpODCase, as a function of temperature, are shown in Panel A. The ellipticity of each enzyme sample over the range 190–260 nm was corrected for concentration of enzyme (63 [●], 64 [○], 59 [■], 51 [□], 58 [◆], 49 [◊], 42 [▲] or 58 μM [Δ]) and pathlength of sample (0.1 cm), to give the molar ellipticity. Each trace is the average of six individual spectra recorded at 4 (●), 10 (○), 15 (■) 20 (□), 25 (◆), 30 (◊), 37 (▲) or 50 °C (Δ). The extent of α–helical character was estimated from the molar ellipticity at 222 nm ($[\theta]_{222}$), and used to define the melting point (T_m) of CpODCase. T_m is the temperature at which $[\theta]_{222}$ is the average of the $[\theta]_{222}$ of the folded and unfolded states ($[\theta]_f$, and $[\theta]_u$, respectively). $[\theta]_{222}$ is plotted as a function of temperature in Panel B. Error bars represent the first standard deviation from the mean of the molar ellipticities obtained from the six spectra. The data were fit to eqn. 5.3 by non-linear regression analysis using *KaleidaGraph* v.3.5 (Synergy Software, Reading, PA). The thus-calculated $[\theta]_{222}$ of the folded and unfolded states are -0.403 ± 0.013, and $-0.014 \pm 0.029 \times 10^3$ deg·cm^2·dmol^{-1}, respectively, and the T_m is 33.7 ± 1.0 °C. Detailed methods are described in § 5.2.16.

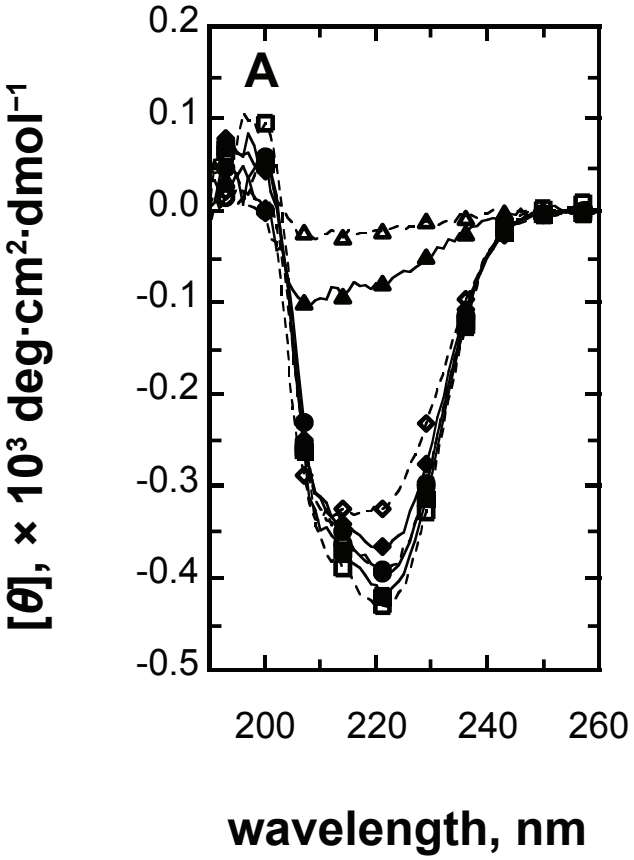
A
0.2
0.1
0.0
-0.1
-0.2
-0.3
-0.4
-0.5
200
220
240
260
wavelength, nm
[θ], × 10³ deg·cm²·dmol⁻¹

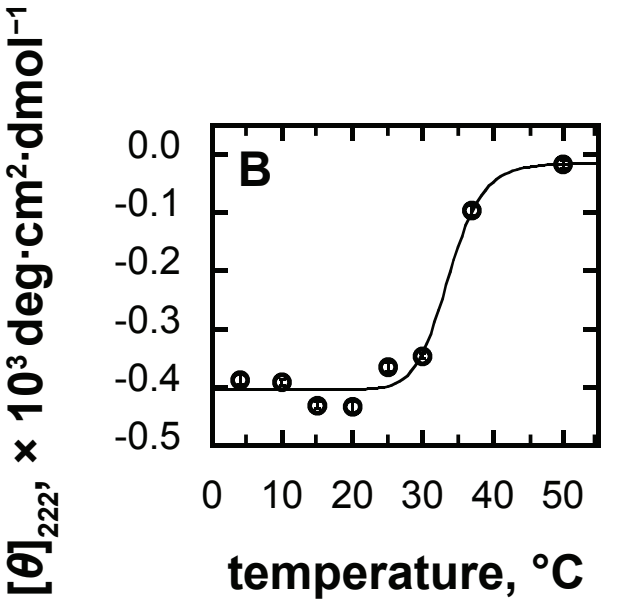
B
0.0
-0.1
-0.2
-0.3
-0.4
-0.5
0
10
20
30
40
50
temperature, °C
[θ]222, × 10³ deg·cm²·dmol⁻¹

Figure 3.6

Figure 3.7 van't Hoff and Eyring–Polanyi Plots of CpODCase-Activity
Comparison of the kinetic and equilibrium constants at varying temperature revealed the extent to which ΔH and ΔS, contributed to the overall energetics of the chemical transitions investigated herein. The activity of CpODCase was assayed as a function of OMP concentration at 10, 15, 20, 25, 30, 35, 40, 45, 50, 55, and 60 °C to derive K_m, k_{cat}, and k_{cat}/K_m at each of these temperatures. From these values, and with the known correlation between k_{non} and temperature (predicted by Radzicka & Wolfenden [1995] using the decarboxylation of 1–methylorotic acid as a model), K_{tx} was calculated using eqn. 1.4. Van't Hoff plots of $1/K_{tx}$ and K_m, as functions of temperature, are shown in Panels A and B, respectively. Eyring–Polanyi plots of k_{cat} and k_{cat}/K_m as functions of temperature, are shown in Panels C and D, respectively. Error bars represent the estimated error in the prediction of the kinetic and equilibrium constants from non-linear regression using eqn. 1.9. Each of the plots was fit to eqn. 1.11–1.14 (Panel A–D) by linear regression analysis using *KaleidaGraph* v.3.5 (Synergy Software, Reading, PA), to elucidate the ΔH and ΔS of the associated chemical transitions. The estimated values of ΔH and ΔS are listed in Table 3.3. Detailed methods are described in § 1.7.1, 5.2.17, and 5.2.20.

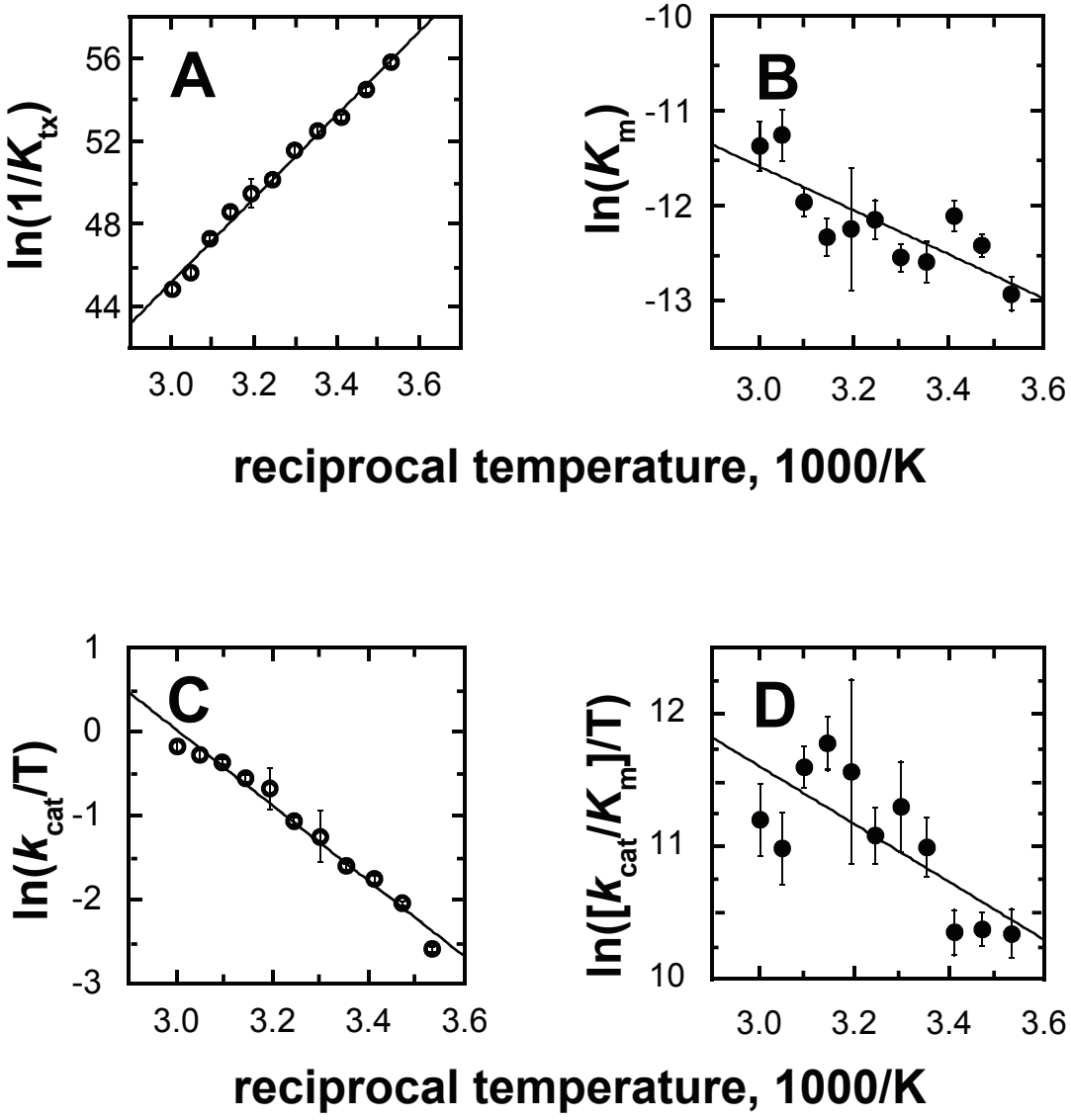
A
B
C
D
ln(1/K_tx)
ln(K_m)
ln(k_cat/T)
ln([k_cat/K_m]/T)
reciprocal temperature, 1000/K
reciprocal temperature, 1000/K

Figure 3.7

Table 3.3

Individual Contributions of Enthalpy and Entropy Changes to the Energetics of CpODCase-Catalysed Decarboxylation of OMP[a]

$E + \{S\}^{\ddagger} \rightleftharpoons \{ES\}^{\ddagger}$		
ΔG_{tx},[b] kcal/mol	ΔH_{tx}, kcal/mol	ΔS_{tx}, cal/mol·K
− 31.0 ± 1.7	− 40.1 ± 1.2	− 30.3 ± 4.0
$ES \rightleftharpoons E + S$		
ΔG_{m},[b] kcal/mol	ΔH_{m}, kcal/mol	ΔS_{m}, cal/mol·K
7.2 ± 1.5	4.5 ± 1.1	− 9.1 ± 3.5
$ES \rightarrow \{ES\}^{\ddagger}$		
$\Delta G_{es}^{\ddagger}$,[b] kcal/mol	$\Delta H_{es}^{\ddagger}$, kcal/mol	$\Delta S_{es}^{\ddagger}$, cal/mol·K
15.00 ± 0.52	8.93 ± 0.43	− 20.3 ± 1.0
$E + S \rightarrow \{ES\}^{\ddagger}$		
$\Delta G_{e+s}^{\ddagger}$,[b] kcal/mol	$\Delta H_{e+s}^{\ddagger}$, kcal/mol	$\Delta S_{e+s}^{\ddagger}$, cal/mol·K
7.6 ± 1.3	4.3 ± 1.2	− 11.1 ± 1.2

[a] As outlined in Scheme 1.1

[b] Calculated for 25 °C using eqn. 1.10

Chapter 4 RESULTS & DISCUSSION: COMPARATIVE ANALYSES OF ODCase VARIANTS

The previous two chapters described the characterisation of two variants of ODCase, one derived from the psychrotolerant bacterium *P. arcticus* 274–3, and one from the psychrophilic bacterium *C.* psych*rerythraea* 34H. This chapter compares my characterisation of Pa- and CpODCase to the characterisations of ODCase-variants derived from mesophiles or thermophiles in the literature (*i.e.*, the mesozymes Sc-, Ec-, and *Homo sapiens sapiens* [Hs]ODCase, and the thermozyme MtODCase). In this broader comparison of ODCase-variants, trends begin to emerge that indicate how ODCases are adapted to low- or high-temperature environments.

4.1 Comparing the Kinetics of ODCase-Variants

The ODCase-variants considered in the discussion that follows are derived from the organisms listed in Table 4.1. Also included in Table 4.1 are the kinetic constants (apparent turnover number, k_{cat}, and the apparent equilibrium constant, K_m) and the thermal stability (indicated by T_m) of the relevant ODCase-variants, and the optimal growth temperature of their parent organisms (T_{opt}). These data are relevant to a theory presented by D'Amico *et al.*, (2003) (see § 1.8.2.2) that proposes a distinct folding-funnel morphology for enzymes from psychrophiles (*i.e.*, psychrozymes) and enzymes from thermophiles (*i.e.*, thermozymes). In particular D'Amico and coworkers (2003) describe the folding funnel of psychrozymes as being energetically

Table 4.1
Correlation between kinetic and equilibrium parameters, thermal stability, and organism growth temperature for selected ODCase variants.

organism	Accession #	k_{cat}, 1/s	K_m, mM	enzyme T_m, °C	organism T_{opt}, °C
Saccharomyces cerevisiae	P03962[a]	15[g]	0.0016[g]	42[l]	~37
Colwellia psychrerythraea 34H	Q482F9.1[b]	60[h]	0.0034[a]	34[h]	8[b]
Psychrobacter arcticus 273-4	Q4FRL9.1[c]	37[h]	0.020[h]	26[h]	22[n]
Escherichia coli	P08244[d]	28[i]	0.001[i]	–	~37
Methanobacterium thermoautotrophicum ΔH	O26232[e]	4.7[j]	0.0015[j]	>65[j]	65[o]
Homo sapiens sapiens	P11172.1[f]	8.1[k]	0.0017[k]	37-55[m]	37

The original sources of these ODCase variants are found within the following references: [a](Rose, Grisafi, & Botstein, 1984), [b](Methé et al., 2005), [c](Ayala-del-Río et al., 2010), [d](Turnbough, Kerr, Funderburg, Donahue, & Powell, 1987), [e](Smith et al., 1997), and [f](Suttle, Bugg, Winkler, & Kanalas, 1988)
Kinetic parameters were determined at 25 °C herein[h], or by the authors of the following references: [g](Barnett, Amyes, Wood, Gerlt, & Richard, 2008), [i](Harris, Navarro Poulsen, Jensen, & Larsen, 2000), [j](Toth et al., 2009), or [k](Poduch, Wei, Pai, & Kotra, 2008)
Thermal stabilities were assessed herein[h], or by the authors of the following references: [l](Miller, Smiley, Short, & Wolfenden, 1999), [j](Toth et al., 2009), or [m](Brown, Fox, & O'Sullivan, 1975)
Optimal growth conditions were determined by the authors of the following references: [b](Methé et al., 2005), [n](Bakermans et al., 2006), or [o](Zeikus & Wolfe, 1972)

shallow, broad, and flat, while the folding funnel of thermozymes is described as deep, narrow and jagged (see Figure 1.3). The shallow folding funnel of psychrozymes raises the energy of the ES-complex, and effectively lowers the activation barrier, increasing the apparent turnover number, k_{cat} (D'Amico *et al*., 2003). However, the broad and flat bottom of the psychrozyme folding funnel also confers flexibility, which reduces the affinity of E for S, and the stability of the ES-complex, resulting in greater values of the apparent dissociation constant, K_m (D'Amico *et al*., 2003). Finally, the shallow folding-funnel is inherently energetically closer to the unfolded state, and thus psychrozymes are predicted to have lower values of T_m (D'Amico *et al*., 2003). The converse arguments can all be made for thermozymes as well. Ultimately, there is an anticipated correlation between lower values of T_m and larger values of k_{cat} and K_m or *vice versa*.

Indeed, as Table 4.1 shows, the kinetic constants, and the T_m- and T_{opt}-values for Pa- and CpODCase are consistent with the hypothesis that enzymes derived from organisms with a lower T_{opt} typically have higher k_{cat} and K_m values at 25 °C, and lower T_m values, as compared to enzymes derived from mesophiles. This observation was predicted by the theory and observations discussed in § 1.8.2.2, and originally described elsewhere (D'Amico *et al*., 2003; Georlette *et al*., 2004; Hammes *et al*., 2011). The converse is observed for MtODCase, excepting the reported K_m value, reiterating the correlation between overall thermal stability, substrate affinity, and turnover number, observed previously (D'Amico *et al*., 2003). However, it is interesting to note that, although the CpODCase T_m lies between those of ScODCase

and PaODCase, CpODCase has the greatest k_{cat}, indicating that the magnitude of k_{cat} may be an inaccurate predictor of relative thermal stability. As a whole, these data reveal a general trend towards higher values of k_{cat} and K_m for ODCase-variants with a lower T_m, and *vice versa*, but there are no rigorously-defined rules to interrelate these values.

4.2 Thermodynamics

4.2.1 Analysis of Previously Determined Data for Sc-, Ec-, and MtODCase

To gain a greater understanding of the thermodynamic strategies used by Pa- and CpODCase, I examined them in the context of other ODCase-variants. The following section includes an exploration of trends arising from the thermodynamic parameters corresponding to Pa-, Cp-, Sc-, Ec-, and MtODCase, as well as the thermodynamic parameters corresponding to the uncatalysed reaction.

Although the desired thermodynamic parameters for the uncatalysed reaction were directly available from a report by Wolfenden (2003), some of the desired parameters for Sc-, Ec-, and MtODCase needed to be calculated from data collected by Toth *et al*. (2009). With these data, I was able to calculate the values of ΔH and ΔS corresponding to the equilibrium constants, K_m and K_{tx}, using the method of van't Hoff (Tellinghuisen, 2006), and the values of $\Delta H^{\ddagger}$ and $\Delta S^{\ddagger}$ corresponding to the kinetic constants, k_{cat} and k_{cat}/K_m, using the method of Eyring (1935) and Polanyi (Evans & Polanyi, 1935). The plots used in this determination are shown in Figure 4.1, 4.2, and 4.3, for Sc-, Mt-, and EcODCase, respectively.

Figure 4.1 van't Hoff and Eyring–Polanyi Plots of ScODCase-Activity.

Comparison of the kinetic and equilibrium constants, as a function of temperature, revealed the extent to which ΔH and ΔS contributed to the overall energetics of the chemical transitions investigated herein. The activity of ScODCase was assayed as a function of OMP concentration by Toth *et al*. (2009), at 5, 10, 15, 25, 35, 45, and 50 °C, to derive K_m, k_{cat}, and k_{cat}/K_m at each of these temperatures. From these values, and with the known correlation between k_{non} and temperature (predicted by Radzicka & Wolfenden [1995] using the decarboxylation of 1–methylorotic acid as a model), I calculated K_{tx} using eqn. 1.4. Van't Hoff plots of $1/K_{tx}$ and K_m, as functions of temperature, are shown in Panels A and B, respectively. Eyring–Polanyi plots of k_{cat} and k_{cat}/K_m as functions of temperature, are shown in Panels C and D, respectively. Error bars represent the estimated error in the prediction of the kinetic and equilibrium constants obtained previously (Toth *et al*., 2009). Each of the plots was fit to eqn. 1.11–1.14 (Panel A–D) by linear regression analysis using *KaleidaGraph* v.3.5 (Synergy Software, Reading, PA), to elucidate the ΔH and ΔS of the associated chemical transitions. The predicted contributions of ΔH and ΔS are listed in Table 4.2. Detailed methods are described by Toth *et al*. (2009), and § 1.7.1, 5.2.17, and 5.2.20.

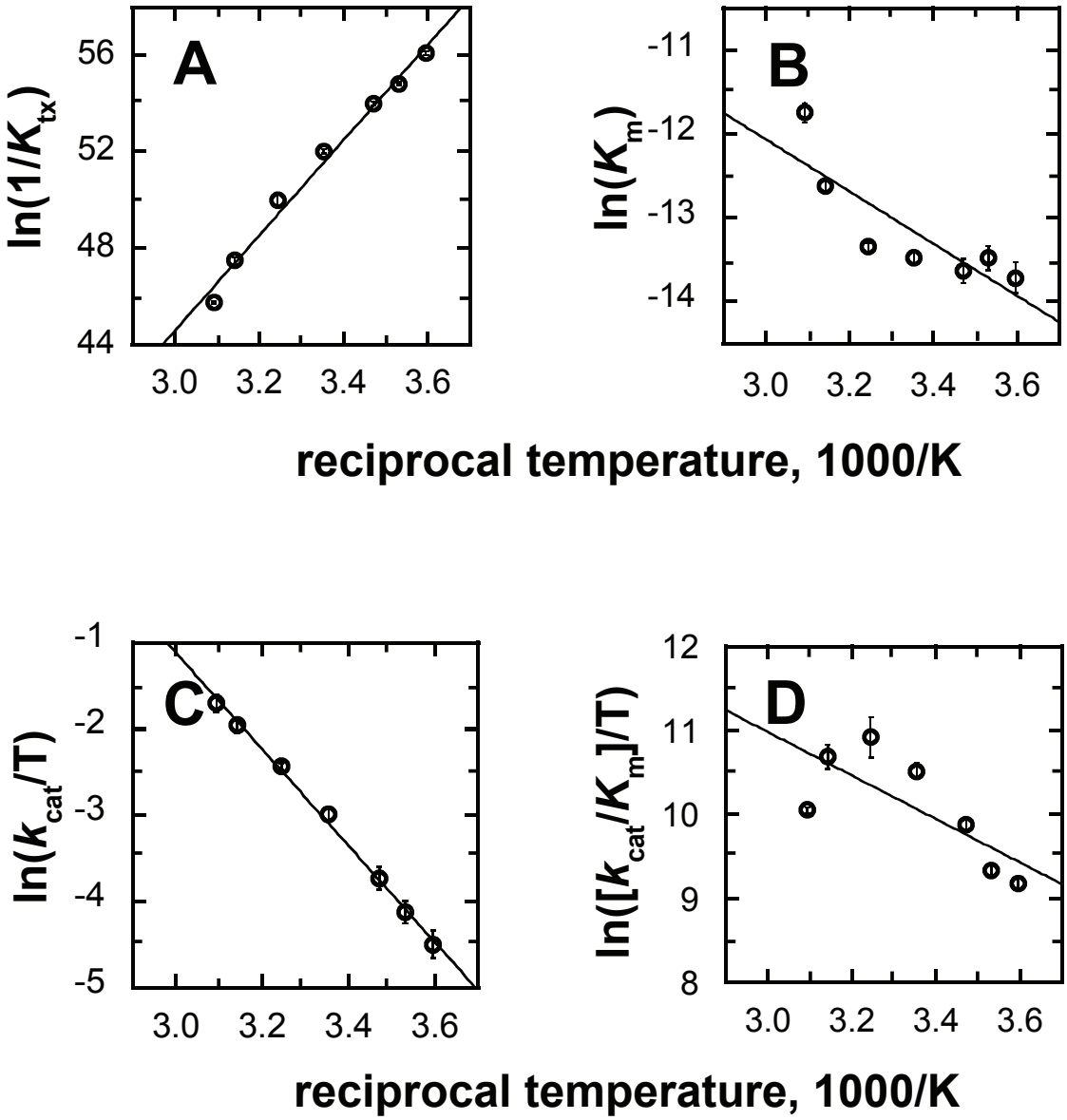
A
B
C
D
ln(1/K_tx)
ln(K_m)
ln(k_cat/T)
ln([k_cat/K_m]/T)
reciprocal temperature, 1000/K
reciprocal temperature, 1000/K

Figure 4.1

Table 4.2

Individual Contributions of Enthalpy and Entropy Changes to the Energetics of ScODCase-Catalysed Decarboxylation of OMP[a]

$E + \{S\}^{\ddagger} \rightleftharpoons \{ES\}^{\ddagger}$		
ΔG_{tx},[b] kcal/mol	ΔH_{tx}, kcal/mol	ΔS_{tx}, cal/mol·K
− 30.3 ± 2.6	− 39.2 ± 1.9	− 29.1 ± 6.6
$ES \rightleftharpoons E + S$		
ΔG_{m},[b] kcal/mol	ΔH_{m}, kcal/mol	ΔS_{m}, cal/mol·K
7.6 ± 2.3	6.1 ± 1.7	− 5.2 ± 5.7
$ES \rightarrow \{ES\}^{\ddagger}$		
$\Delta G_{es}^{\ddagger}$,[b] kcal/mol	$\Delta H_{es}^{\ddagger}$, kcal/mol	$\Delta S_{es}^{\ddagger}$, cal/mol·K
15.89 ± 0.31	11.08 ± 0.26	− 16.10 ± 0.47
$E + S \rightarrow \{ES\}^{\ddagger}$		
$\Delta G_{e+s}^{\ddagger}$,[b] kcal/mol	$\Delta H_{e+s}^{\ddagger}$, kcal/mol	$\Delta S_{e+s}^{\ddagger}$, cal/mol·K
8.0 ± 2.0	5.0 ± 2.0	− 9.9 ± 1.7

[a] As outlined in Scheme 1.1

[b] Calculated for 25 °C using eqn. 1.10

Figure 4.2 van't Hoff and Eyring–Polanyi Plots of MtODCase-Activity. Comparison of the kinetic and equilibrium constants, as a function of temperature, revealed the extent to which ΔH and ΔS contributed to the overall energetics of the chemical transitions investigated herein. The activity of ScODCase was assayed as a function of OMP concentration by Toth *et al*. (2009), at 5, 10, 15, 25, 35, 45, and 50 °C, to derive K_m, k_{cat}, and k_{cat}/K_m at each of these temperatures. From these values, and with the known correlation between k_{non} and temperature (predicted by Radzicka & Wolfenden [1995] using the decarboxylation of 1–methylorotic acid as a model), I calculated K_{tx} using eqn. 1.4. Van't Hoff plots of $1/K_{tx}$ and K_m, as functions of temperature, are shown in Panels A and B, respectively. Eyring–Polanyi plots of k_{cat} and k_{cat}/K_m as functions of temperature, are shown in Panels C and D, respectively. Error bars represent the estimated error in the prediction of the kinetic and equilibrium constants obtained previously (Toth *et al*., 2009). Each of the plots was fit to eqn. 1.11-1.14 (Panel A–D) by linear regression analysis using *KaleidaGraph* v.3.5 (Synergy Software, Reading, PA), to elucidate the ΔH and ΔS of the associated chemical transitions. The predicted contributions of ΔH and ΔS are listed in Table 4.2. Detailed methods are described by Toth *et al*. (2009), and § 1.7.1, 5.2.17, and 5.2.20.

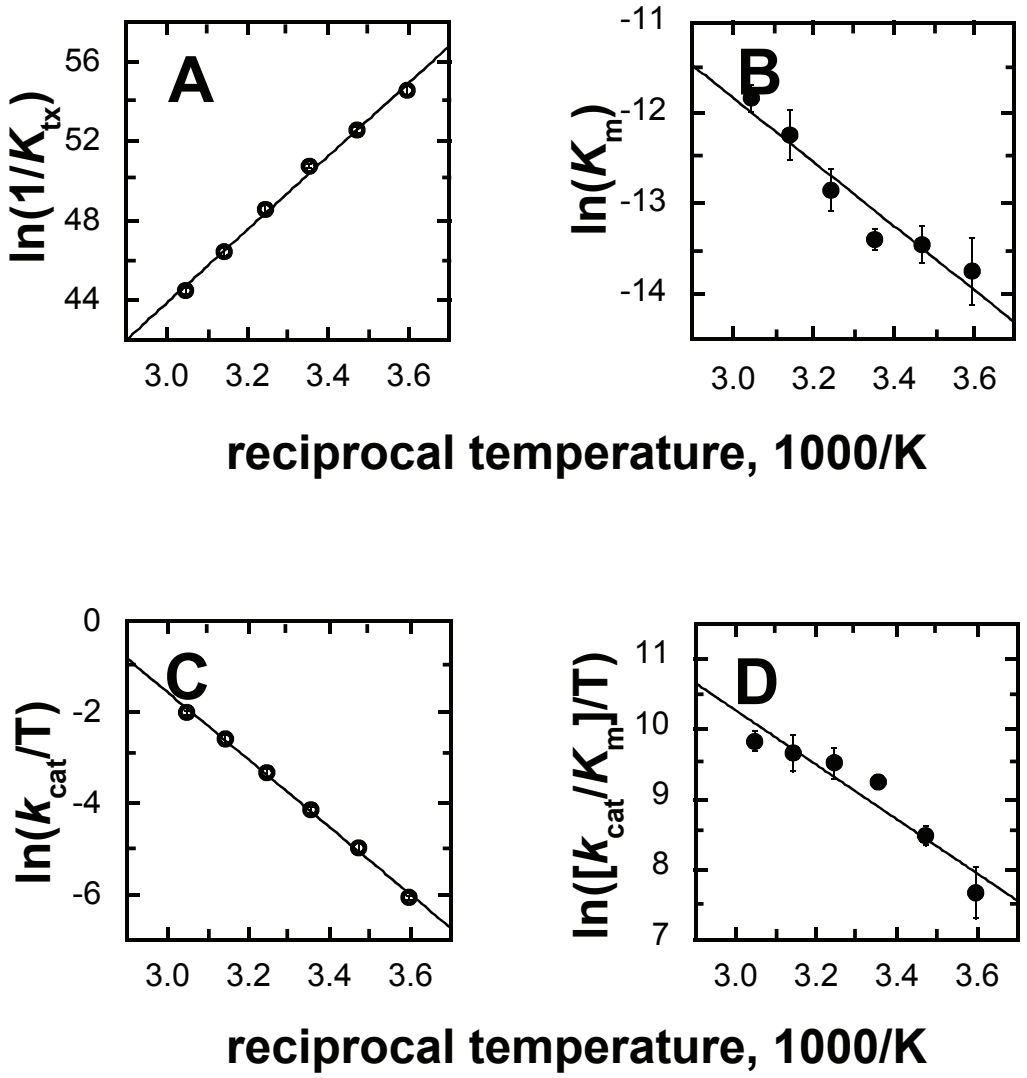
A
B
C
D
ln(1/K_tx)
ln(K_m)
ln(k_cat/T)
ln([k_cat/K_m]/T)
reciprocal temperature, 1000/K
reciprocal temperature, 1000/K

Figure 4.2

Table 4.3

Individual Contributions of Enthalpy and Entropy Changes to the Energetics of MtODCase-Catalysed Decarboxylation of OMP.[a]

$E + \{S\}^{\ddagger} \rightleftharpoons \{ES\}^{\ddagger}$		
ΔG_{tx},[b] kcal/mol	ΔH_{tx}, kcal/mol	ΔS_{tx}, cal/mol·K
− 29.8 ± 1.6	− 36.7 ± 1.1	− 23.1 ± 3.8
$ES \rightleftharpoons E + S$		
ΔG_{m},[b] kcal/mol	ΔH_{m}, kcal/mol	ΔS_{m}, cal/mol·K
7.7 ± 1.3	7.02 ± 0.93	− 2.1 ± 3.1
$ES \rightarrow \{ES\}^{\ddagger}$		
$\Delta G_{es}^{\ddagger}$,[b] kcal/mol	$\Delta H_{es}^{\ddagger}$, kcal/mol	$\Delta S_{es}^{\ddagger}$, cal/mol·K
16.53 ± 0.35	14.69 ± 0.35	− 6.16 ± 0.18
$E + S \rightarrow \{ES\}^{\ddagger}$		
$\Delta G_{e+s}^{\ddagger}$,[b] kcal/mol	$\Delta H_{e+s}^{\ddagger}$, kcal/mol	$\Delta S_{e+s}^{\ddagger}$, cal/mol·K
8.7 ± 1.2	7.6 ± 1.1	− 3.80 ± 0.33

[a] As outlined in Scheme 1.1

[b] Calculated for 25 °C using eqn. 1.10

Figure 4.3 Eyring–Polanyi Plot of EcODCase-Activity.
Correlation of the turnover number with assay temperature revealed the extent to which $\Delta H_{es}^{\ddagger}$ and $\Delta S_{es}^{\ddagger}$ contributed to the of promotion of ES to $\{ES\}^{\ddagger}$. The activity of EcODCase was assayed as a function of OMP concentration by Toth *et al*. (2009), at 5, 10, 15, 25, 35, and 45 °C, to derive k_{cat} at each of these temperatures. The Eyring–Polanyi plot of k_{cat} as a function of temperature, is shown below. Error bars represent the estimated error in the prediction of the turnover number obtained previously (Toth *et al*., 2009). This plot was fit to eqn. 1.13 by linear regression analysis using *KaleidaGraph* v.3.5 (Synergy Software, Reading, PA), to elucidate $\Delta H_{es}^{\ddagger}$, and $\Delta S_{es}^{\ddagger}$. The predicted contributions of $\Delta H_{es}^{\ddagger}$ and $\Delta S_{es}^{\ddagger}$ are listed in Table 4.3. Detailed methods are described by Toth *et al*. (2009), and § 1.7.1, 5.2.17, and 5.2.20.

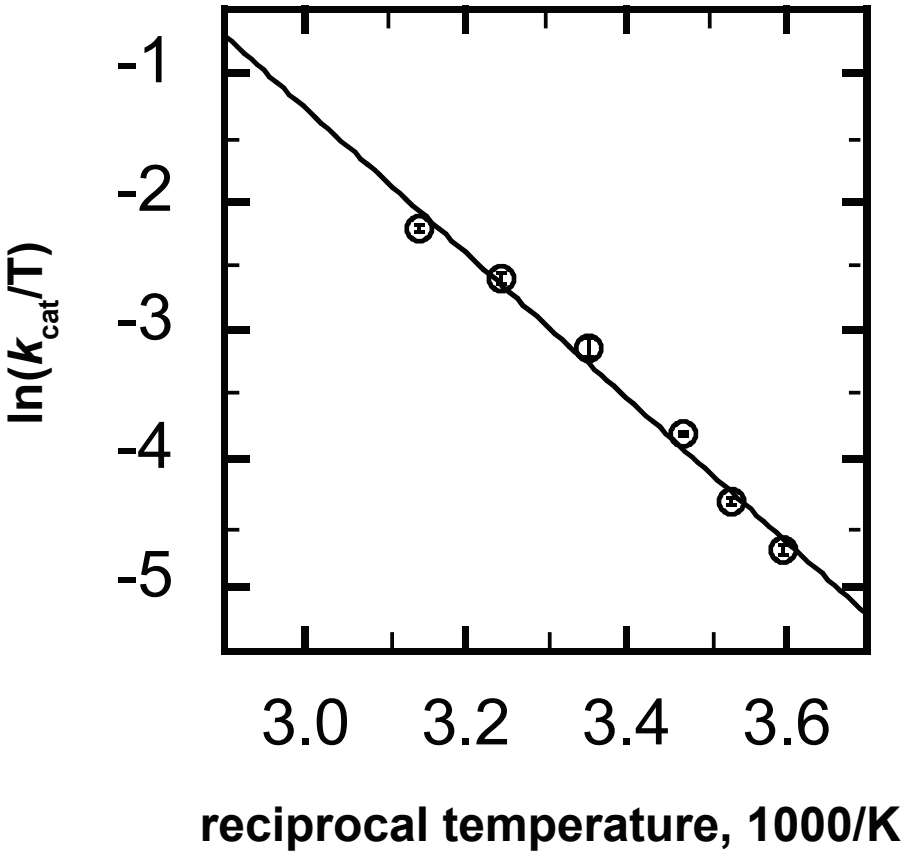

Figure 4.3

Table 4.4

Individual Contributions of Enthalpy and Entropy Changes to the Energetics of EcODCase-Catalysed Decarboxylation of OMP.[a]

ES → {ES}‡		
$\Delta G_{es}^{\ddagger}$,[b] kcal/mol	$\Delta H_{es}^{\ddagger}$, kcal/mol	$\Delta S_{es}^{\ddagger}$, cal/mol·K
15.99 ± 0.71	11.19 ± 0.62	− 16.1 ± 1.1

[a] As outlined in Scheme 1.1

[b] Calculated for 25 °C using eqn. 1.10

Table 4.5

Individual Contributions of Enthalpy and Entropy Changes to the Energetics of Uncatalysed Decarboxylation of OMP.[a,]

$E + S \rightarrow E + \{S\}^{\ddagger}$		
$\Delta G_{non}^{\ddagger}$,[b] kcal/mol	$\Delta H_{non}^{\ddagger}$, kcal/mol[c]	$\Delta S_{non}^{\ddagger}$, cal/mol·K[c]
38.67 ± 0.40	44.41 ± 0.28	19.36 ± 0.95

[a] As outlined in Scheme 1.1
[b] Calculated for 25 °C using eqn. 1.10
[c] Obtained from Radzicka & Wolfenden (1995)

Using eqn 1.10, the corresponding values of $\Delta G_{es}^{\ddagger}$ and $\Delta G_{e+s}^{\ddagger}$ were evaluated for catalytic reactions at 25 °C. These thermodynamic parameters are collected in Table 4.2, 4.3, and 4.4, respectively. Further, the corresponding thermodynamic parameters for the uncatalysed reaction are collected in Table 4.5. With these parameters, the thermodynamic strategies of ODCase-variants may be analysed within a broader context, and thus understood with greater depth.

4.2.2 Consequences of the H– and S–Correlations Identified from Thermodynamic Analyses of Pa-, Cp-, Sc-, and MtODCase-Mediated Catalysis

4.2.2.1 Consequences for the Topology of Folding Funnels

A comparison of the values of ΔH and ΔS corresponding to each transition depicted in Scheme 1.1 is shown in Figure 4.4. These data are relevant to the thermodynamic implications of the folding funnels discussed in the introduction (see § 1.8.2.2) and originally described by D'Amico and coworkers (2003). According to D'Amico *et al*., psychrozymes have a folding funnel that is energetically shallow, broad, and flat, while the folding funnel of thermozymes is described as deep, narrow, and jagged. The aforementioned characteristics of the psychrozyme folding funnel are proposed to reduce the enthalpy of activation of the ES-complex, $\Delta H_{es}^{\ddagger}$, but also afford the ES-complex more conformational freedom that must be lost to form the TS, thus making the entropy change upon activation, $\Delta S_{es}^{\ddagger}$, more negative as well (D'Amico *et al*., 2003). Similarly, increased flexibility would be expected to

Figure 4.4 ΔH–ΔS Correlations, Revealed by a Survey of the Thermodynamic Parameters Associated with Mt-, Sc-, Ec-, Cp-, and PaODCase-Mediated Catalysis.

A survey of the thermodynamic parameters associated with Mt-, Sc-, Ec-, Cp-, and PaODCase-mediated catalysis, revealed the extent to which ΔH and ΔS (of the chemical transitions outlined in Scheme 1.1) correlated with one another. This survey includes the two ODCase-variants characterised here (PaODCase [▼] and CpODCase [■]), as well as those characterised by Toth *et al*. (2009) (MtODCase [▲], ScODCase [●], and EcODCase [◆]). The ΔH-values collected in Table 2.3, 3.3, 4.2, 4.3, 4.4, and 4.5 were plotted as a function of the corresponding ΔS-values, to construct plots illustrating the correlation between these parameters during $\{S\}^{\ddagger}$-binding in the TS (Panel A), S-release in the GS (Panel B), and promotion of the ES-complex or free E + S to the TS, $\{ES\}^{\ddagger}$ (Panel C and D, respectively), and the latter most in comparison to the uncatalysed activation of S to $\{S\}^{\ddagger}$ ('+'; Panel E). Error bars represent the estimated error in the prediction of the thermodynamic parameters given in Table 2.3, 3.3, 4.2, 4.3, 4.4, and 4.5. Each of the plots was fit with a line-of-best-fit by linear regression analysis using *KaleidaGraph* v.3.5 (Synergy Software, Reading, PA), to illustrate the apparent linear nature of the ΔH–ΔS correlations. Detailed methods are described in § 1.7.1, 5.2.17, and 5.2.20.

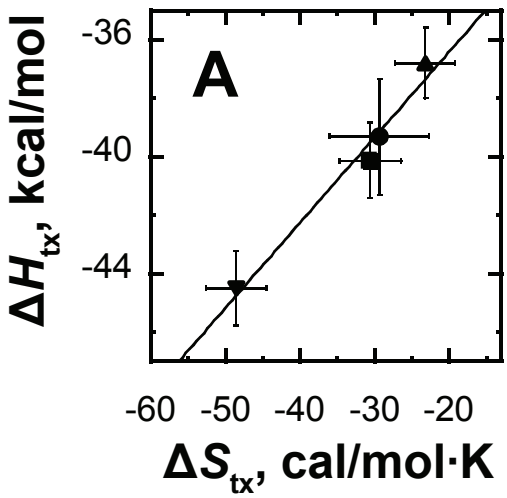

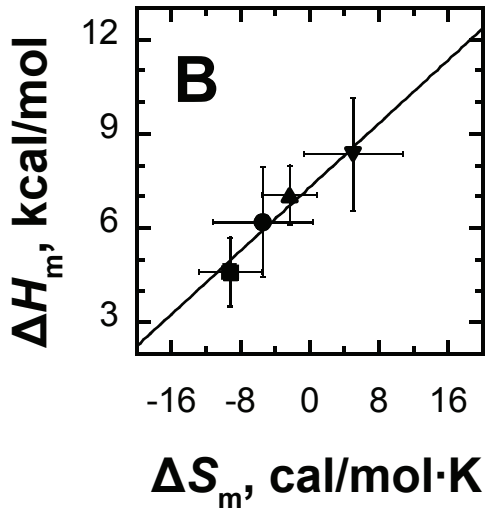

Figure 4.4 (page 1 of 2)

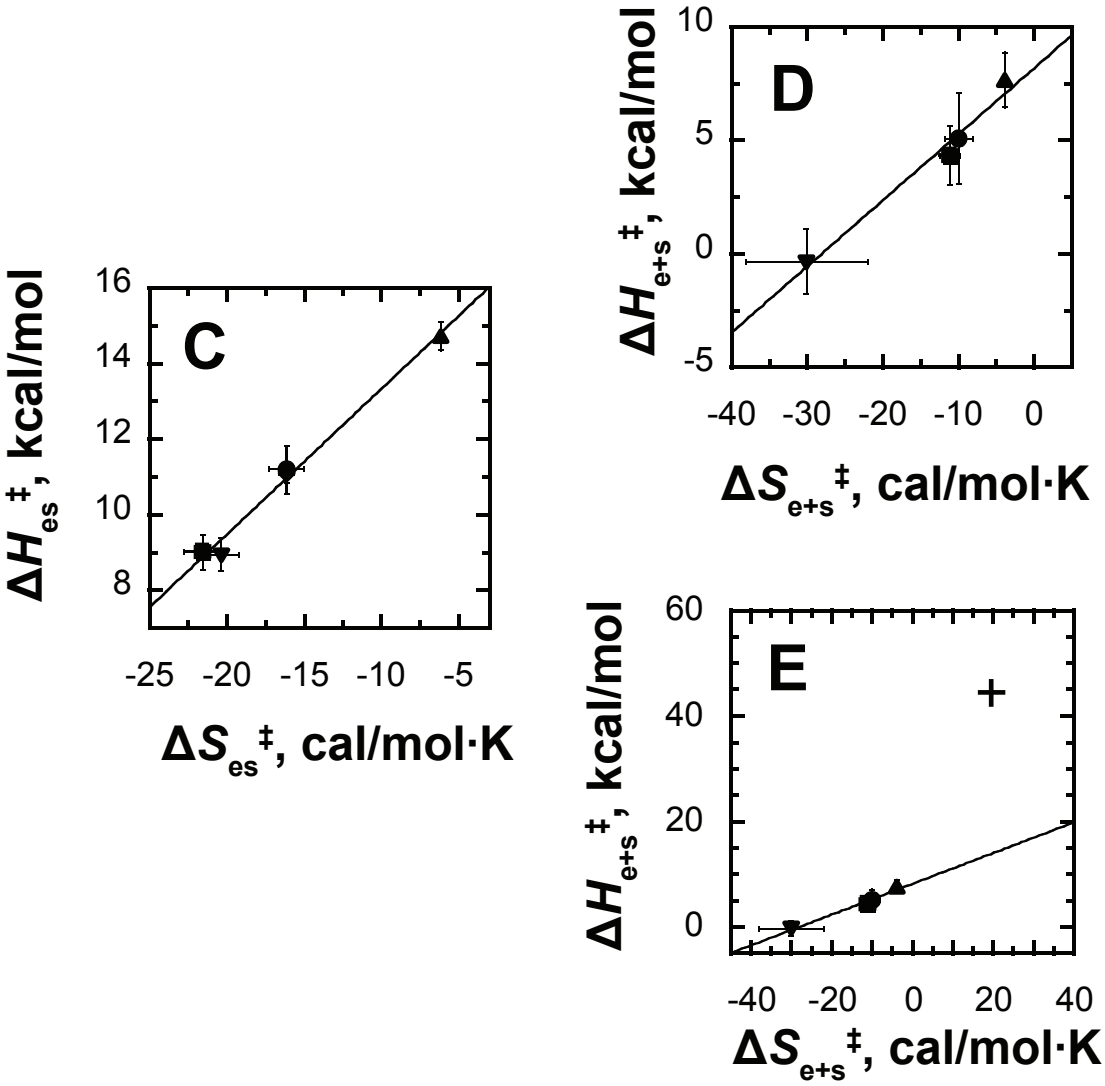

Figure 4.4 (page 2 of 2)

ultimately destabilise the GS-complex, and be reflected in less positive and/or more negative values of ΔH_m and ΔS_m (D'Amico *et al*., 2003). As before, the converse arguments can be made for each of the aforementioned thermodynamic parameters in the context of thermozymes. Summarily, enzymes with lower thermal stability, as reflected by lower values of T_m, are anticipated to have lower values of $\Delta H_{es}^{\ddagger}$, $\Delta S_{es}^{\ddagger}$, ΔH_m, and ΔS_m. Indeed, the plots in Figure 4.4 Panel B and C are consistent with the hypothesis that lower values of T_m correlate with reduced values of $\Delta H_{es}^{\ddagger}$, $\Delta S_{es}^{\ddagger}$, ΔH_m, and ΔS_m, and *vice versa*, excepting the values of ΔH_m and ΔS_m associated with PaODCase. Regardless, ODCase-variants with lower thermal stability, T_m, also have lower values of $\Delta H_{e+s}^{\ddagger}$ and $\Delta S_{e+s}^{\ddagger}$ (Figure 4.4, Panel D).

4.2.2.2 Consequences for Determination of the Importance of TS-Stabilisation

The previous subsection describes a theory, proposed by D'Amico *et al*. (2003), intended to account for the strategies that extremozymes use to effect catalysis, solely on the basis of folding-funnel topology. Such a theory only accounts for GS-effects, and assumes a relatively consistent TS-enthalpy and TS-entropy among the enzyme-variants; however, this assumption need not be valid. If a group of ODCase-variants have different TS-affinities (*i.e*., values of ΔG_{tx}), then TS-effects must be considered in a comparison of them. Indeed, a comparison of ΔG_{tx} values associated with Pa-, Cp-, Sc-, and MtODCase as the linear function of temperature described by eq. 1.10, reveals a distinct TS-stabilisation for each variant at all temperatures, excepting two intersection-points (Figure 4.5, Panel A). These

Figure 4.5 Variation of ΔG_{tx}, ΔG_{m}, $\Delta G_{es}^{\ddagger}$, and $\Delta G_{e+s}^{\ddagger}$, as a Function of Temperature for Mt-, Sc-, Cp-, and PaODCase-Mediated Catalysis

Evaluation of ΔG_{tx}, ΔG_{m}, $\Delta G_{es}^{\ddagger}$, and $\Delta G_{e+s}^{\ddagger}$, as a function of temperature, revealed both differences and commonalities among the thermodynamic strategies used the ODCase-variants examined below. This survey includes the two ODCase-variants characterised here (PaOODCase [▼] and CpODCase [■]), as well as those described by Toth *et al*. (2009) (MtODCase [▲], and ScODCase [●]). ΔG_{tx}, ΔG_{m}, $\Delta G_{es}^{\ddagger}$, and $\Delta G_{e+s}^{\ddagger}$, were calculated from K_{tx}, K_{m}, k_{cat}, and k_{cat}/K_{m}, using eqn. 1.5, 1.2, 1.3, and 1.7, respectively, and plotted as a function of temperature. Error bars represent the standard deviation from the mean. The plots were fit by linear regression analysis using *KaleidaGraph* v.3.5 (Synergy Software, Reading, PA), to illustrate the distinct strategies applied by each ODCase-variant to effect decarboxylation of OMP. Also included is the evaluation of $\Delta G_{non}^{\ddagger}$ as a function of temperature, as predicted by Radzicka & Wolfenden (1995) using the decarboxylation of 1–methylorotic acid as a model (—). Detailed methods are described in § 1.7.1, 5.2.17, and 5.2.20.

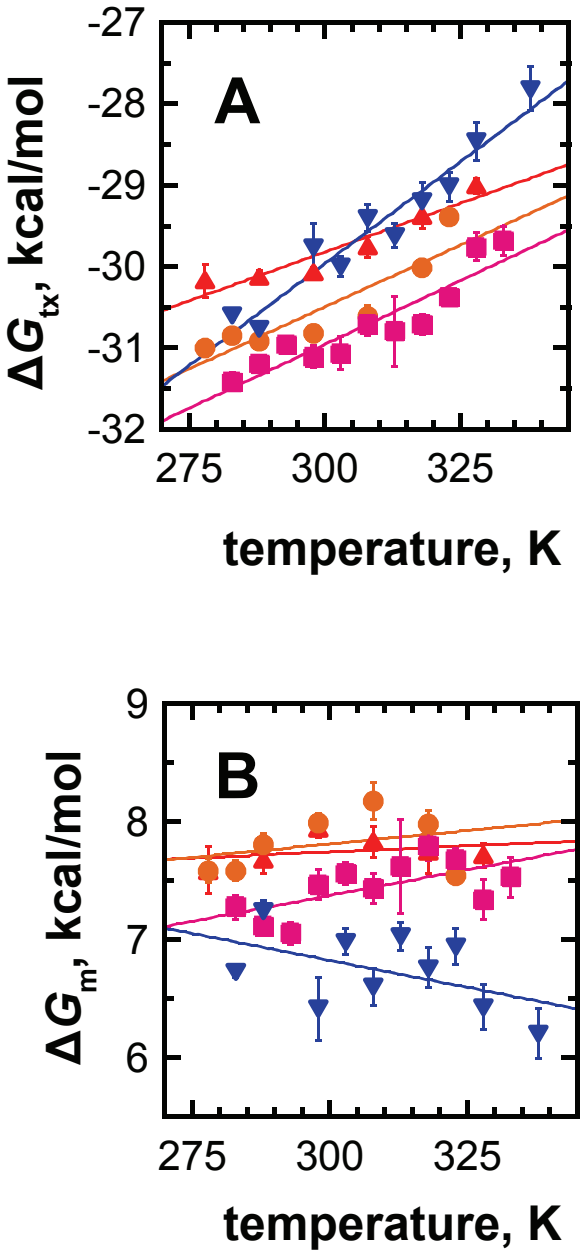

Figure 4.5 (page 1 of 2)

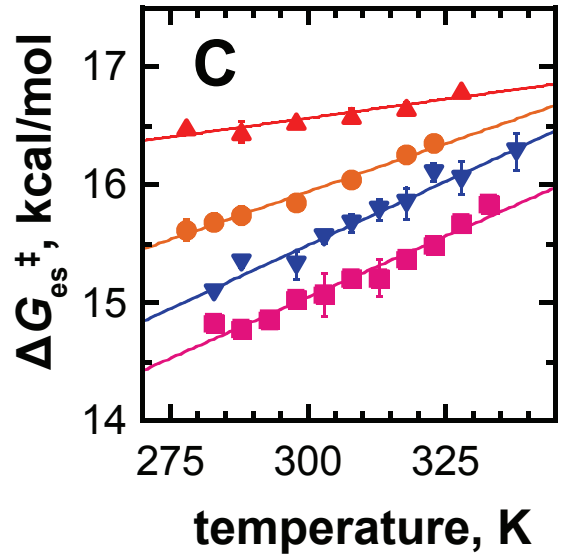

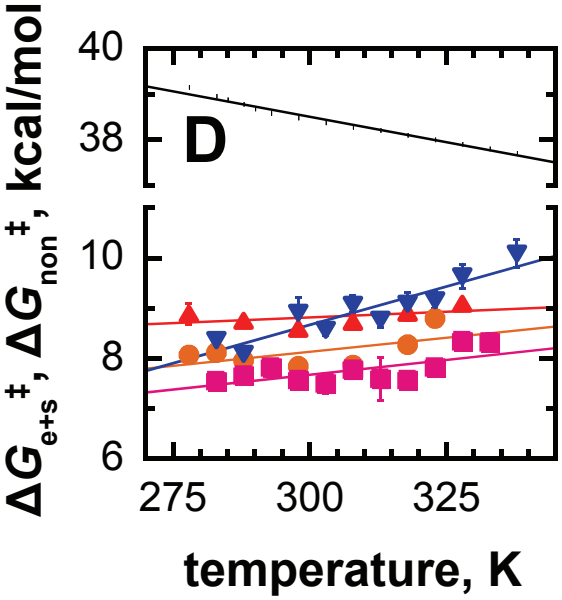

Figure 4.5 (page 2 of 2)

intersection-points represent an equivalence of ΔG_{tx} values; however, the ΔH_{tx} and ΔS_{tx} values, related to the intercepts and slopes described by eqn 1.10, indicate thermodynamically-distinct TS-complexes for each ODCase-variant, at all temperatures. Consequently, the catalytic strategies used by these ODCase-variants cannot be explained by GS-effects alone, and TS-effects must be considered.

$$\Delta G = \Delta H - T \cdot \Delta S \tag{1.10}$$

4.2.2.3 Consequences for Elucidation of the Catalytic Strategy Implemented by an ODCase-Variant

As asserted above, the roles of TS-stabilisation and GS-destabilisation must be examined together to explain the activity of ODCase-variants. Consequently a discussion of the plots of ΔG_m or ΔG_{tx}, as a function of temperature (Figure 4.5, Panel A or B, respectively) is indicated. Further, a discussion of stabilisation or destabilisation necessitates a consistent reference-point be defined: the reference points for the discussion that follows are the thermodynamic parameters associated with the mesozyme, ScODCase, which are listed in Table 4.2, and plotted in Figure 4.4 and 4.5.

The psychrozymes, PaODCase and CpODCase, appeared to use distinct strategies to effect catalysis at low-temperatures. PaODCase effected GS-destabilisation (*i.e.*, making ΔG_m less positive) largely through entropy effects, as

could be seen from the sharply negative slope in Figure 4.5, Panel B, that indicates a relatively large increase in entropy upon substrate release (*i.e.*, a relatively large positive value of ΔS_m). Despite having the largest intercept, which indicates a superlative increase in enthalpy upon substrate release (ΔH_m, Figure 4.4, Panel B), PaODCase retained a low value of ΔG_m, and a consequently high value of K_m, at all temperatures. By contrast, CpODCase effects GS-destabilisation through largely enthalpic effects. Although CpODCase was observed to have the most negative ΔS_m, as indicated by the large positive slope in Panel B of Figure 4.5, it was also observed to have the least positive ΔH_m (Figure 4.4, Panel B). This ultimately lead to values of ΔG_m and K_m that were similar to PaODCase at low temperatures, yet approached those of ScODCase and MtODCase at high temperatures. Furthermore, CpODCase appeared to effect stabilisation of the TS through enthalpy effects. Despite having a slope similar to ScODCase in Panel A, indicating a similar ΔS_{tx}, the strongly negative value of ΔH_{tx} ultimately lead to lower values of ΔG_{tx} at all temperatures examined. Similarly, PaODCase displayed a strongly negative ΔH_{tx} and ΔS_{tx} that ultimately lead to values of ΔG_{tx} which are larger than even MtODCase at high temperatures, yet approach ScODCase at low temperatures. Summarily, PaODCase can be said to operate primarily through entropy-driven GS-destabilisation, akin to that described by D'Amico *et al.* (2003), and CpODCase, primarily through enthalpy-driven TS-stabilisation, akin to that described by Wolfenden (2003).

The thermozyme, MtODCase, was observed to have values of ΔH_m, ΔS_m, ΔG_m, and ΔS_{tx} similar to those of ScODCase, yet greater values of ΔH_{tx} and ΔG_{tx}.

Consequently, MtODCase can be said to sacrifice enthalpy of TS-stabilisation. This may be due to a lack of selective pressure to reduce the enthalpy of activation—as might be expected for a population of organisms with ample ambient thermal energy. Alternatively, it could be an indirect cost of increased thermal stability. Regardless, the thermodynamic strategy of MtODCase does not appear to afford greater rate-acceleration, efficiency, or proficiency than its meso- or psychrozyme counterparts, at any of the temperatures assessed by Toth *et al*., (2009).

4.2.2.4 Consequences for Predicting Tolerance to Low Substrate-Availability

The impacts of GS-destabilisation and TS-stabilisation are combined in the mechanisms of Pa- and CpODCase in order to adapt these enzymes to the low-temperatures at which they must operate. The relative importance of these two strategies to the mechanism of an ODCase variant is indicative of the amount of substrate that each enzyme has been optimised to operate on. As described in the introduction (see § 1.7.1), when an ODCase-variant is operating under the regime where [S] >> K_m, it accelerates decarboxylation of OMP primarily by increasing k_{cat} (*i.e*., by reducing $\Delta G_{es}^{\ddagger}$). This may be achieved in two ways, which can be summarised in the context of eqn 1.15–1.17, or the rearrangements of them given by eqn. 4.1–4.3. Because $\Delta G_{non}^{\ddagger}$ is immutable, catalysis must be effected by raising the 'bottom' of $\Delta G_{es}^{\ddagger}$, by making ΔG_m less positive (*i.e*., GS-destabilisation, such as the catalytic strategies described by D'Amico *et al*. [2003]), or by lowering the 'top' of $\Delta G_{es}^{\ddagger}$ by making ΔG_{tx} more negative (*i.e*., TS-stabilisation, as described by

Wolfenden [2003]). However, if substrate becomes less plentiful and [S] << K_m, then decarboxylation is accelerated primarily by increasing k_{cat}/K_m (*i.e.*, by reducing $\Delta G_{e+s}^{\ddagger}$). This, too, can be effected in two ways, one of which is lowering the 'top' of $\Delta G_{e+s}^{\ddagger}$ by reducing ΔG_{tx} (i.*e.*, TS-stabilisation, as described by Wolfenden [2003]). This catalytic strategy is exactly analogous to the barrier-lowering strategy used when substrate is abundant. However, the other strategy is to lower the 'top' of $\Delta G_{e+s}^{\ddagger}$, by making ΔG_m more positive and making ΔG_{tx} correspondingly more negative (*i.e.*, equal GS- and TS-stabilisation)—a strategy that leaves $\Delta G_{es}^{\ddagger}$ unchanged.

$$\Delta G_{es}^{\ddagger} = \Delta G_{tx} + \Delta G_{non}^{\ddagger} + \Delta G_m \tag{4.1}$$

$$\Delta H_{es}^{\ddagger} = \Delta H_{tx} + \Delta H_{non}^{\ddagger} + \Delta H_m \tag{4.2}$$

$$\Delta S_{es}^{\ddagger} = \Delta S_{tx} + \Delta S_{non}^{\ddagger} + \Delta S_m \tag{4.3}$$

Consistent with the anticipated observations for an enzyme optimised to operate with ample substrate, described above, PaODCase was revealed to have a moderate value of $\Delta G_{e+s}^{\ddagger}$ and ΔG_{tx}, and a small positive value of ΔG_m at low temperatures. Furthermore, these parameters diverged considerably with increasing temperature, making the distinctions between PaODCase and the other variant even more pronounced. By contrast, PaODCase maintained the second-lowest value of $\Delta G_{es}^{\ddagger}$ over the full range of temperatures. Collectively, these parameters indicated that

PaODCase is an enzyme that has improved catalytic activity over its meso- and thermozyme counterparts, in the presence of ample substrate. However, as substrate pools diminish, PaODCase is anticipated to fall behind the other ODCase-variants, especially at higher temperatures.

4.2.3 Predictions and Trends Arising from Thermodynamic Parameters of ODCase-Variants

Returning to Table 4.1—now in the context of Figure 4.4 and 4.5, Panel A and C—the following maxims may be proposed: psychrozyme-variants of ODCase are characterised by lower *(i.e.*, less positive or more negative) values of T_m, ΔH_{tx}, ΔS_{tx}, ΔG_m, $\Delta H_{es}^{\ddagger}$, $\Delta S_{es}^{\ddagger}$, and $\Delta G_{es}^{\ddagger}$, and higher (*i.e.*, more positive or less negative) values of k_{cat} and K_m at low temperatures; and thermozyme-variants of ODCase are characterised by higher values of T_m, ΔH_{tx}, ΔS_{tx}, $\Delta H_{es}^{\ddagger}$, $\Delta S_{es}^{\ddagger}$, and $\Delta G_{es}^{\ddagger}$, and lower values of k_{cat} at high temperatures. These maxims are consistent with prior investigations discussed above (see § 1.8.2.2) and originally described elsewhere (D'Amico *et al.*, 2003; Georlette *et al.*, 2004; Hammes *et al.*, 2011).

From the correlations listed above, it may be possible to make predictions for other ODCase-variants, or perhaps other enzymes in general. Prediction of the reaction thermodynamics of a particular ODCase-variant, using its thermal stability, appears to be more reliable than a prediction afforded by the T_{opt} of its host organism. In principle, this means that a survey of thermal stability could rapidly and confidently identify enzymes of potential use in high- or low-temperature-catalyst

development (Gibbs *et al*., 2005). Although identification on the basis of T_{opt} alone is not indicated by these results, it may still contribute to selection of a survey sample (for example, by eliminating source organisms with a T_{opt} that exceeds the desired operating temperature, which arguably cannot possess enzymes that undergo thermal denaturation below their growth temperature).

4.2.3.1 Possible Sources of the Observed Correlation between Thermal Stability, and Catalytic Activity

The underlying cause of the observed correlation between thermal stability, and ΔH_{tx} and ΔS_{tx}, which is apparent from Figure 4.4, Panel A, and Table 4.1, is unclear. It is possible that the reduction of enthalpy of TS-formation requires a concomitant reduction in entropy of TS-formation, and that this directly translates to ΔH and ΔS of the folding equilibrium. If this is the case, then overall structural integrity should be sufficient to predict the relative TS-stabilisation of all variants of ODCase; however, this need not be the case. An alternate possibility arises from the predicted evolutionary course followed by extremophiles. For example, thermal stability is a valuable trait among the enzymes of thermophiles, but activity at lower temperatures is not, and may be lost to genetic drift. Similarly, improved activity at low temperature is a valuable trait for the enzymes of psychrophiles, but loss of thermal stability may occur as well, due to genetic drift. An analogy can be made to antibiotic resistance: a mutation that confers resistance is strongly selected for, even if it compromises structure and function; subsequent stable mutations typically

accommodate the original mutation, while coincidentally compromising vestigial features (Jakubowska & Korona, 2009). This raises the possibility that the apparent correlation is not a result of a requirement for increased flexibility among psychrozymes. If this is the case, then the correlation would be poor or non-existent for enzymes from nascent psychrophiles, and it would be possible to design an enzyme that has both high thermal stability, and high activity at low temperatures. Regardless, thermal stability is a potential indicator of ΔH_{tx} and ΔS_{tx}. The same predictions may also be made using the temperature of maximal activity, which has been shown to correlate with T_m (Giver *et al*., 1998).

4.2.4 Implications of the Relationship between Overall ODCase-Catalysed Turnover, and Uncatalysed Turnover, of OMP to UMP

The discussion above concerns the catalytic strategy of ODCase-variants relative to one another, but has not attended to the relationship between the overall barrier to the enzyme-catalysed reaction ($\Delta G_{e+s}^{\ddagger}$), the non-enzymatic reaction ($\Delta G_{non}^{\ddagger}$), and their corresponding temperature-dependencies. This relationship is attended to in Figure 4.5, Panel D, where it is shown that all the ODCase-variants examined by this plot, used the same basic strategy to effect catalysis: reduction of the TS-enthalpy, $H^{\ddagger}$ (corresponding to lower intercepts at the ordinate-axis), at the cost of reduced TS-entropy, $S^{\ddagger}$ (corresponding to increased slopes), ultimately yielding a reduced TS-free energy, $G^{\ddagger}$. This statement reiterates one of the most fundamental concepts in catalysis; namely, that a substrate is bound by a catalyst to

guide its transition through a subset of reaction pathways that are less energetically costly than those pathways that the transition would require otherwise (Fischer, 1894; D. E. Koshland, 1958; Pauling, 1948; Polanyi, 1921).

4.2.5 Investigation of the Apparent Correlation between ΔH and ΔS

In Figure 4.4, the values of ΔH and ΔS appear to have a direct linear correlation, to one another. However, there is reason to believe that the strength of this correlation could be an artifact, rather than something more provocative, such as the oft-proposed, and hotly debated phenomenon of extrathermodynamic *H–S* compensation (Wilfong *et al.,* 2011; Freed, 2011; Douglas, Dudowicz, & Freed, 2009; Cornish-Bowden, 2002; Cooper *et al*., 2001; Sharp, 2001; Qian, 1998; Krug, Hunter, & Grieger, 1976; Leffler, 1963; Leffler, 1955). An artificial correlation can arise from results such as these, due to the narrow range of reciprocal temperatures typically used to evaluate the slope of a van't Hoff-, or Eyring–Polanyi-plot, relative to the gap between the reciprocal temperatures and the ordinate-axis, where the intercept is evaluated (Krug, *et al*., 1976).

In considering the factors that give rise to the artifact described above, recall that the "pivot-point" of a linear-regression fit is effectively located at the geometric centre of the constellation of data-points. Consequently, the pivot point of a van't Hoff, or Eyring–Polanyi plot lies on the vertical line corresponding to $T = T_{\mathrm{hm}}$, the harmonic mean of the experimental temperatures, at a height that is proportional to $\Delta G_{\langle 1/T \rangle}$, the Gibbs free energy change associated with the equilibrium or activation of

interest, evaluated at $\langle 1/T \rangle$, the "expected-value" of the reciprocal temperatures (*i.e.*, the pivot points are found by evaluating eqn. 1.10–1.14 at the average reciprocal temperature). Specifically, the pivot point is evaluated as the ordered-pair (T_{hm} , $-[\Delta G_{\langle 1/T \rangle}/RT_{hm}]$), or ($T_{hm}$, $[\ln(k_B/h) - \Delta G_{\langle 1/T \rangle}/RT_{hm}]$) in the context of a van't Hoff or Eyring–Polanyi plot, respectively. Clearly, if the range of experimental temperatures is too narrowly distributed, then the data-points will collectively approach the pivot point.

When the cluster of data points on a van't Hoff, or an Eyring-Polanyi plot is focused, even small experimental errors would cause the regression line to pivot extensively. Consequently, there will be a large, coincident, and linearly-related change in both the slope and intercept of these plots, leading to correlation of the error-values associated with ΔH and ΔS, and ultimately, increased correlation between the values themselves (Krug, *et al.*, 1976). This problem is exacerbated by experimental systems in which the variation of ΔG as a function of temperature is expected to be small, and thus the data are predisposed to form a tight cluster.

The precise nature of the artifactual correlation between ΔH and ΔS, can best be understood in the context of eqn. 1.10. Because of the aforementioned consistency of ΔG, and small range of temperatures, T approximates T_{hm}, and ΔG approximates $\Delta G_{\langle 1/T \rangle}$, the free energy at the arithmetic mean of the inverse temperatures; consequently, eqn. 1.10 may approximate the linear function of ΔH and ΔS, shown in eqn. 4.4. This equation implies a plot of ΔH *vs.* ΔS evaluated for a set of related equilibria, or activations, will give a line of *H–S* ordered pairs, with a slope of T_{hm},

and an intercept of $\Delta G_{<1/T>}$. Eqn. 4.4 and the aforementioned plot apply equally well to the error associated with ΔH and ΔS, thus: if the line of best-fit on a van't Hoff or Eyring–Polanyi plot pivots freely due to limited variation of ΔG and T, then the constellation of data-points on a plot of ΔH *vs*. ΔS will extend into a line with a slope equal to T_{hm}. Furthermore, because the errors are expected to be relatively large, they are likely to overpower the influence of any underlying, true *H–S* correlation.

$$\Delta H = \Delta G_{<1/T>} + T_{hm} \cdot \Delta S \tag{4.4}$$

4.2.6 Interpretation of ΔH vs. ΔS in Light of an H–S Correlation Artifact

Despite the caveat described above, the interpretations made throughout this chapter of the plots displayed in Figure 4.4, are entirely unaffected: Figure 4.4 should be taken to mean that the ODCase-variants can be ordered in terms of the thermodynamics of their TS-stabilisation, and the order of ΔH and ΔS is correlated with other properties of their corresponding ODCase-variants. The caveat described in § 4.2.5 contributes a confounding variable to plots of ΔH *vs*. ΔS that causes the plot to be linear. Thus the linearity is real, in a manner of speaking, but it may not be due to any property of Pa-, Cp-, Sc-, Ec-, and MtODCase. Although such a relationship could exist (if binding interactions are introduced to reduce an enthalpy barrier, then motion, and thus entropy, may be correspondingly restricted), its existence is collateral to the interpretations and discussions given in previous sections. However, the existence of a correlation between ΔH and ΔS is intriguing in its own right. For

example, it could be indicative of an underlying cost-benefit ratio that decides which of the aforementioned catalytic strategies is ultimately used. Not only would this contribute to greater understanding of the evolution, design, and function of enzymes, but it would also serve to guide *de novo* enzyme design.

4.2.7 Uncovering the True Relationship between ΔH and ΔS

The caveats associated with determining ΔH and ΔS by the method described above are practically unavoidable when working within the temperature limitations of biomolecules and aqueous solutions. However, through judicious use of established literature methods they can be attenuated (*e.g.*, by widening the range of temperatures assayed), or even partially circumvented (as in the method described in the following section). Suffice it to say that the true test of these correlations is a fastidious statistical treatment, of robust data, that lends itself to the formulation of robust conclusions.

One component of the caveat associated with plots of ΔH *vs.* ΔS (described in § 4.2.5) arises from the disparity between the experimentally feasible temperatures, and the temperature at which the intercept of a van't Hoff or Eyring–Polanyi plot is technically determined ($1/T = 0$). There are two problems that can arise from this: amplification of errors arising from long-range extrapolations from the data, and misleading correlations arising from strong coupling between experimental errors in the slope and intercept. The former problem can be partially attenuated by assaying over a wide range of temperatures, but is ultimately limited by the experimental

system (*e.g.*, solvent volatility and fusibility, thermal limitations of equipment, *etc.*). Fortunately, the latter problem of error-coupling leading to artifactual correlation can be effectively obviated using an adaption of the method described by Krug and coworkers (1976). In essence, the method implements an affine transformation that centres the data points about the ordinate-axis by translating everything by T_{hm}. Consequently the intercept is calculated at the "pivot-point" of the data set, and is evaluated independently of the slope. By adapting this approach to the van't Hoff and Eyring–Polanyi equations (eqn. 1.11–1.14), a set of transformed expressions is obtained: eqn. 4.5–4.8.

$$\ln K_m = -(\Delta H_m / R) \cdot [(1/T)-\langle 1/T\rangle] + (\Delta S_m / R) - (\Delta H_m / R) \cdot \langle 1/T\rangle \tag{4.5}$$

$$\ln(1 / K_{tx}) = -(\Delta H_{tx} / R) \cdot [(1/T)-\langle 1/T\rangle] + (\Delta S_{tx} / R) - (\Delta H_{tx} / R) \cdot \langle 1/T\rangle \tag{4.6}$$

$$\begin{aligned} \ln(k_{cat} / T) = &-(\Delta H_{es}^{\ddagger} / R) \cdot [(1/T)-\langle 1/T\rangle] \\ &+ (\Delta S_{es}^{\ddagger} / R) - (\Delta H_{es}^{\ddagger} / R) \cdot \langle 1/T\rangle + \ln(k_B/h) \end{aligned} \tag{4.7}$$

$$\begin{aligned} \ln[(k_{cat} / K_m) / T] = &-(\Delta H_{e+s}^{\ddagger} / R) \cdot [(1/T)-\langle 1/T\rangle] \\ &+ (\Delta S_{e+s}^{\ddagger} / R) - (\Delta H_{e+s}^{\ddagger} / R) \cdot \langle 1/T\rangle + \ln(k_B/h) \end{aligned} \tag{4.8}$$

As described briefly above, eqn. 4.5–4.8 are obtained by introducing a term containing T_{hm} to eqn. 1.11–1.14. More accurately, two terms are introduced, both equivalent to the contribution of the slope term at T_{hm}: $-(\Delta H / R) \cdot \langle 1/T \rangle$. One of these is subtracted from the original slope term, and the other is added to the intercept term. Thus the additional terms do not modify equivalence in any way; rather, they present an alternate frame of reference. Instead of plotting the left hand side as a function of inverse temperature ($1/T$), it is plotted as a function of the difference between the inverse temperature, and the average inverse temperature ($(1/T) - \langle 1/T \rangle$). Such a plot is centred about $\langle 1/T \rangle$, rather than $1/T = 0$; accordingly, the intercept is shifted by $-(\Delta H / R) \cdot \langle 1/T \rangle$. Note that eqn. 4.4 defines this new intercept as $\Delta G_{\langle 1/T \rangle} / RT_{hm}$; thus the transformed intercept is a measure of free energy. These transformed equations effectively centre the data set about the ordinate-axis, such that the intercept is determined at the pivot point, where it is least affected by slope-estimation errors. Consequently, the variance of the slope and intercept estimates are uncoupled, and underlying correlations, arising from the thermodynamic parameters of ODCase-activity, can be detected (Krug *et al.*, 1976). Ultimately, the ΔH–ΔS plots in Figure 4.4 are transformed into ΔH–$\Delta G_{\langle 1/T \rangle}$ plots (using eqn. 4.5b–4.8b) in order to test the strength of the ΔH–ΔS correlation; these transformed plots are shown in Figure 4.5.

$$\ln K_m = -(\Delta H_m / R) \cdot [(1/T) - \langle 1/T \rangle] - (\Delta G_{\langle 1/T \rangle, m} / R) \cdot \langle 1/T \rangle \qquad (4.5b)$$

Figure 4.6 Refined ΔH–ΔG Correlations Derived from Figure 4.5 and Originating from a Survey of the Thermodynamic Parameters Associated with Mt-, Sc-, Ec-, Cp-, and PaODCase-Mediated Catalysis

A survey of the thermodynamic parameters associated Mt-, Sc-, Ec-, Cp-, and PaODCase-mediated catalysis, revealed the extent to which ΔH and ΔG (of the chemical transitions outlined in Scheme 1.1) correlated with one another. This survey includes the two ODCase-variants characterised here (PaODCase [▽] and CpODCase [■]), as well as those described by Toth *et al*., (2009) (MtODCase [▲], ScODCase [●], and EcODCase [◆]), and the uncatalysed-pathway (+) determined by Radzicka & Wolfenden (1995), using the decarboxylation of 1–methylorotic acid as a model. The ΔH-values collected in Table 2.3, 3.3, 4.2, 4.3, 4.4, and 4.5 were plotted as a function of the corresponding $\Delta G_{<1/T>}$-values to construct plots illustrating the correlation between these parameters during formation of the virtual equilibrium for $\{S\}^{\ddagger}$-binding in the TS (Panel A), formation of the equilibrium involving S-release in the GS (Panel B), and promotion of the ES-complex, free E + S, or free S, to the TS ($\{ES\}^{\ddagger}$, or $\{S\}^{\ddagger}$, respectively) (Panel C, D, and E, respectively). Panel D is a focused view of the enzyme-derived data points in Panel E. Error bars represent the estimated error in the prediction of the thermodynamic parameters given in Table 2.3, 3.3, 4.2, 4.3, 4.4, and 4.5. Error bars represent the estimated error in the prediction of the thermodynamic parameters given in Table 2.3, 3.3, 4.2, 4.3, 4.4, and 4.5. Each of the plots was fit by linear regression analysis using *KaleidaGraph* v.3.5 (Synergy Software, Reading, PA), to illustrate the effect of ΔH–ΔG compensation. Data points corresponding to PaODCase-mediated catalysis (▽) and the uncatalysed reaction (+) were excluded from the linear regression analysis. Detailed methods are described in § 1.7.1, 5.2.17, and 5.2.20.

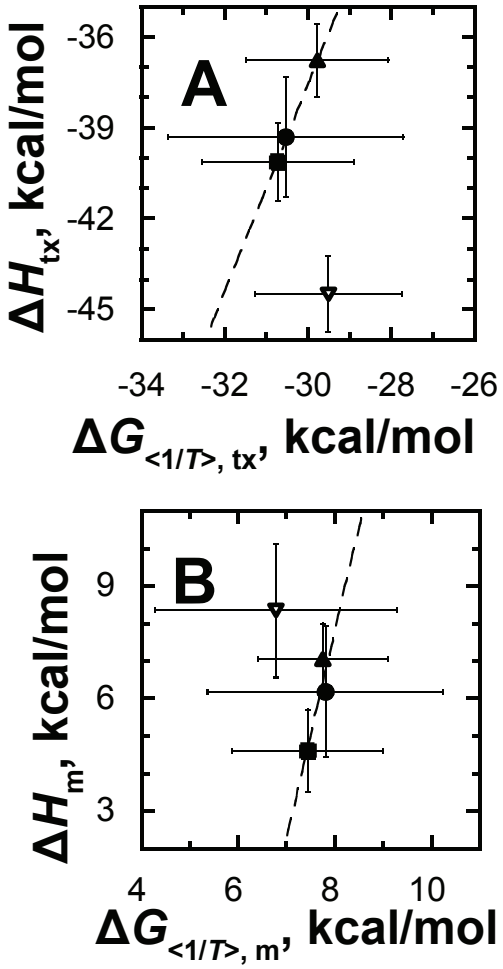

Figure 4.6 (page 1 of 2)

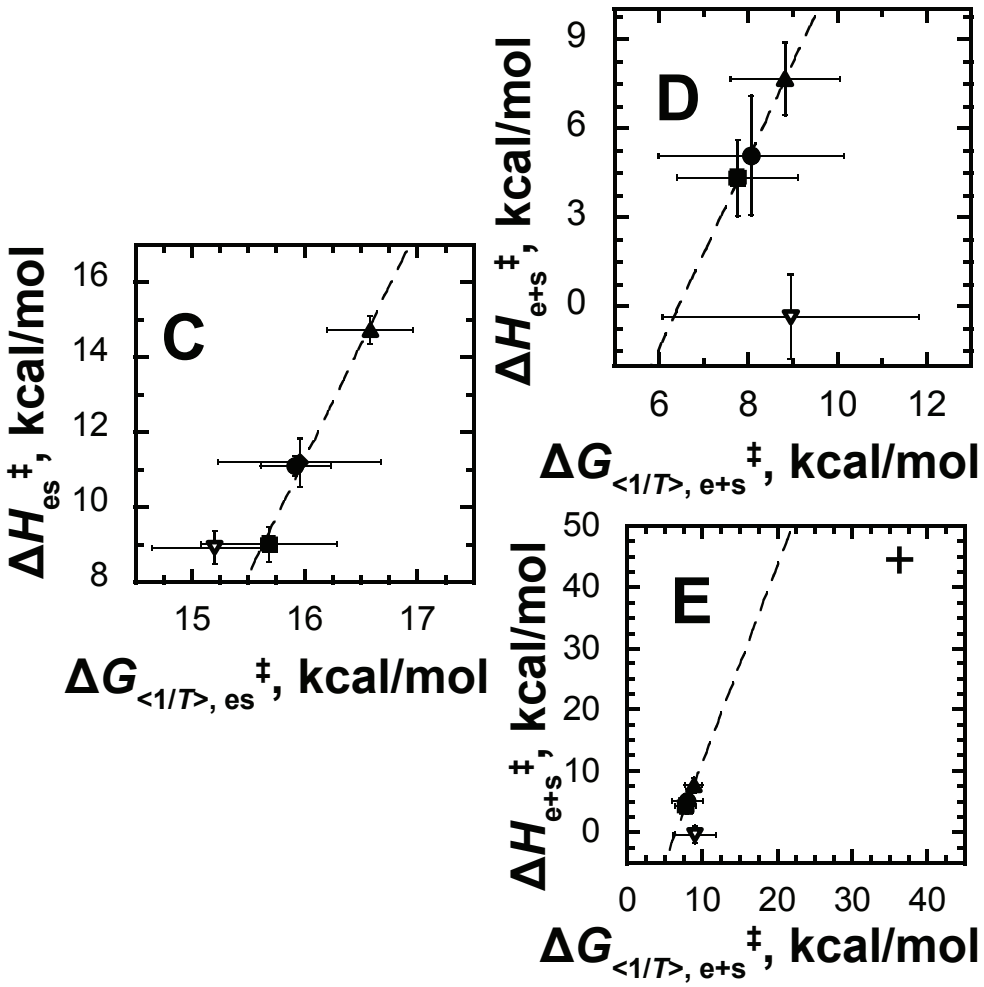

Figure 4.6 (page 2 of 2)

$$\ln(1 / K_{tx}) = -(\Delta H_{tx} / \mathrm{R}) \cdot [(1/T)\text{-}\langle 1/T\rangle] - (\Delta G_{\langle 1/T\rangle,\, tx} / \mathrm{R}) \cdot \langle 1/T\rangle \qquad (4.6b)$$

$$\ln(k_{cat} / T) = -(\Delta H_{es}^{\ddagger} / \mathrm{R}) \cdot [(1/T)\text{-}\langle 1/T\rangle] - (\Delta G_{\langle 1/T\rangle,\, es}^{\ddagger} / \mathrm{R}) \cdot \langle 1/T\rangle + \ln(k_B/h) \qquad (4.7b)$$

$$\ln[(k_{cat} / K_m) / T] = -(\Delta H_{e+s}^{\ddagger} / \mathrm{R}) \cdot [(1/T)\text{-}\langle 1/T\rangle] - (\Delta G_{\langle 1/T\rangle,\, e+s}^{\ddagger} / \mathrm{R}) \cdot \langle 1/T\rangle + \ln(k_B/h) \qquad (4.8c)$$

4.2.8 Decoupling and Removing Divergent Values from Plots of ΔH vs. ΔS

By applying the approach of Krug *et al*. (1976), as described above, to ODCase-mediated and non-enzymatic decarboxylation of OMP, it is possible to identify divergences from true correlations that were undetectable in the plots of ΔH *vs*. ΔS. Indeed, Figure 4.6 reveals that the thermodynamic parameters corresponding to PaODCase and the uncatalysed reaction were inconsistent with the linear correlations apparent for the remaining ODCase-variants. The validity of this apparent correlation between the remaining variants was subsequently analyzed in greater depth. Table 4.6 lists the data relevant to determining the likelihood that the thermodynamic parameters ΔH and $\Delta G_{\langle 1/T\rangle}$ correlated in a linear fashion, and to determine if any further data points needed to be excluded from the fit. Although none of the confidence values were sufficient (>95% confidence) to claim that the

Table 4.6
Statistical Analysis[a] of the Apparent Linear Correlations between Enthalpy and Free Energy Changes Corresponding to ODCase-Catalysed Decarboxylation of OMP Seen in Figure 4.7 and Refined from Figure 4.5

correlation	confidence, %	R^2	χ^2	*n*	*d.f.*	$\Delta G_{<1/T>}$, kcal/mol			
						PaODCase	CpODCase	ScODCase	MtODCase
ΔH_{tx}–$\Delta G_{<1/T>,tx}$	18.17	0.967	3.41	3	2	-124.8 ± 7.3	-129.1 ± 7.5	-127 ± 11	-124.5 ± 7.1
ΔH_{m}–$\Delta G_{<1/T>,m}$	0.26	0.777	11.9	3	2	28 ± 10	30.9 ± 6.4	32 ± 10	32.4 ± 5.6
$\Delta H_{es}^{\ddagger}$–$\Delta G_{<1/T>,es}^{\ddagger}$	6.87	0.975	7.1	4	3	63.1 ± 2.3	67.2 ± 3.0	66.8 ± 1.3	69.4 ± 1.5
$\Delta H_{e+s}^{\ddagger}$–$\Delta G_{<1/T>,e+s}^{\ddagger}$	37.71	0.981	1.95	3	2	36 ± 11	32.2 ± 5.6	33.8 ± 8.7	36.9 ± 5.1
						PaODCase	CpODCase	ScODCase	MtODCase
T_{hm}, K	-	-	-	-	-	309	307	298	302

[a] The coefficients of determination (R^2) and χ^2-values were obtained by linear regression analysis of the plots in Figure 4.7 using *KaleidaGraph* v.3.5 (Synergy Software, Reading, PA). The sample number (*n*) was used to determine the degrees of freedom (*d.f.*), and in turn to conduct a χ^2-test of the linearity of the apparent correlations and determine a level of confidence in each. Also included are the $\Delta G_{<1/T>}$-values calculated for each ODCase variant at its corresponding T_{hm}.

Table 4.7

Statistical Analysis[a] of the Origin of Linear Correlations Observed in Figure 4.7 between Enthalpy and Entropy Changes Corresponding to ODCase-Catalysed Decarboxylation of OMP (excluding PaODCase)

correlation	β, K	n	*s.e.m.*	confidence, %	t	R^2	χ^2	*d.f.*
ΔH_{tx}–ΔS_{tx}	439	3	37	98.7	-6.28	0.99293	0.75	2
ΔH_{m}–ΔS_{m}	359	3	38	94.3	-2.47	0.98878	0.6	2
$\Delta H_{es}^{\ddagger}$–$\Delta S_{es}^{\ddagger}$	367.9	4	8.8	99.96	-13.84	0.99884	0.34	3
$\Delta H_{e+s}^{\ddagger}$–$\Delta S_{e+s}^{\ddagger}$	442	3	28	99.3	-8.438	0.99595	0.43	2

[a] The coefficients of determination (R^2) and χ^2-values were obtained by linear regression analysis of the plots in Figure 4.7 using *KaleidaGraph* v.3.5 (Synergy Software, Reading, PA). The sample number (n) was used to determine the degrees of freedom (*d.f.*). These statistics were used to conduct a t-test to determine if T_{hm}-values were distinct from the β–values (± standard error in the mean, *s.e.m.*) corresponding to the apparent correlations, and determine a value of student's-t (t) and associated level of confidence for each. Only the T_{hm} corresponding to assays of CpODCase (307 K) was used in the analysis, as it was closest to β.

linear relationship between ΔH and $\Delta G_{<1/T>}$ (or by extension, between ΔH and ΔS) did not arise by chance, the coefficients of determination (R^2) were close-enough to unity that they did not merit elimination of additional data points.

4.2.9 Statistical Analysis of a Refined H–S Correlation

Removing the thermodynamic parameters corresponding to PaODCase and the uncatalysed reaction improved the strength of the correlations between the remaining ΔH- and ΔS-values observed in Figure 4.4. Table 4.7 lists the results of the statistical analysis conducted on these remaining data. In contrast to Table 4.6, Table 4.7 addresses the likelihood that the remaining data were inconsistent with the correlation predicted in eqn. 4.4. In order to conduct this analysis in a rigorous fashion, I assumed that the data were linearly correlated in a fashion analogous to eqn. 4.4, as described by eqn. 4.9, and proceeded to test this assumption. In this model, β represents the slope of the line of best-fit in a plot of ΔH *vs.* ΔS, such as those in Figure 4.4, it has the dimensions of temperature, and is typically evoked in purported cases of enthalpy–entropy compensation; for these reasons it is sometimes referred to as the compensation temperature. This parameter may also be referred to as the isokinetic temperature due to its relationship to a set of chemical reactions with similar activation barriers ($\Delta G^{\ddagger}$), but distinct enthalpy–entropy contributions (*i.e.*, $\Delta H^{\ddagger}$ and $\Delta S^{\ddagger}$): namely, that at this temperature the reaction rates converge to the same value. The fundamental difference between eqn. 4.4 and 4.9 is the value of β: if a statistically significant difference exists between the values of β and T_{hm}, then it

would rule out the aforementioned artifact as the cause of any correlation among the remaining values of ΔH and ΔS. Although the confidence values in Table 4.6 provided only circumstantial evidence to suggest a linear correlation between enthalpy and entropy, the confidence values in Table 4.7 strongly reject (>95% confidence) the possibility that—if a correlation does exist—it is due to the correlation artifact. The lone exception was the ΔH_m–ΔS_m correlation, for which this possibility is only border-line rejected, with a confidence of 94.3%.

$$\Delta H = \Delta G_{\beta} + \beta \cdot \Delta S \tag{4.9}$$

4.2.10 Lessons Learned from Analysis of H–S Correlation

In summary, a deeper analysis of the thermodynamic parameters associated with ODCase mediated decarboxylation of OMP reveals that no existing model can confidently be applied to the observed data. In particular, the thermodynamic parameters associated with PaODCase-mediated catalysis do not cluster, nor correlate linearly with the corresponding thermodynamic parameters of the other variants. Even after removal of the PaODCase-data from the set, it is possible that the apparent linear correlation between the remaining ODCase-data is merely due to a randomly generated coincidence; however, it is not the result of an artifact. Thus, this data set may indicate that a pair of extra-thermodynamic correlations exist, one including PaODCase and one including the other variants examined here; but without further

data, this cannot be stated with confidence.

4.3 Structural Comparison of ODCase-Variants

As noted in the introduction, there are no well-defined rules that predict the thermal stability of a protein based upon its structure; rather, there are inconsistently observed trends involving very particular circumstances. Specifically, compared to mesozymes: thermozymes tend to possess more disulfide-bonds, H-bonds, and proline resides, as well as tighter packing and greater contact between hydrophobic residues (Imanaka, 2011); psychrozymes tend to possess fewer proline residues and disulfide-bonds, and a higher occurrence of glycine-clusters (Feller, 2003; Russell, 2000); and both thermozymes and psychrozymes tend to possess more ion-pairs (Kumar & Nussinov, 2004; Smalas *et al*., 2000). This section explores the structural characteristics of selected ODCase-variants in the context of these trends.

4.3.1 Primary Structure

In order to examine the applicability of the aforementioned structural trends to ODCase-variants, the proportions of charged amino acids in the primary structures of Pa-, Cp-, Sc-, Ec-, Hs-, or MtODCase were counted. Further, the prevalence of certain key amino acids residues (glycine, proline, and cysteine) implicated in key structural elements of psychro-, meso-, or thermozymes were also determined; the result of these analyses is given in Table 4.8. These results are also displayed in bar-graph format in Figure 4.7.

Table 4.8

Primary Structure Analysis[a] of Pa-, Cp-, Sc-, Ec-, Hs-, and MtODCase

	# of amino acids	# of charged amino acids					structurally high-impact					
Variant		−	+	total #	%	pI	G	G, %	P	P, %	C	C, %
PaODCase	232	27	21	48	20.7	5.04	12	5.2	7	3.0	5	2.2
CpODCase	231	27	24	51	22.1	5.63	19	8.2	11	4.8	1	0.4
ScODCase	267	36	36	72	27.0	6.91	27	10.1	7	2.6	4	1.5
EcODCase	245	27	24	51	20.8	5.81	16	6.5	12	4.9	3	1.2
HsODCase	259	31	29	60	23.2	6.44	23	8.9	9	3.5	4	1.5
MtODCase	228	34	28	62	27.2	5.12	21	9.2	9	3.9	3	1.3

[a]Counts and percentages of various amino acids, as well as theoretical pI values, were obtained using the "ProtParam" tool on the ExPASy website (http://web.expasy.org/protparam/).

Figure 4.7 Comparison of the Amino Acid Compositions of Pa-, Cp-, Sc-, Ec-, Hs-, and MtODCase

Relative percentages of amino acid content among ODCase-variants, obtained using the "ProtParam" tool on the ExPASy website (http://web.expasy.org/protparam/), are shown. The percentage of negatively charged residues (aspartic and glutamic acid) in the sequence of Pa-, Cp-, Sc-, Ec-, Hs-, or MtODCase is represented by a red bar above the relevant ODCase-variant label. Similarly, blue represents positively charged residues (lysine and arginine), green represents glycine residues, yellow represents proline residues, and orange represents cysteine residues. The remaining amino acids are collectively represented by light grey.

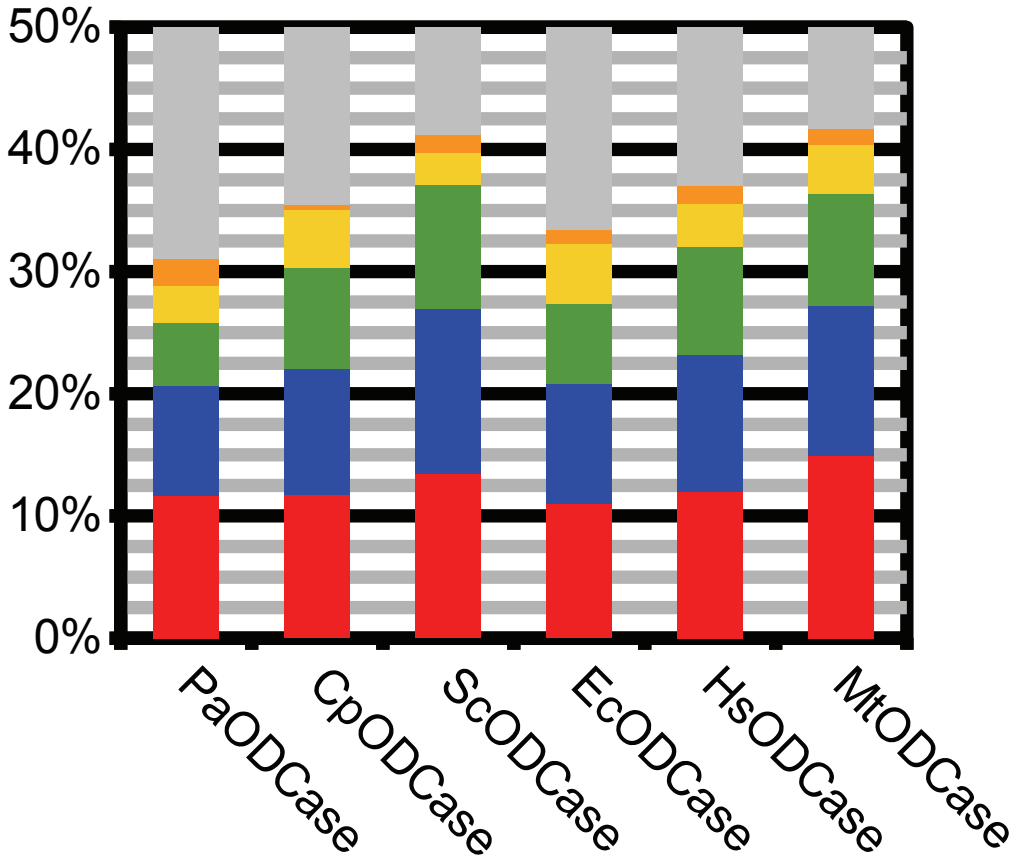
50%
40%
30%
20%
10%
0%
PaODCase
CpODCase
ScODCase
EcODCase
HsODCase
MtODCase

Figure 4.7

Previous surveys of extremozyme structural-features revealed that both psychrozymes and thermozymes tend to have a greater number of ion-pairs relative to their mesozyme counterparts (Kumar & Nussinov, 2004; Smalas *et al*., 2000). Thus, they may be predicted to have a larger proportion of "charged" (*i.e*., lysine, arginine, aspartic acid, and glutamic acid) residues. Indeed, the thermozyme MtODCase has the greatest number of charged residues. However, the mesozyme ScODCase has a similar number of charged residues, while the remaining mesozymes, Ec- and HsODCase, and the psychrozymes, Pa- and CpODCase, have fewer charged residues. On a related note, there is an apparent trend towards a greater proportion of negatively charged (*i.e*., aspartic and glutamic acid) residues among both thermozymes and psychrozymes, which may contribute to improved solubility or flexibility as indicated by earlier surveys of psychrozymes and thermozymes (Gianese *et al*., 2002). Meaningful speculation cannot begin without first determining the 3D structures of Pa-, and CpODCase, such that the precise location and impact of each charged residue can be determined.

The primary structures of psychrozymes may be distinguished from those of thermozymes on the basis of the proportion of glycine and proline residues, and di-sulfide bonds; specifically, psychrozymes are observed to possess more glycine residues, and fewer proline residues and disulfide-bonds (Feller, 2003; Russell, 2000), whereas the opposite is observed among thermozymes (Imanaka, 2011). In the context of the ODCase-variants described in Table 4.8 and Figure 4.7, the reduced number of cysteine residues in the sequence of CpODCase, which implies that few

di-sulfides exist in its structure, is consistent with the prediction of fewer disulfide-bonds among psychrozymes, described above; however, none of the other distinctions are observed.

Although the relative abundances of amino acid residues considered above are not indicative of more general trends, it was noted in the introduction that such trends are typically not consistently applicable; rather, a closer examination of each structure is required to yield more meaningful data. Indeed, a comparison of the primary structures of Pa-, Cp-, Sc-, Ec-, Hs-, or MtODCases phosphate gripper loops, and the tertiary structures of the corresponding ODCase active sites, suggests that the aforementioned trends are more accurately defined as situation-dependent tools; this hypothesis is considered in the following section.

4.3.2 ODCase Active Site Phosphate Gripper Loop

The phosphate gripper loop described by Toth *et al*., (2009) is a segment of random coil that caps the active site of Sc-, Mt-, Ec-, and HsODCases (Figure 4.8, Panel B, C, D, and E, respectively) and contacts the phosphate group of OMP. A multiple sequence alignment of the primary structures in this region of Pa-, Cp-, Sc-, Ec-, Hs-, and MtODCase (Figure 4.8, Panel A) reveals that the phosphate gripper loop is 19 residues long in Sc-, Ec-, and HsODCase, but is syncopated to 9 residues in MtODCase; an observation that is thought to contribute to the maintenance of catalytic activity at high temperatures (Toth *et al*., 2009). By extension, it might be anticipated that the psychrozymes Pa- and CpODCase would possess an extended

Figure 4.8 Comparison of the Phosphate Gripper Loop Length among the Thermozyme Mesozyme, and Psychrozyme ODCase-Variants

A multiple sequence alignment (created using Clustal Omega, available from the EMBL–EBI web site [http://www.ebi.ac.uk/Tools/msa/clustalo/]) reveals the conserved prolines and valine that bracket the phosphate gripper loop (∗, Panel A). Sequences are aligned to ScODCase, the numbering for which is provided for reference. Amino acids 1–221 of the bifunctional enzyme to which HsODCase belongs (HsODCase numbering) roughly correspond to HsOPRTase, and was omitted from the alignments. The loop is shown as a section of random coil (magenta and cyan) in the crystal structures of ScODCase (19 residues, P202–V220, Panel B, PDB entry 3GDL [Chan *et al*., 2009]), EcODCase (19 residues, P189–P207, Panel C, PDB entry 1EIX), MtODCase (10 residues, P180–P189, Panel D, PDB entry 3G1A [Harris, Navarro Poulsen, Jensen, & Larsen, 2000]), and HsODCase (19 residues, P417–P435, Panel E, PDB entry 3MW7 [data not published]). An intervening sequence (cyan), corresponding to the length of the syncopation observed in the sequence of MtODCase, the succeeding α–helix (orange), and *β*–strand (red), are coloured for visual reference. Crystals were formed with TS-analogues or GS-analogues bound in the active site: 6–aza–uridine 5'–monophosphate (Panel B and D), 1–(5'–phospho–β–D–ribofuranosyl)barbituric acid (Panel C), or 5–fluoro–uridine 5'–monophosphate (Panel E). The atoms of the bound analogues are coloured according to the following scheme: carbon is white, oxygen is red, nitrogen is blue, phosphorous is orange, and fluorine is pale blue.

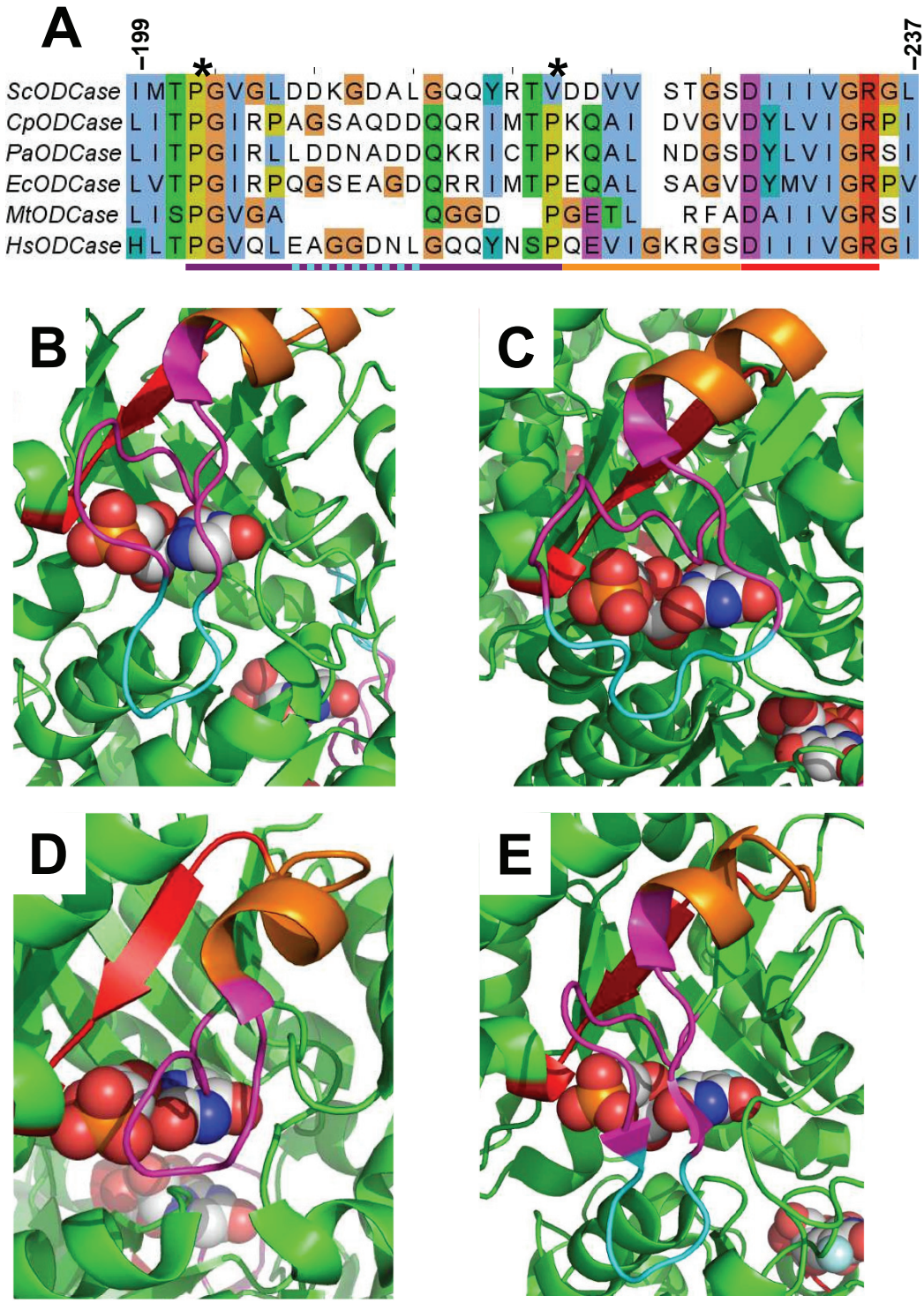
A
199
237
ScODCase IMTPGVGLDDKGDALGQQYRTVDDVV STGSDIIIVGRGL
CpODCase LITPGIRPAGSAQDDQQRIMTPKQAI DVGVDYLVIGRPI
PaODCase LITPGIRLLDDNADDQKRICTPKQAL NDGSDYLVIGRSI
EcODCase LVTPGIRPQGSEAGDQRRIMTPEQAL SAGVDYMVIGRPV
MtODCase LISPGVGA QGGGD PGETL RFADAIIVGRSI
HsODCase HLTPGVQLEAGGDNLGQQYNSPQEVIGKRGSDIIIVGRGI
B
C
D
E

Figure 4.8

loop; however, this is not the case. The loop does not appear to be extended beyond 19 residues in the sequences of Cp- or PaODCase, which is consistent with the notion that gross structural changes are not required to adapt an enzyme to reduced temperatures, and that the architectural strategies employed by psychrozymes is not always the opposite of those employed by the thermozymes.

A more detailed comparison the active site structures in Figure 4.8 reveals a few illuminating differences between thermo-, meso-, and psychrozyme variants of ODCase. The phosphate gripper loop of MtODCase is not only syncopated, but the remaining sequence is rich in glycine residues (four out of ten); which facilitates tighter packing. Indeed, there is a trend towards drawing the "butts" of α–helices towards the active site, and using backbone amides to hydrogen bond the substrate, rather than side chains; an observation that is consistent with the tighter packing observed for thermozymes in general (Imanaka, 2011). The added amino acids that are present in the phosphate gripper loops of Sc-, and HsODCase, are predominantly charged, and are in positions with available solvent or counter-ions. Furthermore, the active-site substrate-interactions implemented by these variants are predominantly side-chain-mediated. Although EcODCase is most similar to Cp-, and PaODCase by sequence similarity, there are no obvious active-site structural features to distinguish it from Sc-, or HsODCase; a similar argument could be made for CpODCase using the sequence alignment as a guide. By contrast, the phosphate gripper loop of PaODCase is enriched with charged amino acids (seven out of nineteen); particularly in consecutive pairs of like-charges. Further, there are four aspartic acid residues in

positions that align with contacts to the phosphate moiety in the structures of Sc-, Ec-, and HsODCase. These high local concentrations of like-charges could be sufficient to destabilise the phosphate gripper loop, and by extension, OMP-binding, to the extent observed in Table 4.1. This strategy has been previously observed in the active-site of a psychrozyme variant of citrate synthase, described in the introduction (Kumar & Nussinov, 2004). These charges may also contribute to increased solubility of the phosphate gripper loop, thus improving flexibility the rate of active site opening and closing, a strategy common to many psychrozymes (Kumar & Nussinov, 2004; Smalas *et al*., 2000).

The comparison described above exemplifies the incompatibility of gross structural differences with attempts to distinguish thermo-, meso-, and psychrozymes in a reliable manner. Similarly, there appears to be no definitive distinctions at the level of the amino acid sequences of these ODCase-variants, either. For example, the thermodynamics of EcODCase-mediated decarboxylation of OMP indicate that it is a mesozyme; however, its phosphate gripper loop is most similar to that of the psychrozymes (Figure 4.8, Panel A). Furthermore, a radial tree-diagram of the primary structure similarity among ODCase-variants (Figure 4.9) reveals that this is also the case for the full sequences. This observation may indicate that the facets of structure which endow "cold-resistance" are more subtle than the gross comparisons made here. Of course, EcODCase may indeed have comparatively low thermal stability; a T_m-determination for EcODCase would further attend to the question of which sequence elements confer thermal stability or lability to these enzymes.

Figure 4.9 Primary Structure Similarity between Pa-, Cp-, Sc-, Ec-, Hs-, and MtODCase

The radial tree representation of amino acid sequence similarity between the ODCase-variants examined below, reveals that EcODCase (highlighted yellow) is most similar to CpODCase and PaODCase, despite being derived from a mesophile. ScODCase and HsODCase share more similarity to one another than to the other variants, and MtODCase is most distinct. The evolutionary distance (see scale) between two sequences is modelled as the expected fraction of amino acid substitutions per site given the fraction of mismatched amino acids in the aligned region (created using the corresponding tool provided with multiple sequence alignments created using the Protein BLAST function of the NCBI website (http://blast.ncbi.nlm.nih.gov/).

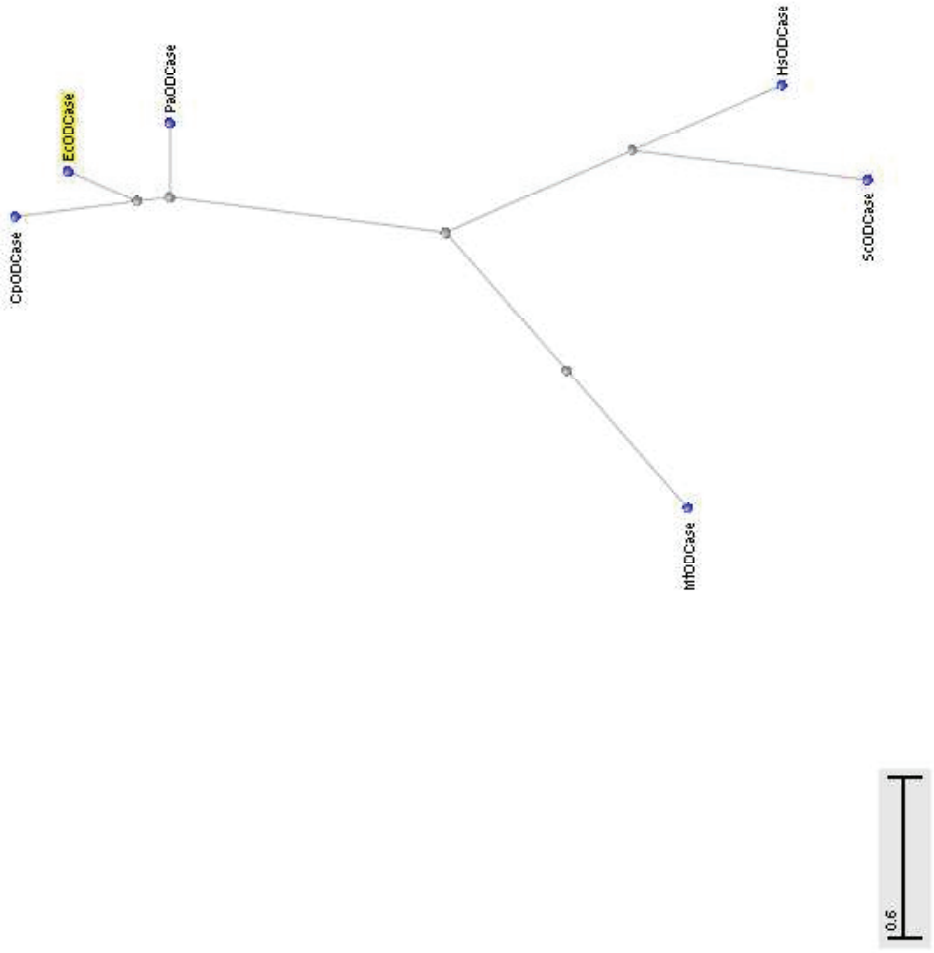
HsODCase
PaODCase
EcODCase
ScODCase
CpODCase
MfODCase
0.6

Figure 4.9

Chapter 5 MATERIALS & METHODS

5.1 Materials, Equipment, & Sources

Unless otherwise mentioned, OMP and all other chemicals were purchased from Sigma–Aldrich Canada Ltd. (Oakville, ON). Restriction enzymes, DNA ladders, and protein molecular weight markers were purchased from New England Biolabs Ltd. (Mississauga, ON). His•Bind resin, thrombin cleavage and capture kits, *E. coli* BL21(DE3) and DH5α cells, and the pET–15b expression system were purchased from Novagen Inc. (Madison, WI). Oligonucleotide primers for amplification of ORFs were commercially synthesised by ID Labs (London, ON). *C. psychrerythraea* gDNA (GenBank accession number: CP000083.1) was obtained from the ATCC (Burlington, ON). gDNA from *Psychrobacter arcticus* 273–4 was provided by the laboratory of Dr. James Tiedje (Center for Microbial Ecology, Michigan State University, East Lansing, MI). *E. coli* BL21(DE3), containing the plasmid, pET–15b–PaODC (pET–15b background, with the ORF of $PaODCase_{+tag}$, from *P. arcticus* 273–4 [GenBank accession number: CP000082.1]), prepared previously by Brandi Mahaney (Bearne Lab). Plasmid and PCR purifications were conducted using the QIAprep® Spin Miniprep Kit and QIAquick® PCR Purification Kit, respectively (Quiagen Inc., Mississauga, ON). DNA sequencing was performed by the Robarts Research Institute (London ON). Growth media and antibiotics were purchased from BioShop Canada Inc. (Burlington, ON). DNA-ligation and PCR-mediated DNA-amplification were conducted with reagents and buffers from the

Invitrogen line of products (Life Technologies, Grand Island, NY). Additional protein-purification was conducted using an ÄKTA FPLC system in conjunction with a 5-mL HiTrap™ Q FF ion-exchange column (GE Healthcare, Baie d'Urfé, PQ). CD-spectroscopic data were collected using a J-810 spectropolarimeter (Jasco Inc., Easton, MD). UV-vis spectrophotometric data were collected using an 8453 UV-visible spectrophotometer (Agilent Technologies Canada Inc., Mississauga, ON).

5.2 Methods

Common buffers and stock solutions were prepared to the specifications listed in Table 5.1.

5.2.1 Amplifying the ORF of C. psychrerythraea 34H (Cp)ODCase Using PCR

PCR-mediated DNA amplification was conducted on a 50-μL scale using the program described in Table 5.2. Reactions consisted of 2.5 U *Pyrococcus furiosus* DNA polymerase, dNTPs (0.2 mM, equal portions of dATP, dGTP, dCTP, and dTTP), gDNA (5 μg), forward primer (0.4 μM), and reverse primer (0.4 μM), all in the proprietary "*Pfu* buffer" supplied by Life Technologies. The sequence of the reverse primer used was: 5' – GCG ACT GGA TCC **TTA GCG GAT GGT ACC** – 3' (overlap with the ORF is 15 bp [**bold**]; melting temperature (T_m) is 63.9 °C; sequence has a *Bam*HI cut site [underlined]; strongest folding T_m is 49.2 °C [predicted]); and the sequence of the forward primer was: 5' – GGA GCT CCA T**AT G**AA CGA TCC **AAA AGT AGT TGT CG** – 3' (overlap with the ORF is 25 bp [**bold**]; T_m is 62.4 °C;

Table 5.1

Recipes for the Most Common Solutions Described in this Thesis

solution	components and conditions
cleavage buffer	70 mM HEPES–NaOH, 0.5 mM EGTA, pH 8.0
wash buffer	60 mM imidazole, 0.50 M NaCl, 20 mM Tris–HCl, pH 7.9
binding buffer	5.0 mM imidazole, 0.50 M NaCl, 20mM Tris–HCl, pH 7.9
strip buffer	400 mM EDTA, 0.50 M NaCl, 20 mM Tris–HCl, pH 7.9
assay buffer[a]	10 mM MOPS–NaOH, 100 mM NaCl, pH 8.0
SDS–PAGE running buffer	24 mM Tris–HCl, 20 mM glycine, 1‰ SDS
TAE buffer	40 mM Tris–HCl, 20 mM acetic acid, 1 mM EDTA, pH 8.0
ampicillin stock	50 mg/mL ampicillin, 50% ethanol
IPTG stock	1 M IPTG, filter sterilised
FPLC start buffer	20 mM Tris–HCl, pH 7.9
FPLC purge buffer	20 mM Tris–HCl, 1 M NaCl, pH 7.9

[a] See § 5.2.17 and 5.2.18 for a full description of assay components

Table 5.2

Temperature Program Used for PCR

step[a]	time (s)	temperature (°C)
1	varied	95 (equilibration)
2	60	95
3	60	95
4	60	55
5	60	72
6	600	72
7	varied	room temperature (equilibration)

[a] Steps 2–5 were reiterated 30 times before proceeding to step 6.

the sequence has an *Nde*I cut site [underlined]; strongest folding T_m is 31.5 °C [predicted]).

5.2.2 Construction of a Plasmid Containing the ORF of CpODCase (pET–15b–CpODC)

Digestions, ligations, and purifications of DNA-strands were conducted in accordance with the guidelines found in their respective product literature. In separate 50-μL volumes, purified pET–15b plasmids (42.5 μL) or PCR products (20 μL) were incubated at 37 °C, for 3 h, with *Nde*I (20 U), *Bam*HI (20 U), bovine serum albumin (5 μg), and 5 μL of the supplied NEBuffer 3 (to yield a final concentration [by addition of ddH_2O] of 50 mM Tris–HCl, pH 7.9, 10 mM $MgCl_2$, 100 mM NaCl, and 1 mM dithiothreitol). The doubly-digested DNA products were then purified to yield 50 μL of each. The purified products of the digestion reaction were ligated to one another to form the novel plasmid, pET–15b–CpODC. Ligation involved first combining the digested pET15b plasmids (2 μL) and PCR products (5 μL) with 0.5 μL of the supplied T4 Ligase Buffer (to yield a final concentration of 50 mM Tris–HCl, pH 7.5, 10 mM $MgCl_2$, 10 mM dithiothreitol, and 1 mM adenosine 5′–triphosphate [ATP]) in a 1.5-mL microcentrifuge tube. The tube was incubated at 37 °C for 2 min, and then put on ice for 1 min. Then the proprietary "Ligase buffer" (10×; supplied by Life Technologies), and T4 DNA-ligase (1 U), were added and the resulting ligation reaction was incubated at 16 °C for 27 h. At the conclusion of the 27-h period, the vessel was removed, and the ligation product was purified, to yield

the pET–15b–CpODC plasmid in a volume of 50 μL. The entire ORF was subsequently sequenced to confirm that no unintended mutations had been introduced.

5.2.3 Resolution of Linear DNA Fragments via Agarose Gel Electrophoresis

Agarose gels for electrophoresis were cast from low-EEO agarose in TAE buffer containing ethidium bromide (1 ppm) to give a 1% (w/v) gel. DNA samples were electrophoretically separated with a constant voltage of 80 V, in a bath of TAE buffer.

5.2.4 Preparation of Culture Media

Lysogeny broth (LB) media were prepared as originally described (Bertani, 1951), excepting glucose, and heat-sterilised. LB+AMP media were prepared by the addition of ampicillin (100 mg/L), subsequent to heat-sterilisation. LB or LB+AMP agarose plates were prepared by the addition of agarose (15 g/L) prior to heat-sterilisation.

5.2.5 Preparing Competent E. coli Cells

E. coli DH5α or BL21(DE3) cells were incubated in LB medium (5 mL), on a rotary shaker (37 °C, 210 RPM), for 20 h. An aliquot of this culture (200 μL) was transferred to a 50-mL centrifuge tube and diluted with LB medium (20 mL). The diluted culture was again incubated until the optical density, determined at a

wavelength of 600 nm using a UV–vis spectrophotometer, reached 0.6 AU (~ 3 h), at which point it was subjected to centrifugation (288,000 × *g*, 30 min). All further steps were conducted "on ice". The supernatant was decanted away from the pelleted cells and discarded; the remaining pellet was resuspended in an ice-cold, heat-sterilised, solution of $MgCl_2$ (1.5 mL, 0.1 M), and incubated for 1 h before it was again subjected to centrifugation (9108 × *g*, 30 min). The decanting, resuspension, and centrifugation steps were repeated exactly as immediately before, then the cells were incubated in LB medium (20 mL) for 30 min before being separated into 100-μL aliquots, combined with glycerol (12.5% [v/v]), and stored at −80 °C.

5.2.6 Transformation of E. coli DH5α or BL21(DE3) Cells with pET–15b–CpODC

Purified plasmid (20 μL, see § 5.2.2) and competent *E. coli* DH5α or BL21(DE3) cells (100 μL, see § 5.2.5) were gently mixed, then incubated at 42 °C for 45 s. The mixture was cooled on ice for 5 min, then diluted with LB medium (900 μL), and incubated on a rotary shaker for 1 h (37 °C, 210 RPM). The culture was then subjected to centrifugation (2,300 × *g*, 3 min) and decanted to a volume of 100 μL, which was applied to LB+AMP agarose plates for overnight incubation at 37 °C. Each of the plates were examined the following day; if a punctate growth pattern appeared on the plate, then it was sealed with parafin wax, and stored at 4–10 °C.

5.2.7 Preparing Stocks of E. coli BL21(DE3) Containing pET–15b–PaODC or pET–15b–CpODC

Cultures of the relevant *E. coli* cells were grown in LB+AMP medium (5 mL), to approximately linear log phase (10–14 h), and subsequently added to a heat-sterilised solution of glycerol (50%) in distilled deionised water (ddH_2O), at a ratio of 1:4 (v/v), and stored at −80 °C.

5.2.8 Cultivating, Harvesting, and Storing E. coli BL21(DE3) cells for Protein Purification

LB+AMP medium (5 mL) was inoculated from a glycerol stock of transformed *E. coli* BL21(DE3) cells, and incubated overnight on a rotary shaker (210 RPM, 37 °C). The resulting culture was diluted with additional LB+AMP medium (1 L), and incubated for a further 10–14 h (as before). Then the culture was infused with IPTG (1 mL of stock) and additional ampicillin (1 mL of stock), and incubated for a final 3–7 h (as before). Following incubation, the culture was chilled to ~ 4 °C, split into identical portions (by mass, to the nearest 0.1 g), and subjected to centrifugation (11385 × *g*, 4 °C, 10 min). The resulting supernatants were decanted and discarded, before the pellets were resuspended in binding buffer (~ 200 mL, 4 °C), combined into a single vessel, and subjected to centrifugation for a further 10 min (11385 × *g*, 4 °C). The supernatant was again decanted from the pellet. This pellet was stored at −20 °C, for use in protein purification.

5.2.9 Isolating Recombinant Pa-, and CpODCase from E. coli Cells

Unless otherwise mentioned, all steps were carried out at 4 °C. Purification of recombinant Pa- and CpODCase was conducted using procedures analogous to those previously established (Toth *et al*., 2009), from *E. coli* BL21(DE3) cells that were harvested as described above (see § 5.2.8). His•Bind columns for protein purification were prepared as follows: first, the columns were packed with 3 cm^3 of His•Bind resin, then washed with ddH_2O (10 mL), charged with a nickel sulfate solution (50 mM, 7 mL), and subsequently equilibrated with binding buffer (50 mL), in similar fashion to the instructions provided by Novagen (1997). A pellet of harvested *E. coli* cells was thawed until the colour of the pellet changed from brown to yellow, then suspended in binding buffer (30 mL). The suspended cells were lysed using a Branson-brand sonifier (output control set to 5; duty cycle set to 40%; 5 sets of 20 pulses, separated by 20 s intermissions). Subsequent centrifugation (288,000 × *g*, 30 min) separated the viscous cell lysate from insoluble cellular debris. This clarified cell lysate was loaded onto a His•Bind column, where soluble Pa-, or $CpODCase_{+tag}$, were purified using Ni^{2+}-affinity chromatography. The His•Bind column was loaded with a procession of buffers (see Table 5.1): binding buffer (~ 45 mL), then wash buffer (~ 25 mL), and strip buffer (~ 10 mL). Upon addition of the strip buffer, 5–7 mL of the ensuing eluent was collected and dialysed against assay buffer or cleavage buffer (500 mL, two iterations, 6 h each), depending on need. In lieu of an intervening proteolytic-cleavage step, the purified protein was immediately separated into aliquots, and stored at −20 °C.

5.2.10 Determining the Solution-Concentration of ODCase

The concentration of an ODCase-variant was determined by measuring the UV absorption of the solution at 280 nm (A_{280}) and comparing it to the predicted extinction coefficient (ϵ_{280}) of PaODCase (8480 $M^{-1}cm^{-1}$) and CpODCase (15470 $M^{-1}cm^{-1}$). Predicted ϵ_{280} values were calculated using the "ProtParam" tool on the ExPASy website (http://web. expasy. org/protparam/) assuming no disulfide bonds. The precise concentration was determined using the Beer–Lambert–Bouguer law (Beer, 1852; Lambert, 1760; Bouguer, 1729) (eqn. 5.1; c is the molarity, b is the pathlength [in cm]). It was assumed that the only enzyme present in solution was ODCase, on the basis of the SDS–PAGE results (see § 5.2.11)

$$c = A_{280} / (b \cdot \varepsilon_{280}) \tag{5.1}$$

5.2.11 Qualitative Assessment of Protein-Content Using SDS-PAGE

Gels were cast from 29:1 acrylamide:bis–acrylamide to give a 15% resolving gel (0.4-M Tris–HCl, pH 8.8, 1‰ SDS), beneath a 5% stacking gel (0.06-M Tris–HCl, pH 6.8, 1‰ SDS). Electrophoresis was conducted with a constant voltage (30 V for stacking gel, 75 V for resolving), in a bath of SDS-PAGE running buffer. Following electrophoretic separation, the polyacrylamide gel was developed in a Coomassie Brilliant Blue R–250 staining solution (0.25% R–250, 10% acetic acid, 45% methanol) for 10 min. The staining solution was decanted and replaced with a destaining solution (10% acetic acid, 45% methanol). The gel was developed for ~ 1

h in this destaining solution, and for another ~ 1 h in a fresh destaining solution. If required, the gel was developed further in distilled water for 16–24 h, or as long as required to bring the background to consistent colour and clarity.

5.2.12 Removing the Hexahistidine Tag from Pa-, and CpODCase$_{+tag}$

A solution of purified Pa-, or CpODCase$_{+tag}$, was incubated with biotinylated thrombin (0.5 U per 1 mg of ODCase), at 4 °C, in cleavage buffer, with gentle rocking, overnight. Then, streptavidin agarose beads were added (5.0 μL of settled volume, per milligram of purified enzyme), and incubation continued for a further 30 min (as before). Following incubation, the solution was vacuum filtered, and transferred to a dialysis bag (MWCO 12,000–14,000). Dialysis was conducted against assay buffer or start buffer (500 mL, two iterations, 6 h each), depending on need. In lieu of an additional purification step, the purified protein was immediately separated into aliquots, and stored at −20 °C.

5.2.13 Assaying the Extent of Thrombin–Cleavage

Succeeding the initial purification-stage (see § 5.2.9), two 20-μL aliquots of the purified CpODCase$_{+tag}$ were removed, and set aside: one at 4 °C, the other at −20 °C. To the remaining CpODCase$_{+tag}$, biotinylated-thrombin was added (0.5 U per 1 mg of CpODCase$_{+tag}$), and the solution was gently rocked at 4 °C. At various intervals, two additional 20-μL aliquots were removed, combined with SDS-PAGE loading buffer (5 μL), boiled for 5 min, and set aside: one at 4 °C, and the other at −

20 °C. The aliquots to be kept at − 20 °C were placed into 1.5-mL vessels, and rapidly cooled to − 20 °C in pre-cooled acetone, prior to storage. Finally, the first two aliquots were combined with SDS-PAGE loading buffer, then all the aliquots were boiled for 5 min, and subsequently analysed using SDS-PAGE (see § 5.2.11).

5.2.14 Purifying CpODCase$_{-tag}$

A 5-mL HiTrap fast-flow anion-exchange column was connected to an ÄKTA FPLC and used under recommended conditions (Toth *et al*., 2009). The column was pre-equilibrated with FPLC start buffer (25 mL), loaded with the cleavage products, and washed with additional FPLC start buffer (40 mL). A gradient elution, with FPLC purge buffer (0−100% over 100 mL), was monitored *via* two in-line sensors: a conductivity detector and a UV spectrophotometer (280 nm). During elution, fractions (10 mL) were collected, and those fractions having the largest UV-absorption peak were pooled, transferred to a dialysis bag (MWCO 12,000−14,000), dialysed against assay buffer (500 mL, two iterations, 6 h each), separated into aliquots (400 μL), and stored at −20 °C.

5.2.15 CD-Spectra of ODCase-Variants

In each case, an aliquot of purified Pa- or CpODCase in assay buffer was transferred to a quartz cuvette (1 mm pathlength) that had been previously incubated in the CD-spectropolarimeter until it reached the same temperature as the enzyme aliquot. Care was taken to ensure that the concentration of enzyme used gave a

reading from the photodiode that was within its detection-limit (<700 mV) through the range 190–260 nm. The spectra were collected six times using the following instrument settings: 190–260 nm, 20 nm/min scanning speed, 1 nm bandwidth, 1 s response time, and "high" sensitivity. The spectra were averaged and reported after subtraction of a zero spectrum obtained in precisely the same manner, but using assay buffer (the zero spectrum was never observed to contribute to the ultimate spectrum).

5.2.16 Protein Melting Studies

A pair of 400-μL aliquots of PaODCase$_{-tag}$ or CpODCase$_{-tag}$ were incubated at a set temperature for a period of time ranging from 48 h to 28 d. At various intervals, a portion (100 μL) of the aliquot was removed and its CD-spectra were obtained (6 exposures, same settings as in § 5.2.15) at the incubation temperature. The portion was then diluted five-fold, and the concentration of protein was determined using UV–vis spectrophotometry (see § 5.2.10). Once melting appeared to reach equilibrium, the last six iterations were combined, and the molar ellipticities ([θ]) were calculated using eqn. 5.2. In eqn. 5.2, θ is the ellipticity (in mdeg) at a particular temperature, c is the concentration of protein (in M), and l is the pathlength (in cm). The extent of α–helical character, measured using the molar ellipticity at 222 nm, was used to define structural integrity of ODCases. Using a two-state model of unfolding, the melting temperature, T_m, was defined as the temperature at which the molar ellipticity is the average of the molar ellipticities of the folded and unfolded states, $[\theta]_f$ and $[\theta]_u$, respectively. These parameters were determined by plotting $[\theta]_{222}$

as a function of incubation temperature, *T*, and then fitting to eqn. 5.3 (adapted from the work of Greenfield [2007]) using non-linear regression analysis. The index, α, is a dimensionless value, and is defined in eqn. 5.4a, 5.4b, and 5.4c. K_f is the equilibrium established between the folded and unfolded states, F and U, respectively.

$$[\theta] = \frac{\theta}{10 \cdot l \cdot c} \tag{5.2}$$

$$[\theta]_{222} = [\theta]_u + \frac{[\theta]_f - [\theta]_u}{1 + (T/T_m)^{\alpha}} \tag{5.3}$$

$$\alpha = \log_{(T/Tm)} K_f \tag{5.4a}$$

$$(T/T_m)^{\alpha} = K_f \tag{5.4b}$$

$$K_f = [F]/[U] \tag{5.4c}$$

5.2.17 Measuring Pa-, and CpODCase-Activity

Unless otherwise mentioned, Pa-, and CpODCase-activity was assessed as described in this section. Disappearance of OMP was measured using a continuous spectrophotometric assay (0.1–0.5 s data-collection intervals) by following the decrease in absorption at a wavelength of 279 nm, resulting from the conversion of OMP to UMP (Toth *et al*., 2009) (for the difference between the extinction coefficiens

of OMP and UMP, $\Delta\epsilon_{279}$, see § 5.2.20). A 1.5 mL microcentrifuge tube, containing a frozen aliquot of purified ODCase, was placed in ice until the aliquot thawed. The aliquot was subsequently diluted with assay buffer (4 °C) to a concentration that produced a rate of ~ 1–2 mAU/s under standard assay conditions, which are defined as: 30 μL of diluted ODCase stock, and 28 μM OMP, in assay buffer (total volume 1 mL) at 25 °C. The ODCase stock was kept on ice during use, and the time-dependent decline of specific activity was assessed by repeating the standard assay in triplicate at the start of the use-period, after every hour of use, and at the conclusion of the use-period; however, no significant decline in activity was noted. The concentration of the active forms of Pa-, or CpODCase was assumed to be equal to the concentration of protein (see § 5.2.10) in the stock of that particular variant that had the highest specific activity under standard assay conditions. All other enzyme concentrations were normalised on the basis of their activity under the same conditions. Each assay involved first placing a 1400–μL quartz cuvette (1–cm pathlength) into the UV–vis spectrophotometer and allowing it to come to the relevant assay temperature over a 1-min incubation period. For assays requiring temperatures of 15 °C or less, quartz cuvettes were kept in a container that was ensconced in ice, when not in use. For assays requiring temperatures greater than 30 °C, quartz cuvettes were embedded into an appropriately-warm sand bath when not in use. A 1-min incubation period was chosen based on measurements of the temperature of water in a cuvette that had been used in the manner described above, for each temperature used. To begin the assay, data collection by the

spectrophotometer was initiated, and diluted Pa-, or CpODCase stock (30 μL) was injected into the cuvette, immediately followed by vigorous injection of the trigger solution: a 970-μL solution that defines the unique conditions of the assay. The trigger solutions were prepared from a concentrated solution of OMP in assay buffer (concentration determined at pH 2, $\epsilon_{266} = 9800$ AU/M·cm [Toth *et al.*, 2009]). Trigger solutions were incubated in a water bath, at the temperature of the assay, prior to use. Care was taken to ensure that the trigger solution was injected at a point immediately above the point at which the ODCase stock was injected, along the same inner surface of the cuvette. This order of addition is critical, as it preserves the active dimeric form in prior investigations with ScODCase, as does the 100 mM NaCl in the assay buffer (Porter & Short, 2000); these factors may of similar concern with Cp-, and PaODCase. The injection sequence was repeated, for each unique experimental condition, using each of three identically-designed quartz cuvettes (*i.e.*, in triplicate). Initial rates of Pa- and CpODCase-catalysed decarboxylation of OMP were determined using the first 7–20 s of smoothly-varying absorption data at a wavelength of 279 nm (A_{279}) by fitting the data with a parabolic function by non-linear regression analysis using *KaleidaGraph* v.3.5 (Synergy Software, Reading, PA). The parabola was then differentiated with respect to time, to determine the slope at the onset of the fit. Using eqn. 5.5a, the rate of UMP-generation (d[UMP]/dt) was calculated from the observed rate data (dA_{279}/dt) and the temperature-adjusted differential between the molar extinction coefficients of OMP ($\epsilon_{279,\,\mathrm{OMP}}$) and UMP ($\epsilon_{279,\,\mathrm{UMP}}$), $\Delta\epsilon_{279}$ (eqn. 5.5b; see also § 5.2.20 and Table 5.4).

$$d[P]/dt = (dA_{279}/dt) / \Delta\varepsilon_{279} \quad (5.5a)$$

$$\Delta\varepsilon_{279} = \varepsilon_{279,\,OMP} - \varepsilon_{279,\,UMP} \quad (5.5b)$$

The concentration of OMP was assumed to be unchanged prior to measurement for all data, excepting the measurements of CpODCase-activity as a function of temperature; in these assays, the concentration of OMP at the onset of the fit was approximated by assuming that the A_{279} was due solely to OMP. A brief, simulated comparison of the former (·····) and latter (– – –) methods of estimating the actual concentration of OMP (——) is shown in Figure 5.1. The dashed line in Panel A was calculated using eqn. 5.6. The lines in Panel B were calculated using eqn. 5.7. This method was chosen to improve precision and accuracy in data collection from the CpODCase assays, without sacrificing efficient workflow. In particular, it was chosen to more accurately define the initial OMP concentration and rate despite the fleeting initial-rate period observed for this enzyme, which was due to a potent combination of high substrate affinity and high catalytic efficiency.

$$\textit{estimated}\ \text{remaining fraction of OMP} \approx \frac{\textit{actual}\ \text{remaining fraction of OMP} \cdot \Delta\varepsilon_{279} + \varepsilon_{279,\,UMP}}{\varepsilon_{279,\,OMP}} \quad (5.6)$$

Figure 5.1 Simulated Comparison of OMP-Concentration Estimates Used in ODCase-Activity Assays

Two methods of estimating the true concentration of OMP (——) are used in CpODCase-activity assays, each based on a distinct set of assumptions: that negligible substrate had depleted prior to measurement (·····), or that negligible product had formed, despite depletion of substrate, prior to measurement (– – –). Panel A and B both compare the predicted estimates of OMP-concentration as the reactions approached their midpoints. Panel A displays the fraction of OMP remaining, and estimated to remain, by each method. Panel B displays the relative magnitude of the overestimates of OMP-concentration resulting from each method. Estimates made by assuming that the rate measurement is begun immediately after the combination of ODCase and OMP (*i.e.*, when negligible substrate has depleted) do not adjust for relatively fast reactions or slow mixing (Panel A); consequently, they overestimate by 100% at the reaction-midpoint (Panel B). Estimates made by assuming that the A_{279} at the start of the fit can be attributed solely to OMP, scale linearly with the reaction progress (Panel A); consequently, they are more accurate (Panel B). Both estimates are overestimates of OMP-concentration, and likely yielded overestimated K_m values. Values of the fraction of OMP remaining in Panel A were calculated using eqn. 5.6. The relative overestimates depicted in Panel B were calculated using eqn. 5.7.

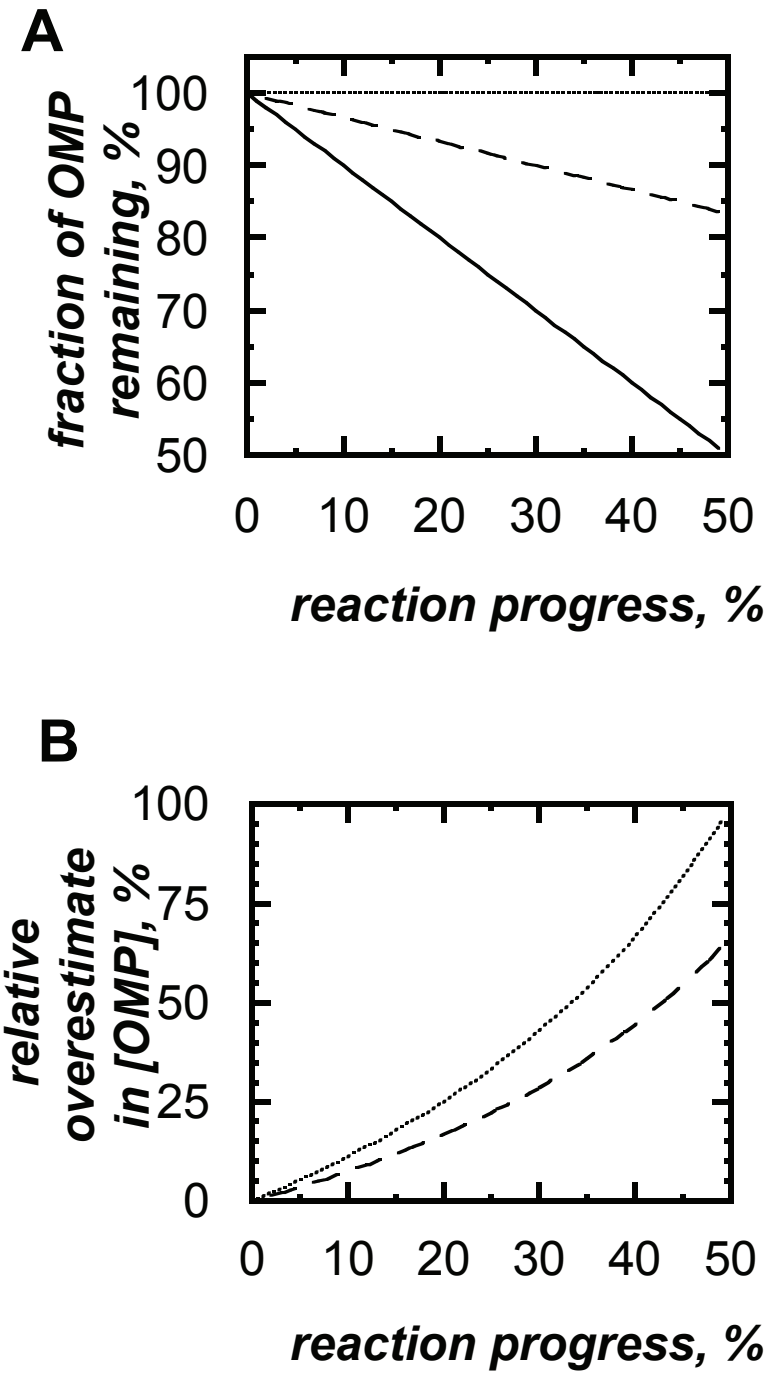
A
fraction of OMP remaining, %
100
90
80
70
60
50
0
10
20
30
40
50
reaction progress, %
B
relative overestimate in [OMP], %
100
75
50
25
0
0
10
20
30
40
50
reaction progress, %

Figure 5.1

$$\text{relative overestimation of [OMP]} = \frac{(\textit{estimated}\text{ remaining fraction of OMP}) - (\textit{actual}\text{ remaining fraction of OMP})}{\textit{actual}\text{ remaining fraction of OMP}} \quad (5.7)$$

5.2.18 Determining the Effect of pH on Pa- and CpODCase-Activity

To assess the effect of pH on Pa-, and CpODCase-activity, an array of trigger solutions (see § 5.2.17) was prepared containing OMP (3.66, 4.39, 5.12, 5.85, 6.58, 7.32, 11.0, 14.6, 29.3, and 58.5 μM), and NaCl (100 mM), over a range of pH values, which were obtained using the buffering agents (10 mM) listed in Table 5.3.

5.2.19 Inhibition of Pa- and CpODCase by UMP

To assess the effect of UMP concentration on Pa- and CpODCase-activity, a set of trigger solutions (see § 5.2.17) was prepared, with identical concentrations of OMP, and varying concentrations of UMP. The assays were conducted under otherwise standard conditions and used to determine values of v_i / v_0 (the fraction of the maximal rate) as a function of UMP-concentration, to determine the IC_{50}-value (*i.e.*, the concentration of UMP [in M] required to achieve 50% activity) and the value of n (the Hill-coefficient of cooperative binding), according to eqn. 5.8 (adapted from Segel [1975]). The plots were fit by non-linear regression analysis using *KaleidaGraph* v.3.5 (Synergy Software, Reading, PA).

$$(v_i / v_0) = (IC_{50})^n / \{(IC_{50})^n + [UMP]^n\} \quad (5.8)$$

Table 5.3

The Six Buffering Agents Used to Control Assay Acidity from pH 6.0 through pH 11.0.

buffering agent	abbreviated name	pH range
2- (*N*-morpholino)ethanesulfonic acid	MES	6.0-6.5
piperazine-*N*,*N*′-bis(2-ethanesulfonic acid)	PIPES	6.5-7.5
4- (2-hydroxyethyl)-1-piperazineethanesulfonic acid	HEPES	7.5-8.5
N-tris(hydroxymethyl)methyl-3-aminopropanesulfonic acid	TAPS	8.5-9.0
N-cyclohexyl-2-aminoethanesulfonic acid	CHES	9.0-10.0
N-cyclohexyl-3-aminopropanesulfonic acid	CAPS	10.0-11.0

5.2.20 Assaying Pa- and CpODCase-Activity as a Function of Temperature

To assess the effect of temperature on Pa- and CpODCase-activity, a set of trigger solutions (see § 5.2.17) was prepared with varying concentrations of OMP, and assays were conducted over a range of temperatures and with the values of $\Delta\epsilon_{279}$, indicated in Table 5.4. The value of $\Delta\epsilon_{279}$ for conversion of OMP to UMP was determined from a pair of linear fits of the data—described by Toth *et al*., (2009)—one from 5–45 °C, and the other from 45–75 °C.

5.2.21 Correlating Pa- and CpODCase Concentration and Activity

A series of dilutions of Pa- and CpODCase were prepared. These dilutions were used in a set of standard assays, at the highest and lowest temperatures (65 and 10 °C for PaODCase and 60 and 10 °C for CpODCase) and OMP concentrations (for PaODCase, 223 and 4.6 μM, and for CpODCase, 142 and 15 μM at 60 °C and 92 and 1.5 μM at 10 °C) used in the assays described above (PaODCase was also assayed at 25 °C). The resulting initial-rate data were plotted against the concentration of ODCase in each assay and fit by linear regression analysis using *KaleidaGraph* v.3.5 (Synergy Software, Reading, PA).

Table 5.4

Values of $\Delta\epsilon_{279}$ for OMP–UMP Adjusted for Assay Temperature[a]

$\Delta\varepsilon_{279}$ ($AU \cdot M^{-1}cm^{-1}$)	temperature (°C)
2249	5
2288	10
2327	15
2367	20
2406	25
2445	30
2484	35
2523	40
2558	45
2584	50
2610	55
2637	60
2664	65
2691	70
2717	75

[a] data obtained from a report by Toth *et al*. (2009).

Chapter 6 SUMMARY, CONCLUSIONS, & FUTURE WORK

This thesis has described my interest in ODCase—an enzyme that is unique and remarkable in its own right—as a model enzyme for better understanding the catalytic strategies used by psychrozymes, and extremozymes in general. It described the kinetic, thermodynamic, and characterisation of two putative psychrozymes, Pa- and CpODCase. The characteristics of these enzymes are considered in the greater context of ODCase-variants as a whole, using existing data from Ec-, Sc-, Mt-, and HsODCase, to compare and contrast the catalytic and structural strategies used by each. The most obvious revelations have come from comparison of the thermodynamics of ODCase-mediated decarboxylation, where it was shown that reduction of $\Delta G_{es}^{\ddagger}$, $\Delta H_{es}^{\ddagger}$, $\Delta S_{es}^{\ddagger}$, ΔH_{tx}, and ΔS_{tx}—and thus magnification of k_{cat}—was the most consistent mark of a psychrozyme. Adaptation to low-temperature was also linked to low thermal stability, as defined by the structural melting transition, T_m. However, identification of further trends was limited by the the number of ODCase variants in my data set, and by the absence of 3D structural data.

In order to proceed with the task of identifying precise strategies for design of enzymes, particularly for use at the extremes of temperature, larger data-sets are required. Larger data-sets would test the validity, and the significance, of the trends observed herein. Although large-scale comparisons of structural and kinetic data have been attended to, they typically concern only a few variants of each enzyme. Thus, an obvious directive is to characterise a large number of variants of the same

enzyme. ODCase makes a good candidate, both because of the exaggerated features it is expected to possess, which enable it to catalyse its reaction with remarkably high proficiency, and because of the long-standing interest in its precise mechanism of action. These comparisons would also be facilitated by additional structural data and computational explorations of the particular structural elements found therein. Once trends have been more confidently identified, the next step should be to confirm these trends by attempting to bestow the properties of one ODCase-variant on another by exchanging amino acids using site-directed mutagenesis. Ultimately, through examinations such as these, a greater mastery of enzyme mechanism and architecture may be achieved.

Appendix: Precursory Kinetic Data and Consolidated Kinetic Constants Underlying and Describing the pH- and *T*-Dependence of Catalysis by Pa- and CpODCase

On the pages of the appendix that follows are plots baring those v_i-values used to derive pK_a-values of PaODCase (Figure A.1), and CpODCase (Figure A.2), and those v_i-values used to parametrize the thermodynamics of catalysis by these enzymes (Figure A.3, and A.4, respectively). Also found herein are servicable data derived from previously reported kinetic assays of Sc-, Mt-, and EcODCase (Toth *et al*., 2009), collected for convenient reference in Table A.2. Finally, the myriad individual v_i-values comprising Figure A.4 have been compiled, and organised for clarity, in Table A.4.

Table A.1
Kinetic and equilibrium constants, of PaODCase and CpODCase, as a function of temperature.

	PaODCase				CpODCase			
T, °C	k_{cat}, s^{-1}	K_m, μM	$1/K_{tx}$, M^{-1}	k_{cat}/K_m, $\times 10^6$ $M^{-1}s^{-1}$	k_{cat}, s^{-1}	K_m, μM	$1/K_{tx}$, M^{-1}	k_{cat}/K_m, $\times 10^6$ $M^{-1}s^{-1}$
10	13.37 ± 0.55	6.45 ± 0.590	(4.15 ± 0.42) × 10^{23}	2.07 ± 0.21	21.27 ± 0.69	2.42 ± 0.44	(1.76 ± 0.33) × 10^{24}	8.8 ± 1.6
15	13.93 ± 0.85	3.21 ± 0.475	(2.16 ± 0.35) × 10^{23}	4.33 ± 0.69	37.1 ± 1.0	4.03 ± 0.49	(4.60 ± 0.57) × 10^{23}	9.2 ± 1.1
20					50.9 ± 2.2	5.53 ± 0.91	(1.20 ± 0.20) × 10^{23}	9.2 ± 1.6
25	36.6 ± 7.5	20.0 ± 8.96	(6.5E ± 3.2) × 10^{21}	1.83 ± 0.90	59.9 ± 2.5	3.38 ± 0.73	(6.3 ± 1.4) × 10^{22}	17.7 ± 3.9
30	38.4 ± 3.4	9.2 ± 1.70	(4.23 ± 0.86) × 10^{21}	4.16 ± 0.85	87 ± 26	3.55 ± 0.53	(2.49 ± 0.84) × 10^{22}	24.5 ± 8.3
35	49.3 ± 6.3	20.9 ± 5.26	(7.14 ± 0.20) × 10^{20}	2.36 ± 0.67	106.0 ± 4.6	5.3 ± 1.1	(6.1 ± 1.3) × 10^{21}	20.0 ± 4.2
40	62.4 ± 9.1	12.4 ± 2.36	(4.70 ± 0.11) × 10^{20}	5.0 ± 1.2	158 ± 40	4.8 ± 3.1	(3.1 ± 2.1) × 10^{21}	33 ± 23
45	86 ± 18	22.8 ± 6.24	(1.14 ± 0.39) × 10^{20}	3.8 ± 1.3	182.2 ± 6.7	4.40 ± 0.87	(1.24 ± 0.25) × 10^{21}	41.4 ± 8.3
50	86.4 ± 9.8	20.3 ± 4.79	(4.2 ± 1.1) × 10^{19}	4.3 ± 1.1	225.0 ± 6.9	6.38 ± 0.98	(3.51 ± 0.55) × 10^{20}	35.3 ± 5.5
55	138 ± 31	52 ± 15.0	(9.0 ± 3.3) × 10^{18}	2.64 ± 0.96	250 ± 17	12.9 ± 3.4	(6.6 ± 1.8) × 10^{19}	19.4 ± 5.3
60	91 ± 14	21.6 ± 5.9	(5.1 ± 1.6) × 10^{18}	4.2 ± 1.3	280 ± 18	11.5 ± 3.0	(2.95 ± 0.79) × 10^{19}	24.4 ± 6.5
65	211 ± 50	98 ± 31.8	(9.5 ± 3.8) × 10^{17}	2.15 ± 0.86				

Table A.2
Kinetic and equilibrium constants[a], of Sc-, Mt-, and EcODCase, as a function of temperature.

	ScODCase				MtODCase				EcODCase
T, °C	k_{cat}, s^{-1}	K_m, μM	$1/K_{tx}$, M^{-1}	k_{cat}/K_m, $\times 10^6$ $M^{-1}s^{-1}$	k_{cat}, s^{-1}	K_m, μM	$1/K_{tx}$, M^{-1}	k_{cat}/K_m, $\times 10^6$ $M^{-1}s^{-1}$	k_{cat}, s^{-1}
5	3.1 ± 0.5	1.1 ± 0.2	(2.28 ± 0.16)× 10^{24}	2.7 ± 0.2	0.64 ± 0.03	1.1 ± 0.4	(5.0 ± 1.8)× 10^{23}	6.0 ± 2.2	2.5 ± 0.1
10	4.6 ± 0.6	1.4 ± 0.2	(6.41 ± 0.40)× 10^{23}	3.2 ± 0.2					3.7 ± 0.1
12	5.1 ± 0.5								
15	6.9 ± 0.9	1.2 ± 0.2	(2.79 ± 0.19)× 10^{23}	5.6 ± 0.4	2.0 ± 0.3	1.5 ± 0.3	(6.99 ± 0.99)× 10^{22}	1.4 ± 0.2	6.4 ± 0.1
17	7.8 ± 0.8								
25	15 ± 1	1.4 ± 0.2	(3.92 ± 0.35)× 10^{22}	1.1 ± 0.1	4.7 ± 0.3	1.5 ± 0.2	(1.10 ± 0.10)× 10^{22}	3.1 ± 0.3	13 ± 1
35	27 ± 1	1.6 ± 0.4	(5.1 ± 1.2)× 10^{2}	1.7 ± 0.4	11 ± 1	2.8 ± 0.6	(1.27 ± 0.27)× 10^{21}	4.2 ± 0.9	23 ± 1
45	45 ± 4	3.3 ± 0.6	(4.19 ± 0.59)× 10^{20}	1.4 ± 0.2	24 ± 2	4.8 ± 1.4	(1.49 ± 0.38)× 10^{20}	5.0 ± 1.3	35 ± 1
50	59 ± 6	7.9 ± 0.9	(7.45 ± 0.29)× 10^{19}	7.5 ± 0.3					
55					44 ± 2	7.3 ± 1.1	(2.08 ± 0.30)× 10^{19}	6.1 ± 0.9	

[a] Values of k_{cat} and K_m are from Toth, *et al.* (2009)

Table A.3
Apparent kinetic and equilibrium constants, of PaODCase and CpODCase, as a function of pH.

buffer and pH	PaODCase			CpODCase		
	k_{cat}, s^{-1}	K_m, μM	k_{cat}/K_m, $M^{-1}s^{-1}$	k_{cat}, s^{-1}	K_m, μM	k_{cat}/K_m, $M^{-1}s^{-1}$
MES						
6	13.2 ± 1.1	12.9 ± 2.9	1.02 ± 0.26			
6.5	19.7 ± 1.7	10.8 ± 2.3	1.82 ± 0.45			
PIPES						
6.5	22.00 ± 0.62	6.83 ± 0.52	3.22 ± 0.29	68 ± 30	290 ± 220	0.23 ± 0.20
7	25.5 ± 1.2	4.53 ± 0.66	5.62 ± 0.97	58.1 ± 2.9	17.1 ± 2.4	3.38 ± 0.47
7.5	28.9 ± 2.0	5.9 ± 1.2	4.9 ± 1.2	56.2 ± 2.6	14.8 ± 1.9	3.79 ± 0.53
HEPES						
7.5	28.2 ± 1.3	7.06 ± 0.88	4.00 ± 0.54	62.4 ± 3.1	10.5 ± 1.7	5.9 ± 1.0
8	28.1 ± 2.0	9.1 ± 1.5	3.10 ± 0.56	68.0 ± 2.8	9.04 ± 1.1	7.5 ± 1.0
8.5	38.0 ± 2.5	7.9 ± 1.3	4.79 ± 0.94	63.7 ± 4.4	4.6 ± 1.5	13.8 ± 5.2
TAPS						
8.5	30.0 ± 1.4	6.63 ± 0.86	66.3 ± 6.9	66.3 ± 6.9	5.9 ± 2.6	11.0 ± 5.8
9	26.7 ± 1.4	8.6 ± 1.1	60.3 ± 1.7	60.3 ± 1.7	4.24 ± 0.61	14.2 ± 2.2
CHES						
9	25.5 ± 1.4	7.4 ± 1.0	67.8 ± 2.3	67.8 ± 2.3	8.2 ± 1.1	8.2 ± 1.1
9.5	22.1 ± 1.1	9.8 ± 1.2	68.0 ± 6.9	68.0 ± 6.9	16.8 ± 5.8	4.04 ± 1.5
10				79.9 ± 7.2	40.3 ± 8.3	1.98 ± 0.45
CAPS						
10				63.4 ± 2.3	18.9 ± 2.3	3.34 ± 0.46
10.5				46.1 ± 5.8	44 ± 13	1.03 ± 0.33
11				17.3 ± 2.6	45 ± 17	0.38 ± 0.15

Figure A.1 Results of PaODCase Kinetic Assays Conducted at pH 6.0–9.5
The activitiy of PaODCase (25 nM [panel A and E], 28 nM [panel B–D, and H], 30 nM [panel F], 33 nM [panel G], 27 nM [panel I], 31 nM [panel J and K], or 32 nM [panel L]) was assayed as a function of OMP concentration (6.58, 7.32, 11.0, 14.6, 29.3, and 58.5 μM [panel A]; 3.66, 4.39, 5.12, 5.85, 6.58, 7.32, 11.0, 14.6, 29.3, and 58.5 μM [panel B–H, and J]; 4.39, 5.12, 5.85, 6.58, 7.32, 11.0, 14.6, 29.3, and 58.5 μM [panel I and K]; or 5.12, 5.85, 6.58, 7.32, 11.0, 14.6, 29.3, and 58.5 μM [panel L]) over a range of pH values (6.0 [panel A], 6.5 [panel B and C], 7.0 [panel D], 7.5 [panel E and F], 8.0 [panel G], 8.5 [panel H and I], 9.0 [panel J and K], 9.5 [panel L]). The reactions contained NaCl (100 mM) and either MES (10 mM; panel A and B), PIPES (10 mM; panel C, D, and E), HEPES (10 mM; panel F, G, and H), TAPS (10 mM; panel I and J), or CHES (10 mM; panel K and L). Initial-rate kinetic data were fit to eqn. 1.9 by non-linear regression analysis using *KaleidaGraph* v.3.5 (Synergy Software, Reading, PA). v_i is the initial rate determined by fitting the corresponding progress curve with a parabolic function. The parameter m_1 corresponds to the apparent V_{max} (in μM/s), and m_2 corresponds to the apparent K_m (in μM). The apparent k_{cat} was obtained by dividing the apparent V_{max} by the normalised concentration of ODCase. The values of apparent k_{cat}, K_m, and k_{cat}/K_m are given in Table 2.1, and the detailed experimental conditions are as described in § 5.2.17 and 5.2.18.

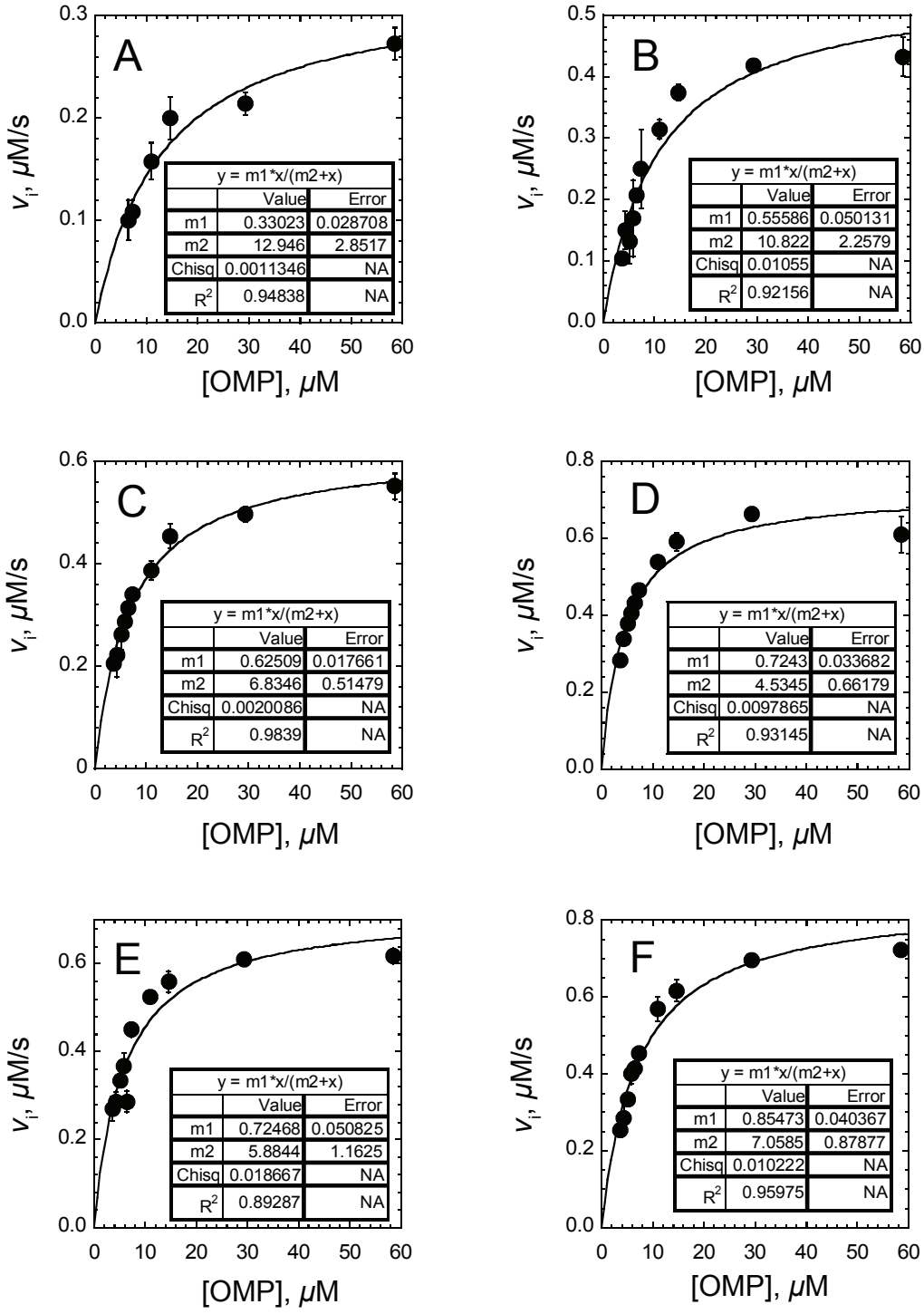

Figure A.1 (page 1 of 2)

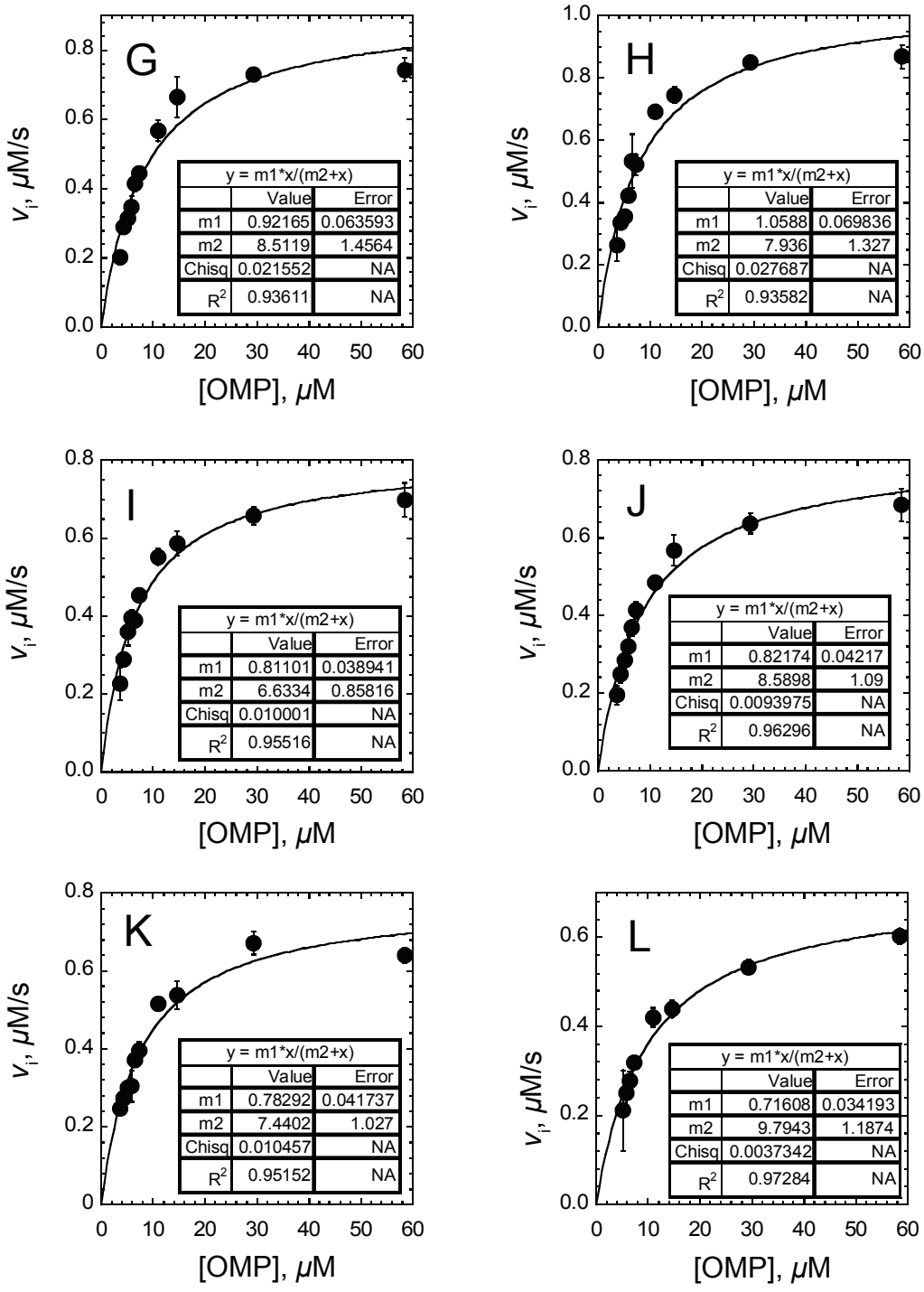

Figure A.1 (page 2 of 2)

Figure A.2 Results of CpODCase Kinetic Assays Conducted at pH 6.5–11.0
The activitiy of CpODCase (16 nM [panel A, D, E, H, J, and N], 17 nM [panel B], 19 nM [panel C and G], 15 nM [panel F and K], 18 nM [panel I], or 14 nM [panel L and M]) was assayed as a function of OMP concentration (38.0, 57.0, 76.0, and 152 μM [panel A]; 2.30, 4.60, 9.20, 13.8, 18.4, 23.0, 34.5, 46.0, 92.0 μM [panel B–E]; 2.70, 5.40, 10.8, 16.2, 21.6, 27.0, 40.5, 54.0, 108 μM [panel F–I]; 4.05, 8.10, 16.2, 24.3, 32.4, 40.5, 60.8, 81.0, and 162 μM [panel J–L]; 8.10, 16.2, 24.3, 32.4, 40.5, 60.8, 81.0, and 162 μM [panel M]; or 5.58, 11.2, 22.3, 33.5, 44.6, 55.8, 83.7, 112, and 223 μM) [panel N] over a range of pH values (6.5 [panel A], 7.0 [panel B], 7.5 [panel C and D], 8.0 [panel E], 8.5 [panel F and G], 9.0 [panel H and I], 9.5 [panel J], 10.0 [panel K and L], 10.5 [panel M], and 11.0 [panel N]). The reactions contained NaCl (100 mM) and either PIPES (10 mM; panel A–C), HEPES (10 mM; panel D–F), TAPS (10 mM; panel G and H), CHES (10 mM; panel I–K), or CAPS (10 mM; panel L–N). Initial-rate kinetic data were fit to eqn. 1.9 by non-linear regression analysis using *KaleidaGraph* v.3.5 (Synergy Software, Reading, PA). v_i is the initial rate determined by fitting the corresponding progress curve with a parabolic function. The parameter m_1 corresponds to the apparent V_{max} (in μM/s), and m_2 corresponds to the apparent K_m (in μM). The apparent k_{cat} was obtained by dividing the apparent V_{max} by the normalised concentration of ODCase. The values of apparent k_{cat}, K_m, and k_{cat}/K_m are given in Table 3.1, and the detailed experimental conditions are as described in § 5.2.17 and 5.2.18.

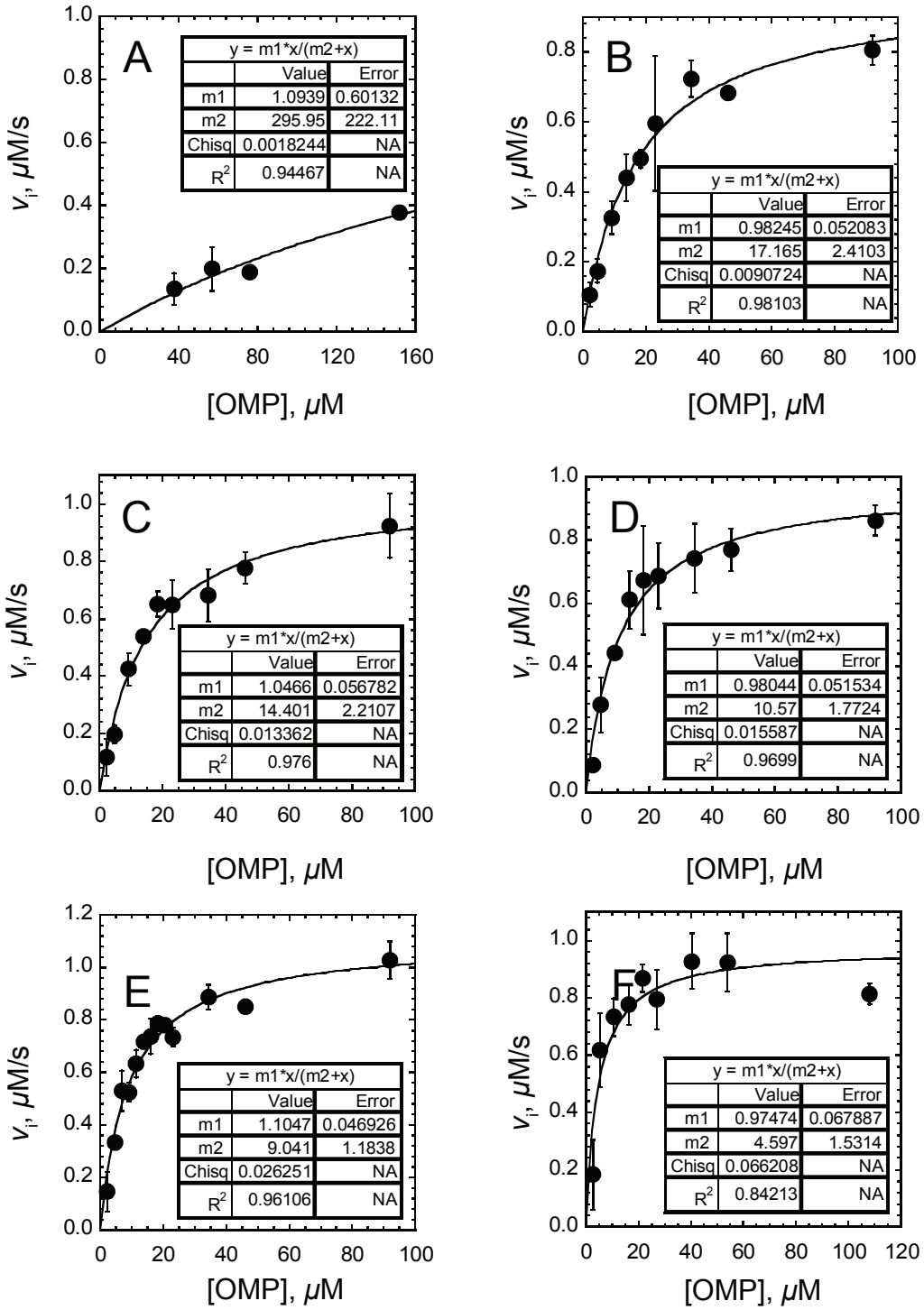

Figure A.2 (page 1 of 3)

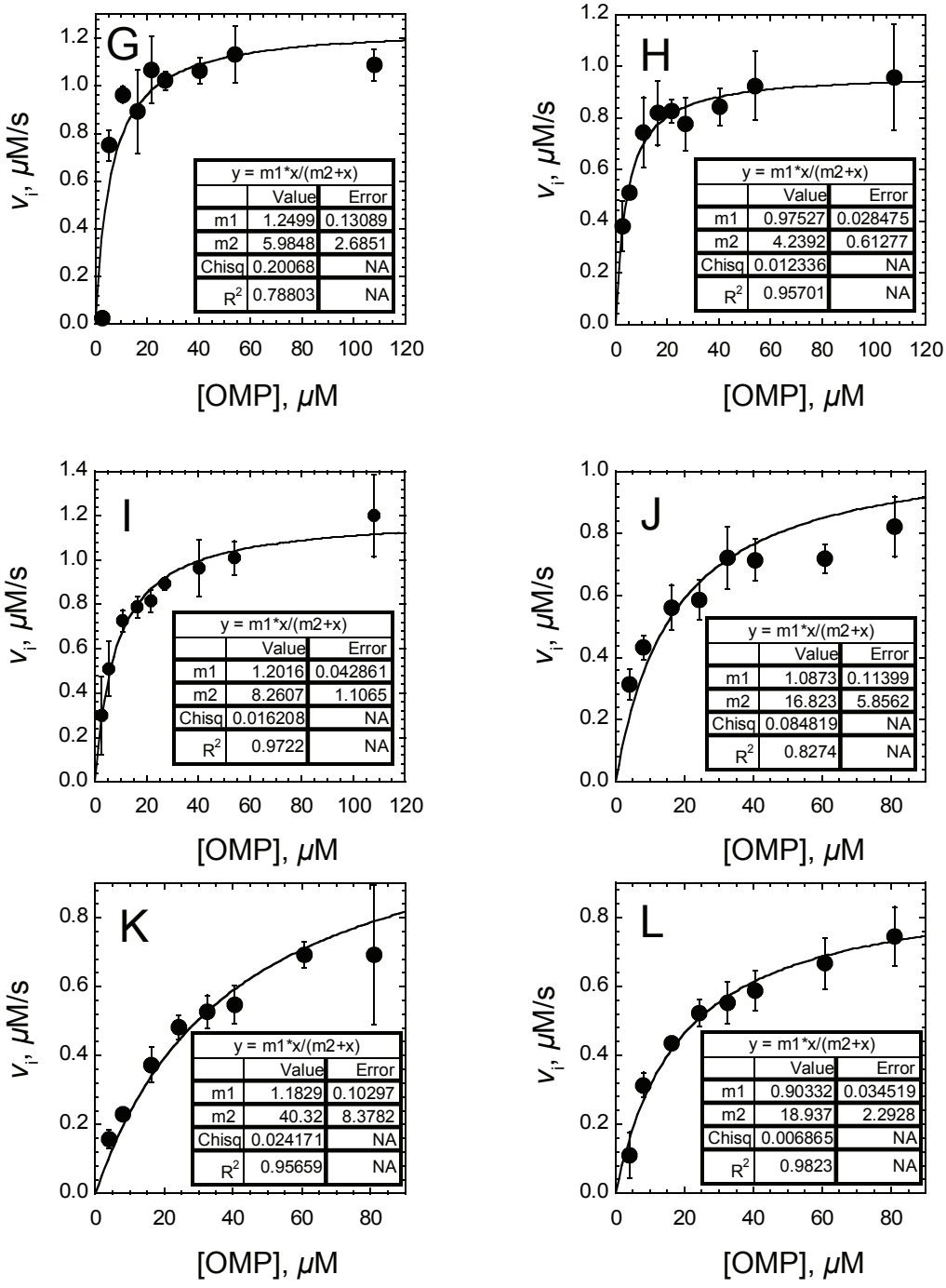

Figure A.2 (page 2 of 3)

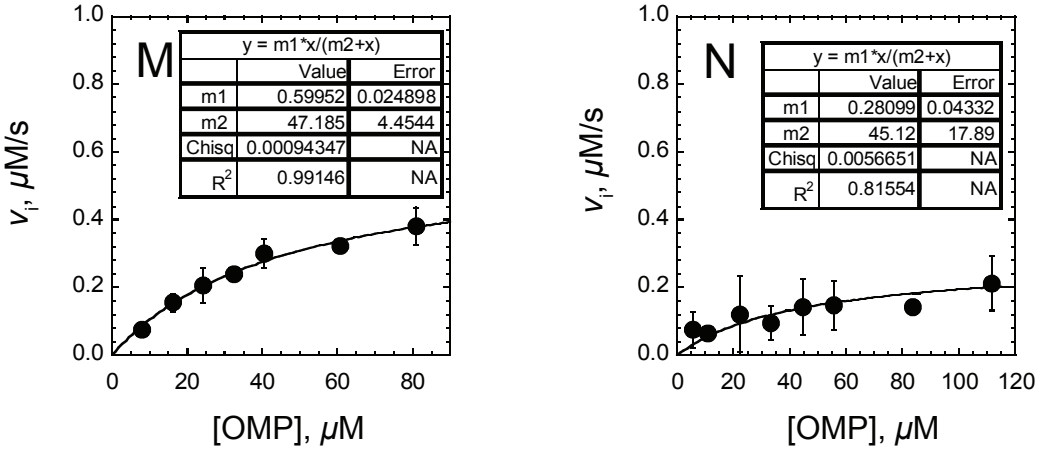

Figure A.2 (page 3 of 3)

Figure A.3 Results of PaODCase Kinetic Assays Conducted at 10–65 °C
The activitiy of PaODCase (28 nM [Panel A], 30 nM [Panel B, C, E], 22 nM [Panel D], 13 nM [Panel F], 27 nM [Panel G, I, K], or 19 nM [Panel H, J]) was assayed as a function of OMP concentration (184, 92.0, 46.0, 23.0, 11.5, 9.2, 6.9, 4.6, 2.3, and 1.15 μM [Panel A]; 117, 58.5, 29.2, 21.9, 14.6, 13.1, 11.7, 10.2, 8.7, 7.3, 5.8, 2.9, and 1.4 μM [Panel B]; 58.5, 29.2, 21.9, 14.6, 13.1, and 11.7 μM [Panel C, F]; 160, 80.0, 40.0, 30.0, 20.0, 18.0, 16.0, 14.0, 12.0, 10.0, 8.0, and 6.0 μM [Panel D]; 58.5, 29.2, 21.9, 14.6, 13.1, 11.7, 10.2, and 8.77 μM [Panel E]; 117.0, 58.52, 29.26, 21.94, 14.63, 13.16, and 11.70 [Panel G, I]; 117, 58.5, 29.2, 21.9, 14.6, 13.1, and 11.7 μM [Panel H]; 184, 92.0, 46.0, 34.5, 23.0, 20.7, 18.4, and 16.1 μM [Panel J]; 141, 117, 58.5, 29.2, 21.9, 14.6, and 13.1 μM [Panel K]) at a series of temperatures (10 °C [Panel A], 15 °C [Panel B], 25 °C [Panel C], 30 °C [Panel D], 35 °C [Panel E], 40 °C [Panel F], 45 °C [Panel G], 50 °C [Panel H], 55 °C [Panel I], 60 °C [Panel J], and 65 °C [Panel K]). Reactions were conducted in assay buffer (10 mM MOPS, pH 8.0, 100 mM NaCl). Initial-rate kinetic data were fit to eqn. 1.9 by non-linear regression analysis using *KaleidaGraph* v.3.5 (Synergy Software, Reading, PA). v_i is the initial rate determined by fitting the corresponding progress curve with a parabolic function. The parameter m_1 corresponds to the apparent V_{max} (in M/s), and m_2 corresponds to the apparent K_m (in μM). The apparent k_{cat} was obtained by dividing the apparent V_{max} by the normalised concentration of ODCase, as in eq. 1.8. The values of k_{cat}, K_m, $1/K_{tx}$, and k_{cat}/K_m are given in Table A.1, and the detailed experimental conditions are as described in the Materials & Methods (§ 5.2.17 and 5.2.20).

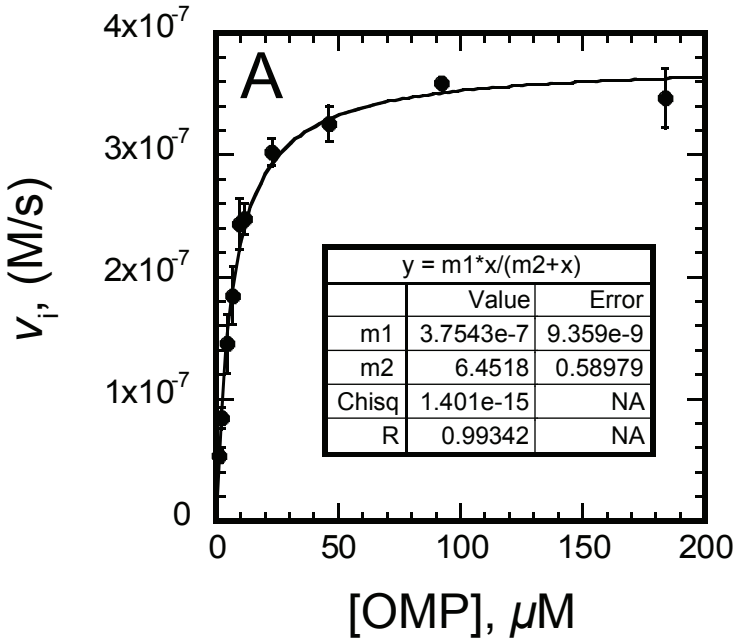

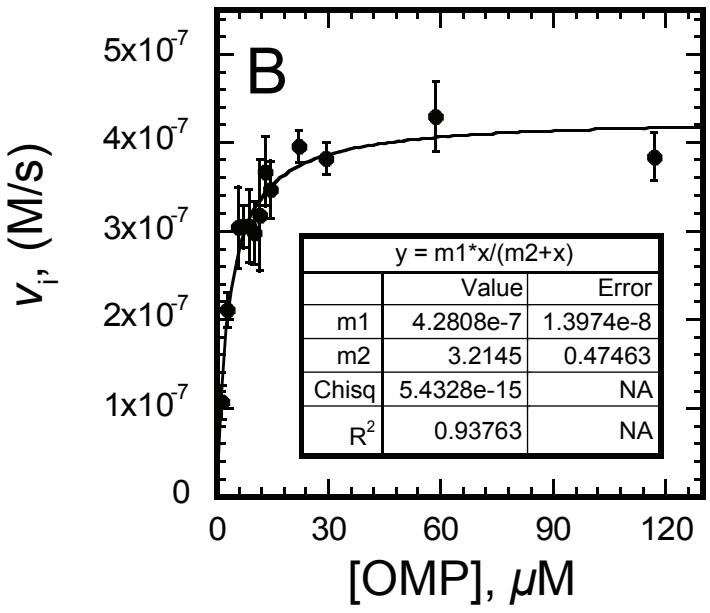

Figure A.3 (page 1 of 6)

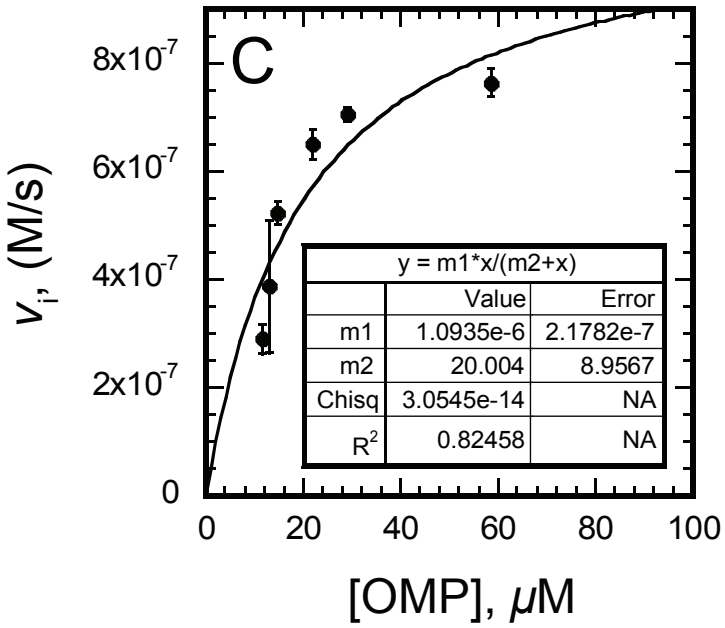

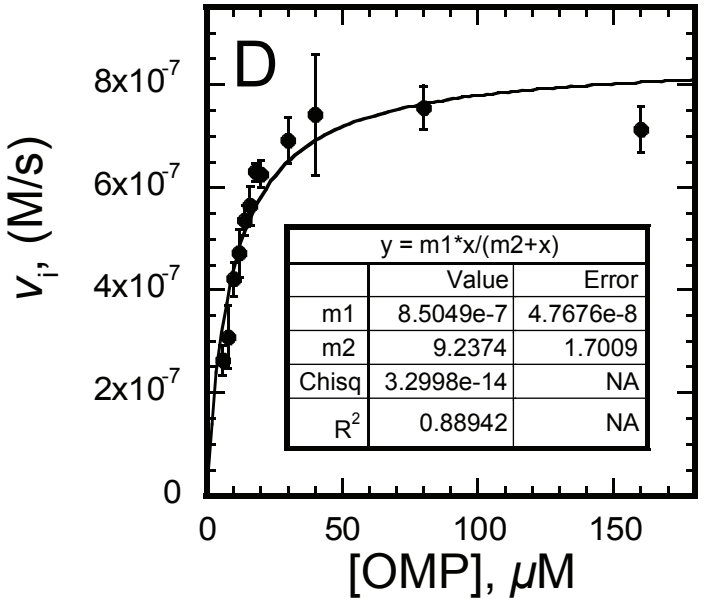

Figure A.3 (page 2 of 6)

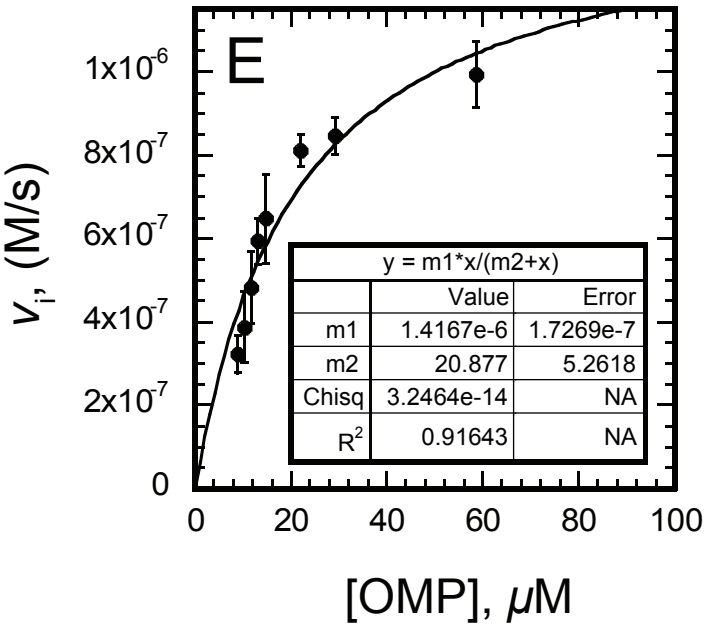

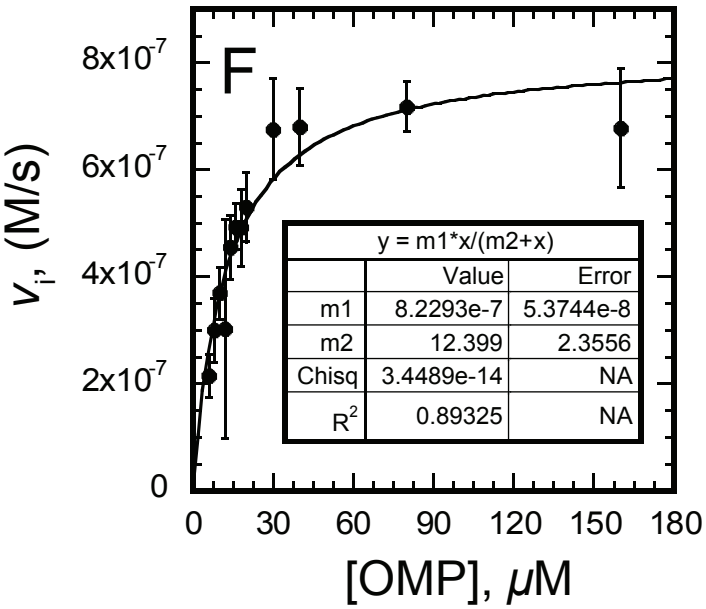

Figure A.3 (page 3 of 6)

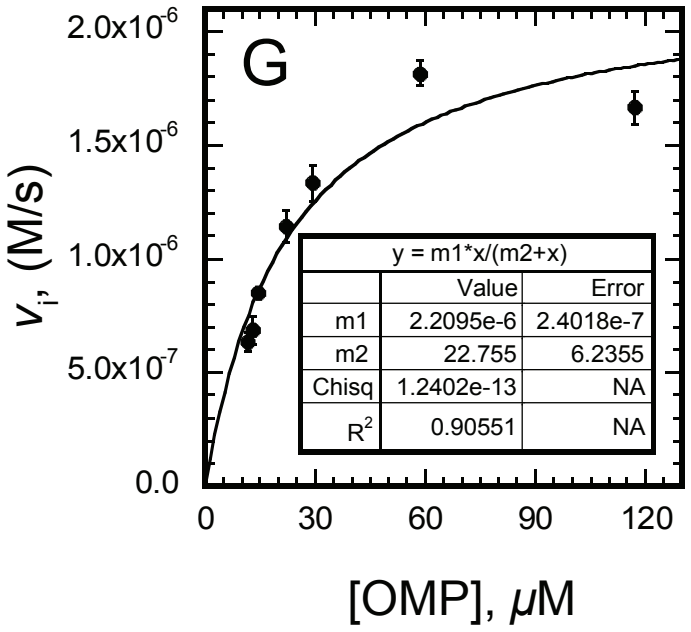

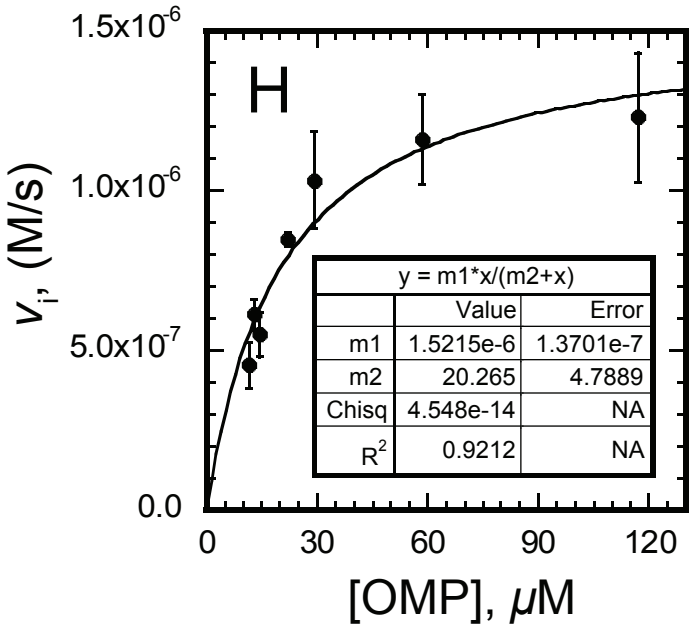

Figure A.3 (page 4 of 6)

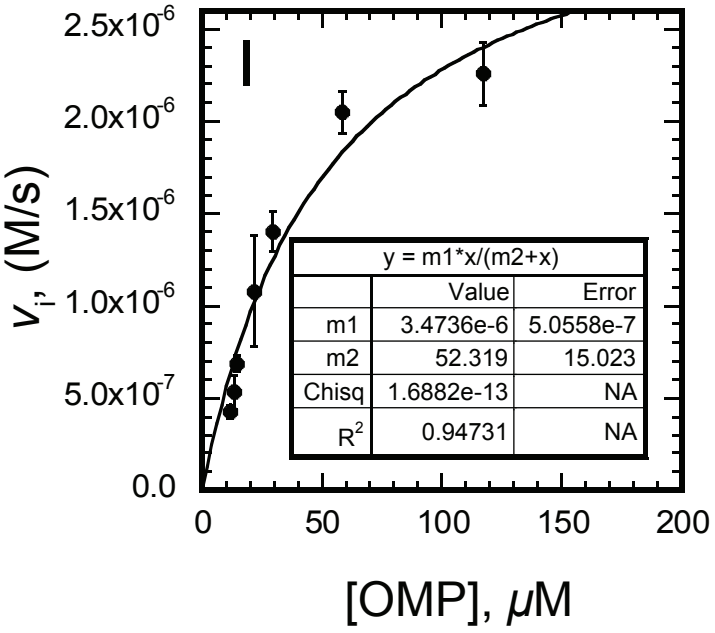

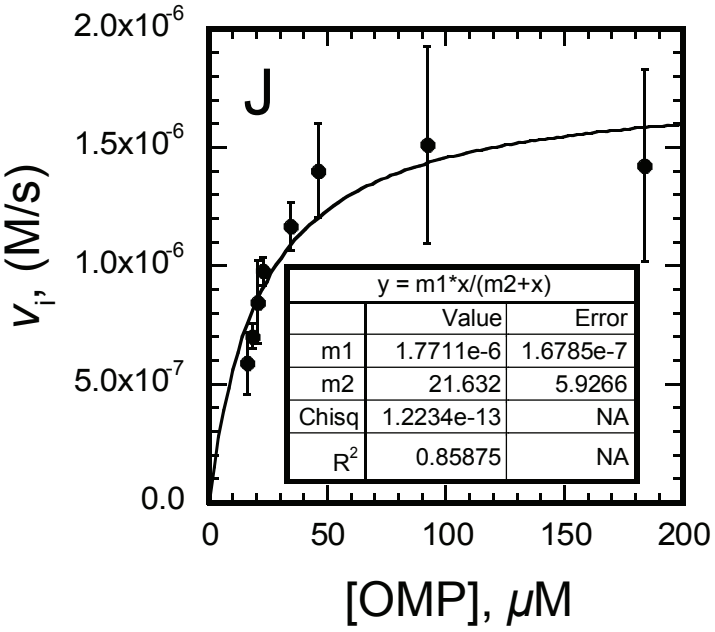

Figure A.3 (page 5 of 6)

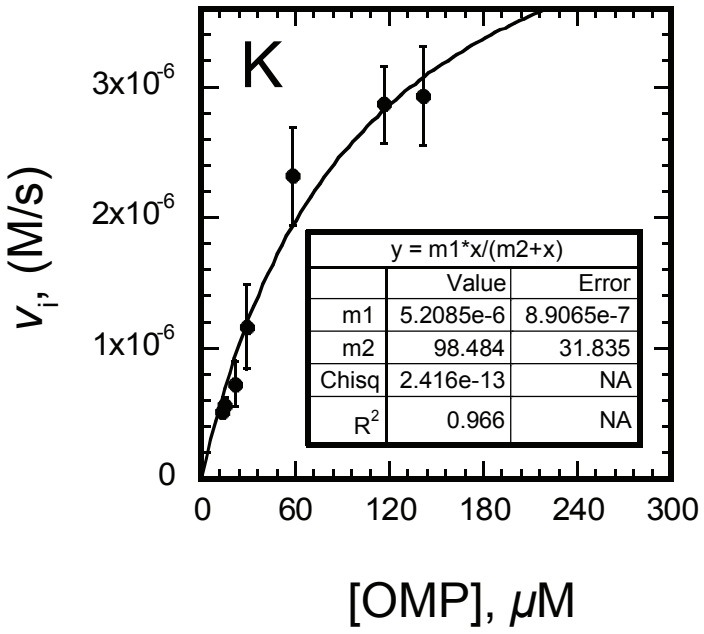

Figure A.3 (page 6 of 6)

Figure A.4 Results of CpODCase Kinetic Assays Conducted at 10–60 °C
The activitiy of PaODCase (19 nM [Panel A], 16 nM [Panel B, C, E, F, J], 17 nM [Panel D, G, K], 14 nM [Panel H], or 15 nM [Panel I]) was assayed as a function of OMP concentration (see Table A.4) at a series of temperatures (10 °C [Panel A], 15 °C [Panel B], 20 °C [Panel C], 25 °C [Panel D], 30 °C [Panel E], 35 °C [Panel F], 40 °C [Panel G], 45 °C [Panel H], 50 °C [Panel I], 55 °C [Panel J], and 60 °C [Panel K]). Reactions were conducted in assay buffer (10 mM MOPS, pH 8.0, 100 mM NaCl). Initial-rate kinetic data were fit to eqn. 1.9 by non-linear regression analysis using *KaleidaGraph* v.3.5 (Synergy Software, Reading, PA). v_i is the initial rate determined by fitting the corresponding progress curve with a parabolic function. The parameter m_1 corresponds to the apparent V_{max} (in M/s), and m_2 corresponds to the apparent K_m (in μM). The apparent k_{cat} was obtained by dividing the apparent V_{max} by the normalised concentration of ODCase, as in eq. 1.8. The values of k_{cat}, K_m, $1/K_{tx}$, and k_{cat}/K_m are given in Table A.1, and the detailed experimental conditions are as described in the Materials & Methods (§ 5.2.17 and 5.2.20).

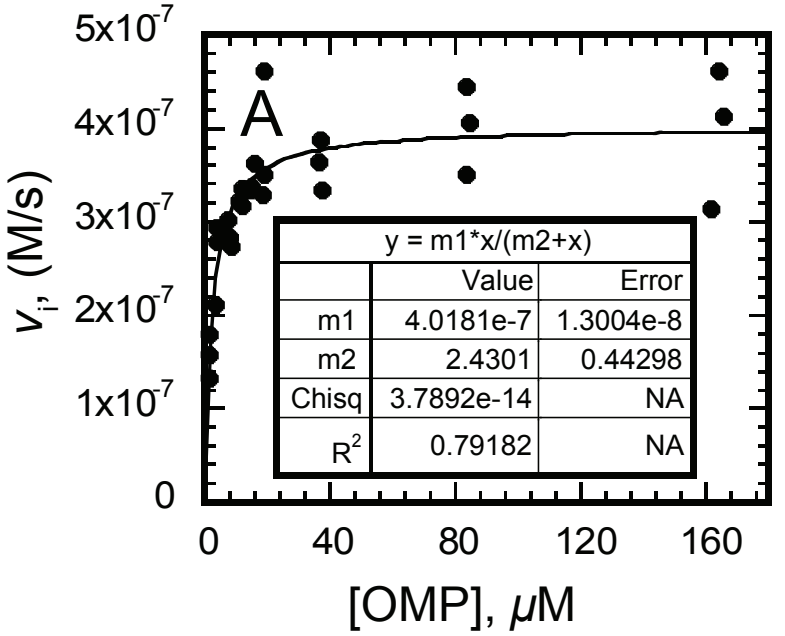

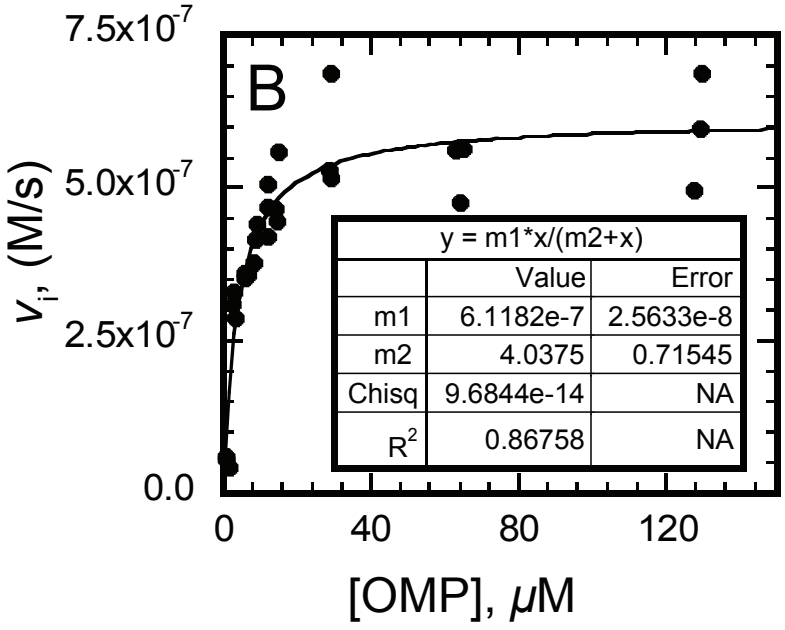

Figure A.4 (page 1 of 6)

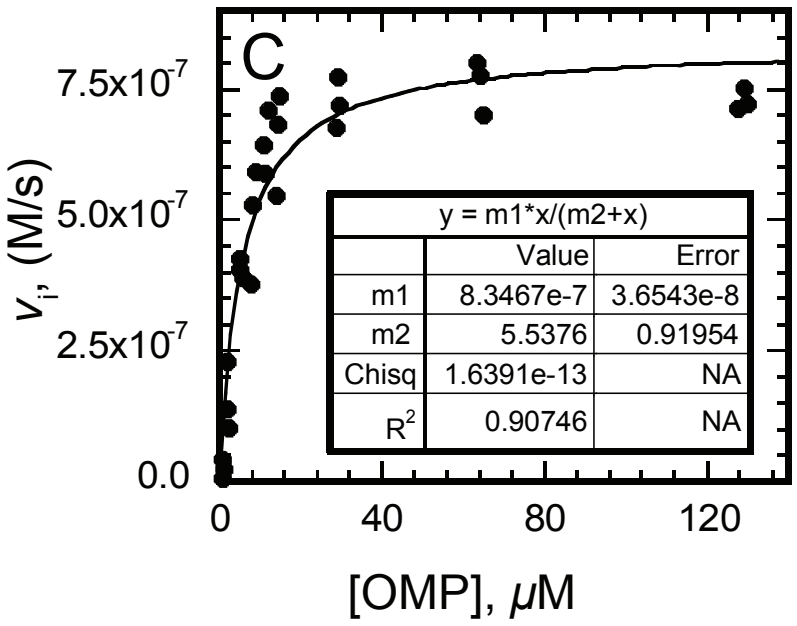

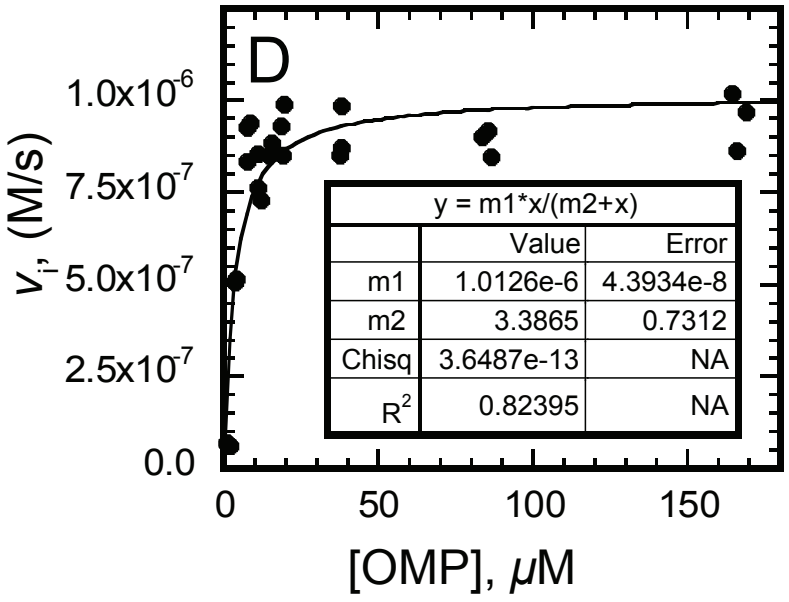

Figure A.4 (page 2 of 6)

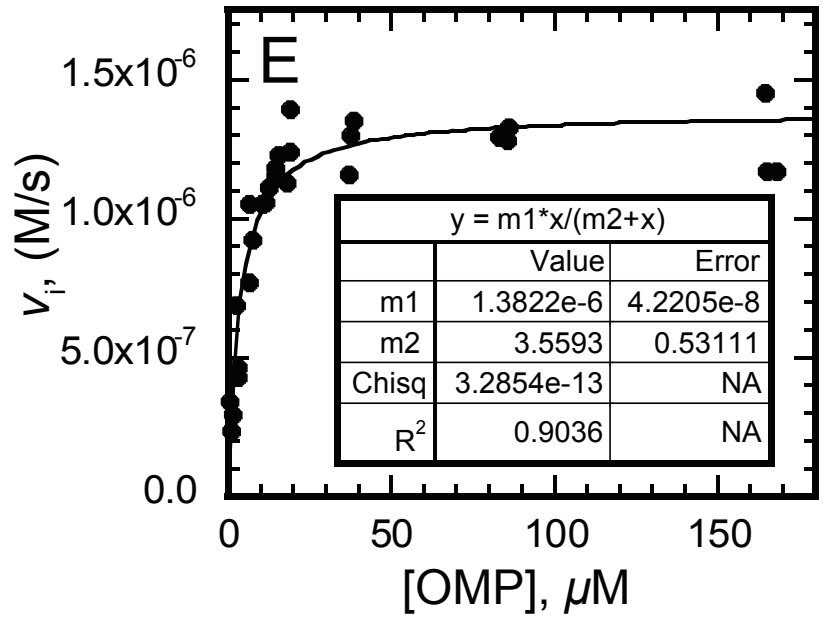

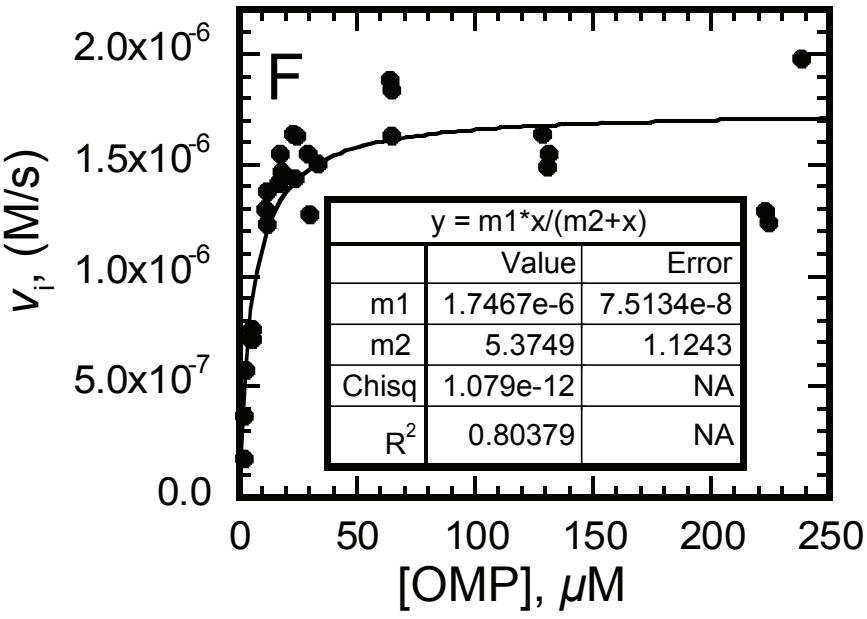

Figure A.4 (page 3 of 6)

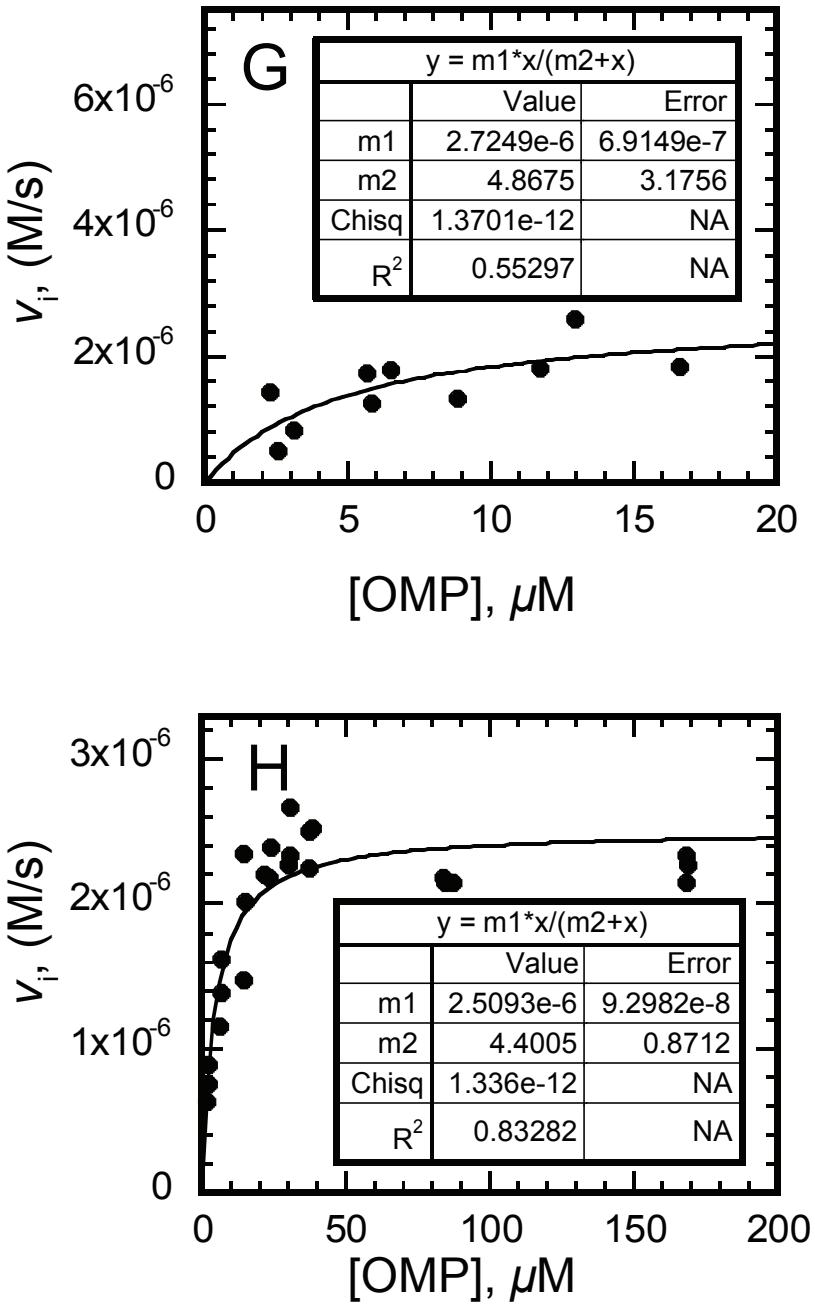

Figure A.4 (page 4 of 6)

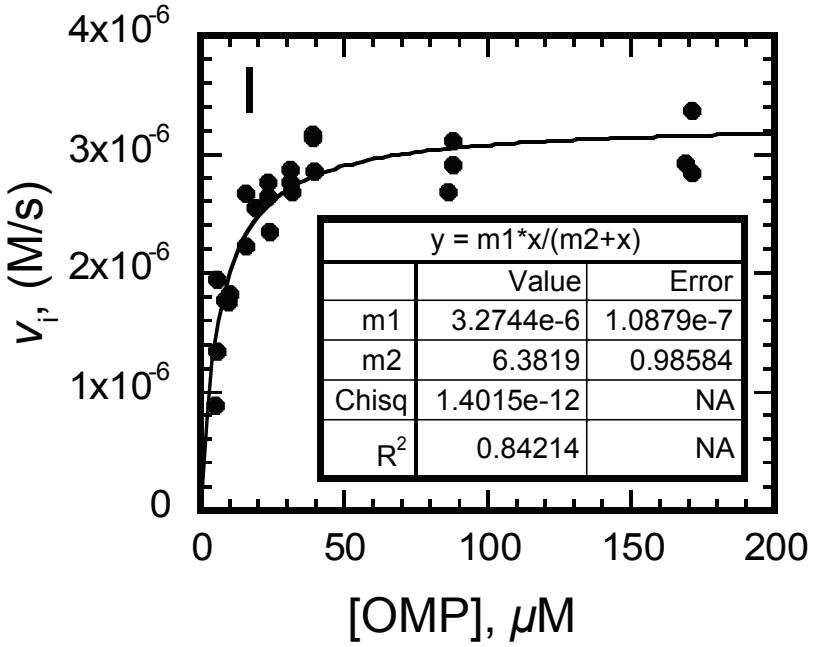

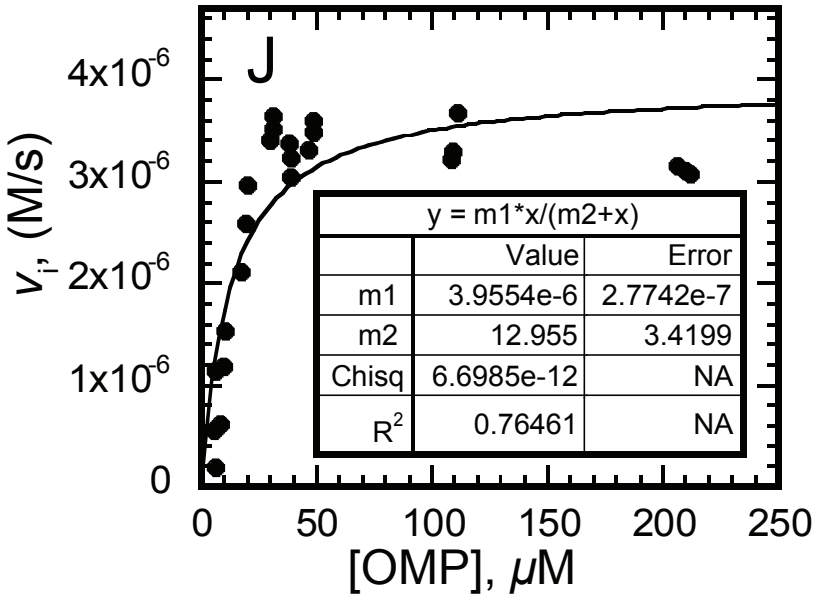

Figure A.4 (page 5 of 6)

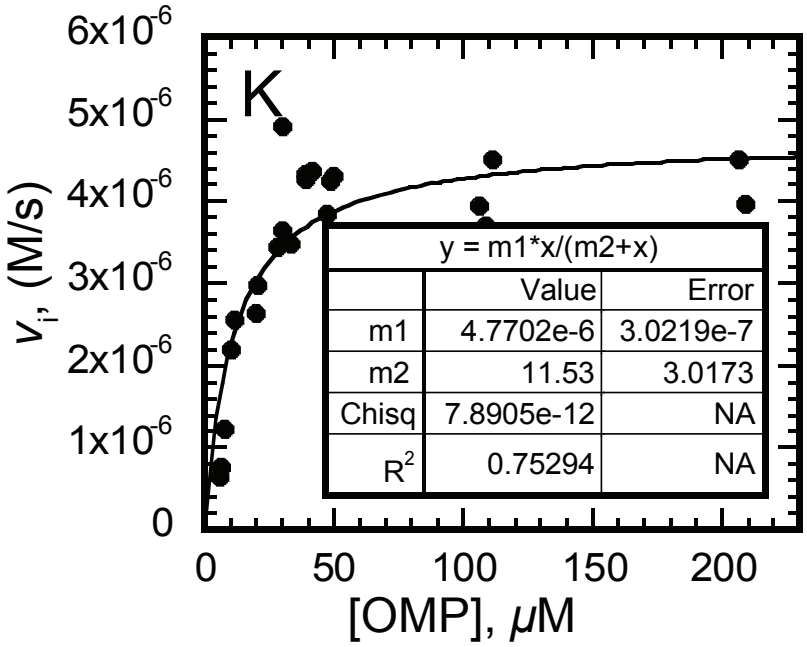

Figure A.4 (page 6 of 6)

Table A.4 (page 1 of 4)
Concentrations of OMP Used in Kinetic Assays of CpODCase over a Range of Temperatures, and their Resulting Initial Rates

10 °C		15 °C		20 °C	
[OMP], μM	v_i, nM/s	[OMP], μM	v_i, nM/s	[OMP], μM	v_i, nM/s
165.57	413	129.72	686	129.95	723
164.12	462	129.00	596	129.05	753
161.45	313	127.34	497	127.55	712
84.46	406	65.11	563	64.88	701
83.77	444	63.98	475	64.22	777
83.60	351	62.92	561	63.54	801
37.63	334	29.11	516	29.38	720
37.00	387	29.06	686	29.11	772
36.40	364	28.97	529	28.82	676
19.12	350	14.85	558	14.68	736
19.03	461	14.77	446	14.31	682
18.49	329	14.09	465	14.08	546
16.03	362	12.12	468	11.92	711
15.12	337	12.09	506	11.23	588
14.65	334	12.08	420	11.09	644
12.09	317	9.20	440	9.05	593
11.89	335	8.60	415	8.11	529
11.09	322	8.31	378	7.86	377
8.57	274	6.72	358	5.78	390
8.14	283	5.86	361	5.15	427
7.66	302	5.80	353	5.15	405
3.94	278	3.31	287	2.52	103
3.83	293	2.86	329	1.97	229
3.65	212	2.57	310	1.91	140
1.77	157	1.62	42	1.32	24
1.51	179	0.95	61	0.75	7
1.38	132	0.69	55	0.68	42

Table A.4 (page 2 of 4)
Concentrations of OMP Used in Kinetic Assays of CpODCase over a Range of Temperatures, and their Resulting Initial Rates

25 °C		30 °C		35 °C	
[OMP], μM	v_i, nM/s	[OMP], μM	v_i, nM/s	[OMP], μM	v_i, nM/s
169.17	970	168.03	1173	237.98	1981
165.92	865	165.12	1170	224.54	1244
164.52	1019	164.52	1452	223.28	1288
86.58	846	86.09	1326	131.37	1547
85.32	917	85.46	1277	130.43	1487
83.55	901	83.00	1287	128.63	1635
38.20	871	38.58	1349	64.72	1839
37.92	986	37.54	1299	64.46	1635
37.38	853	37.08	1161	64.22	1884
19.58	989	19.06	1241	33.14	1507
18.89	849	19.02	1391	29.77	1280
18.34	929	18.18	1130	29.09	1554
16.20	859	15.38	1230	24.25	1625
15.72	884	14.77	1179	23.32	1438
14.66	850	14.46	1145	23.25	1640
11.91	731	12.37	1109	17.98	1473
11.05	857	11.28	1056	17.54	1549
10.80	761	10.43	1051	17.03	1422
8.37	937	7.34	924	11.97	1383
7.74	927	6.69	769	11.49	1231
7.35	836	6.55	1052	11.40	1304
4.00	515	3.05	430	5.46	760
3.66	508	2.92	462	5.34	720
3.28	506	2.62	689	5.22	713
1.95	63	1.35	293	2.80	579
1.17	68	1.00	236	2.32	372
0.98	70	0.62	343	2.17	177

Table A.4 (page 3 of 4)
Concentrations of OMP Used in Kinetic Assays of CpODCase over a Range of Temperatures, and their Resulting Initial Rates

40 °C		45 °C		50 °C	
[OMP], μM	v_i, nM/s	[OMP], μM	v_i, nM/s	[OMP], μM	v_i, nM/s
16.60	1844	168.82	2275	171.14	3374
12.97	2604	168.43	2147	171.03	2854
11.72	1805	168.29	2342	168.95	2928
8.82	1336	87.37	2154	87.74	3105
6.52	1799	84.37	2148	87.60	2917
5.82	1256	83.86	2179	86.11	2688
5.66	1728	38.26	2519	39.22	2857
3.12	838	37.34	2504	39.14	3169
2.54	511	37.06	2248	38.89	3138
2.29	1439	30.54	2341	31.62	2681
		30.40	2672	31.38	2866
		30.18	2265	30.94	2767
		24.08	2391	23.95	2353
		23.43	2178	23.46	2652
		21.77	2197	23.45	2763
		14.88	2015	18.78	2550
		14.68	1470	15.66	2229
		14.26	2355	15.57	2666
		6.82	1618	9.95	1826
		6.78	1388	9.20	1761
		6.08	1153	8.26	1771
		2.48	887	5.34	1343
		2.46	749	5.31	1946
		1.97	633	4.75	886

Table A.4 (page 4 of 4)
Concentrations of OMP Used in Kinetic Assays of CpODCase over a Range of Temperatures, and their Resulting Initial Rates

55 °C		60 °C	
[OMP], μM	v_i, nM/s	[OMP], μM	v_i, nM/s
211.97	3084	209.08	3970
209.58	3110	207.32	3465
206.26	3164	206.52	4509
111.02	3671	111.38	4508
109.26	3287	108.65	3712
108.12	3221	106.25	3937
48.66	3491	50.02	4315
48.38	3591	48.31	4242
46.80	3315	47.31	3854
38.92	3236	41.37	4373
38.68	3047	38.89	4262
38.35	3366	38.75	4325
31.43	3515	33.02	3492
31.23	3642	30.03	3647
30.03	3414	29.94	4906
20.09	2964	28.05	3437
19.46	2592	20.55	2978
17.38	2125	19.75	2635
10.22	1528	11.85	2548
9.58	1189	10.12	2199
8.54	612	7.48	1225
6.03	188	6.26	769
5.97	1126	5.65	652
5.46	556		

REFERENCES

Acheson, S. A., Bell, J. B., Jones, M. E., & Wolfenden, R. (1990). Orotidine–5'–monophosphate decarboxylase catalysis: Kinetic isotope effects and the state of hybridization of a bound transition-state analogue. *Biochemistry, 29* (13), 3198–3202.

Aguilar, A., Ingemansson, T., & Magnien, E. (1998). Extremophile microorganisms as cell factories: Support from the european union. *Extremophiles, 2* (3), 367–373. doi:10.1007/s007920050080

Antranikian, G., Vorgias, C. E., & Bertoldo, C. (2005). Extreme environments as a resource for microorganisms and novel biocatalysts. In R. Ulber, & Y. Le Gal (Eds.), *Marine biotechnology I* (pp. 219–262) Springer Berlin / Heidelberg. doi:10.1007/b135786

Ayala–del–Río, H. L., Chain, P. S., Grzymski, J. J., Ponder, M. A., Ivanova, N., Bergholz, P. W., *et al*. (2010). The genome sequence of psychrobacter arcticus 273–4, a psychroactive siberian permafrost bacterium, reveals mechanisms for adaptation to low-temperature growth. *Applied and Environmental Microbiology, 76* (7), 2304–2312. doi:10.1128/AEM.02101–09

Bakermans, C., Ayala–del–Río, H. L., Ponder, M. A., Vishnivetskaya, T., Gilichinsky, D., Thomashow, M. F., *et al*. (2006). Psychrobacter cryohalolentis sp. nov. and psychrobacter arcticus sp. nov., isolated from siberian permafrost. *International Journal of Systematic and Evolutionary Microbiology, 56* (6), 1285–1291. doi:10.1099/ijs.0.64043–0

Barnett, S. A., Amyes, T. L., Wood, B. M., Gerlt, J. A., & Richard, J. P. (2008). Dissecting the total transition state stabilization provided by amino acid side chains at orotidine 5'–monophosphate decarboxylase: A two-part substrate approach. *Biochemistry, 47* (30), 7785–7787. doi:10.1021/bi800939k

Beak, P., & Siegel, B. (1976). Mechanism of decarboxylation of 1,3–dimethylorotic acid. A model for orotidine 5'–phosphate decarboxylase. *Journal of the American Chemical Society, 98* (12), 3601–3606.

Beer, A. (1852). Bestimmung der absorption des rothen lichts in farbigen Flüssigkeiten. *Annalen Der Physik, 162* (5), 78–88. doi:10.1002/andp.18521620505

Begley, T. P., Appleby, T. C., & Ealick, S. E. (2000). The structural basis for the remarkable catalytic proficiency of orotidine 5'–monophosphate decarboxylase. *Current Opinion in Structural Biology, 10* (6), 711–718.

Begley, T. P., & Ealick, S. E. (2004). Enzymatic reactions involving novel mechanisms of carbanion stabilization. *Current Opinion in Chemical Biology, 8* (5), 508–515. Retrieved from http://www.sciencedirect.com/science/article/pii/S1367593104001024

Barnett, S. A., Amyes, T. L., Wood, B. M., Gerlt, J. A., & Richard, J. P. (2008). Dissecting the total transition state stabilization provided by amino acid side chains at orotidine 5'-monophosphate decarboxylase: A two-part substrate approach. *Biochemistry, 47*(30), 7785-7787. doi:10.1021/bi800939k

Benkovic, S. J., & Hammes–Schiffer, S. (2003). A perspective on enzyme catalysis. *Science, 301* (5637), 1196–1202. doi:10.1126/science.1085515

Bentahir, M., Feller, G., Aittaleb, M., Lamotte–Brasseur, J., Himri, T., Chessa, J. P., *et al*. (2000). Structural, kinetic, and calorimetric characterization of the cold-active phosphoglycerate kinase from the antarctic pseudomonas sp. TACII18. *The Journal of Biological Chemistry, 275* (15), 11147–11153.

Bertani, G. (1951). Studies On Lysogenesis I. *Journal of Bacteriology, 62* (3), 293–300.

Blackburn, G. M., Kang, A. S., Kingsbury, G. A., & Burton, D. R. (1989). *Catalytic antibodies*.

Bouguer, P. (1729). *Essai d'optique, sur la gradation de la lumiere*. Paris, France: Claude Jombert.

Brown, G. K., Fox, R. M., & O'Sullivan, W. J. (1975). Interconversion of different molecular weight forms of human erythrocyte orotidylate decarboxylase. *Journal of Biological Chemistry, 250*(18), 7352-7358.

Bowman, J. P., McCammon, S. A., Brown, M. V., Nichols, D. S., & McMeekin, T. A. (1997). Diversity and association of psychrophilic bacteria in antarctic sea ice. *Applied and Environmental Microbiology, 63* (8), 3068–3078.

Bruice, T. C. (1976). Some pertinent aspects of mechanism as determined with small molecules. *Annual Review of Biochemistry, 45* (1), 331–374. doi:10.1146/annurev.bi.45.070176.001555

Bruice, T. C. (2002). A view at the millennium: The efficiency of enzymatic catalysis. *Accounts of Chemical Research, 35* (3), 139–148. doi:10.1021/ar0001665

Buchner, E. (1897). Alkoholische gährung ohne hefezellen. *Berichte Der Deutschen Chemischen Gesellschaft, 30* (1), 117–124. doi:10.1002/cber.18970300121

Canganella, F., & Wiegel, J. (2011). Extremophiles: From abyssal to terrestrial ecosystems and possibly beyond. *Naturwissenschaften, 98* (4), 253–279. doi:10.1007/s00114–011–0775–2

Cavicchioli, R. (2006). Cold–adapted archaea. *Nature Reviews Microbiology, 4* (5), 331–343. Retrieved from http://dx.doi.org/10.1038/nrmicro1390

Cha, Y., Murray, C., & Klinman, J. (1989). Hydrogen tunneling in enzyme reactions. *Science, 243* (4896), 1325–1330. doi:10.1126/science.2646716

Chan, K. K., Wood, B. M., Fedorov, A. A., Fedorov, E. V., Imker, H. J., Amyes, T. L., *et al*. (2009). Mechanism of the orotidine 5'–monophosphate decarboxylase-catalyzed reaction: Evidence for substrate destabilization, *Biochemistry, 48* (24), 5518–5531. doi:10.1021/bi900623r

Cleland, W., & Kreevoy, M. (1994). Low–barrier hydrogen bonds and enzymic catalysis. *Science, 264* (5167), 1887–1890. doi:10.1126/science.8009219

Cooper, A., Johnson, C. M., Lakey, J. H., & Nöllmann, M. (2001). Heat does not come in different colours: entropy–enthalpy compensation, free energy windows, quantum confinement, pressure perturbation calorimetry, solvation and the multiple causes of heat capacity effects in biomolecular interactions. *Biophysical Chemistry, 93*, 215–230.

Cornish-Bowden, A. (2002). Enthalpy–entropy compensation: a phantom phenomenon. *Journal of Biosciences, 27*, 121–126.

Cui, W., DeWitt, J. G., Miller, S. M., & Wu, W. (1999). No metal cofactor in orotidine 5'–monophosphate decarboxylase. *Biochemical and Biophysical Research Communications, 259* (1), 133–135. doi:10.1006/bbrc.1999.0737

D'Amico, S., Gerday, C., & Feller, G. (2001). Structural determinants of cold adaptation and stability in a large protein. *The Journal of Biological Chemistry, 276* (28), 25791–25796. doi:10.1074/jbc.M102741200

D'Amico, S., Marx, J. C., Gerday, C., & Feller, G. (2003). Activity-stability relationships in extremophilic enzymes. *The Journal of Biological Chemistry, 278* (10), 7891–7896. doi:10.1074/jbc.M212508200

Deming, J. W., & Eicken, H. (2007). Life in ice. In W. T. Sullivan, & J. A. Baross (Eds.), *Planets and life* (pp. 292–312). Cambridge, UK: Cambridge University Press.

Demirjian, D. C., Morís–Varas, F., & Cassidy, C. S. (2001). Enzymes from extremophiles. *Current Opinion in Chemical Biology, 5* (2), 144–151. doi:DOI: 10.1016/S1367–5931 (00)00183–6

Dewar, M. J., & Storch, D. M. (1985). Alternative view of enzyme reactions. *Proceedings of the National Academy of Sciences, 82* (8), 2225–2229.

Douglas, J. F., Dudowicz, J., & Freed, K. F. (2009) Crowding Induced Self-Assembly and Enthalpy-Entropy Compensation. *Physical Review Letters, 103* (135701), 1–4.

Evans, M. G., & Polanyi, M. (1935). Some applications of the transition state method to the calculation of reaction velocities, especially in solution. *Transactions of the Faraday Society, 31*, 875–894. doi:10.1039/TF9353100875"

Eyring, H. (1935). The activated-complex in chemical reactions. *The Journal of Chemical Physics, 3* (2), 107–115. doi:10.1063/1.1749604

Feller, G. (2003). Molecular adaptations to cold in psychrophilic enzymes. *Cellular and Molecular Life Sciences : CMLS, 60* (4), 648–662.

Feller, G., d'Amico, D., & Gerday, C. (1999). Thermodynamic stability of a cold-active alpha–amylase from the antarctic bacterium alteromonas haloplanctis. *Biochemistry, 38* (14), 4613–4619. doi:10.1021/bi982650+

Fischer, E. (1894). **[The influence of configuration on the activity of enzyme].** *Berichte Der Deutschen Chemischen Gesellschaft, 27*, 2985.

Gao, J. (2003). Catalysis by enzyme conformational change as illustrated by orotidine 5′–monophosphate decarboxylase. *Current Opinion in Structural Biology, 13* (2), 184–192. Retrieved from http://www.sciencedirect.com/science/article/pii/S0959440X03000411

Garcia–Viloca, M., Gao, J., Karplus, M., & Truhlar, D. G. (2004). How enzymes work: Analysis by modern rate theory and computer simulations. *Science, 303* (5655), 186–195. doi:10.1126/science.1088172

Georlette, D., Blaise, V., Collins, T., D'Amico, S., Gratia, E., Hoyoux, A., *et al*. (2004). Some like it cold: Biocatalysis at low temperatures. *FEMS Microbiology Reviews, 28* (1), 25–42. doi:10.1016/j.femsre.2003.07.003

Gero, A. (1954). Steric considerations on the chemical structure and physiological activity of methadone and related compounds. *Science, 119* (3082), 112–114. Retrieved from http://www.jstor.org/stable/1681312

Gianese, G., Bossa, F., & Pascarella, S. (2002). Comparative structural analysis of psychrophilic and meso- and thermophilic enzymes. *Proteins, 47* (2), 236–249.

Gibbs, P. R., Uehara, C. S., Neunert, U., & Bommarius, A. S. (2005). Accelerated biocatalyst stability testing for process optimization. *Biotechnology Progress, 21* (3), 762–774. doi:10.1021/bp049609k

Giver, L., Gershenson, A., Freskgard, P., & Arnold, F. H. (1998). Directed evolution of a thermostable esterase. *Proceedings of the National Academy of Sciences, 95* (22), 12809–12813. doi:10.1073/pnas.95.22.12809

Greenfield, N. J. (2007). Using circular dichroism collected as a function of temperature to determine the thermodynamics of protein unfolding and binding interactions. *Nature Protocols, 1* (6), 2527–2535. Retrieved from http://dx.doi.org/10.1038/nprot.2006.204

Hammes, G. G., Benkovic, S. J., & Hammes–Schiffer, S. (2011). Flexibility, diversity, and cooperativity: Pillars of enzyme catalysis. *Biochemistry, 50* (48), 10422–10430. doi:10.1021/bi201486f

Hammes–Schiffer, S. (2006). Hydrogen tunneling and protein motion in enzyme reactions. *Accounts of Chemical Research, 39* (2), 93–100. doi:10.1021/ar040199a

Hamor, G. H. (1961). Correlation of chemical structure and taste in the saccharin series. *Science, 134* (3488), 1416–1417. Retrieved from http://www.jstor.org/stable/1707414

Harris, P., Navarro Poulsen, J., Jensen, K. F., & Larsen, S. (2000). Structural basis for the catalytic mechanism of a proficient enzyme: orotidine 5'–monophosphate decarboxylase. *Biochemistry, 39* (15), 4217–4224. doi:10.1021/bi992952r

Hashimoto, H., Inoue, T., Nishioka, M., Fujiwara, S., Takagi, M., Imanaka, T., *et al*. (1999). Hyperthermostable protein structure maintained by intra and inter-helix ion-pairs in archaeal O6–methylguanine–DNA methyltransferase. *Journal of Molecular Biology, 292* (3), 707–716. doi:10.1006/jmbi.1999.3100

Heppel, L. A., & Hilmoe, R. J. (1951). Purification and properties of 5'–nucleotidase. *Journal of Biological Chemistry, 188* (2), 665–676.

Hough, D. W., & Danson, M. J. (1999). Extremozymes. *Current Opinion in Chemical Biology, 3* (1), 39–46. doi:DOI: 10.1016/S1367–5931 (99)80008–8

Houk, K. N., Tantillo, D. J., Stanton, C., & Hu, Y. F. (2004). What have theory and crystallography revealed about the mechanism of catalysis by orotidine monophosphate decarboxylase? In J. K. Lee (Ed.), *Orotidine monophosphate decarboxylase: A mechanistic dialogue* (pp. 1–22). Heidelberg, Deutschland: Springer Berlin.

Harris, P., Navarro Poulsen, J. C., Jensen, K. F., & Larsen, S. (2000). Structural basis for the catalytic mechanism of a proficient enzyme: Orotidine 5'-monophosphate decarboxylase. *Biochemistry, 39*(15), 4217-4224.

Houk, K. N., Lee, J. K., Tantillo, D. J., Bahmanyar, S., & Hietbrink, B. N. (2001). Crystal structures of orotidine monophosphate decarboxylase: Does the structure reveal the mechanism of nature's most proficient enzyme? *Chembiochem : A European Journal of Chemical Biology, 2* (2), 113–118.

Huston, A. L., Krieger–Brockett, B. B., & Deming, J. W. (2000). Remarkably low temperature optima for extracellular enzyme activity from arctic bacteria and sea ice. *Environmental Microbiology, 2* (4), 383–388. doi:10.1046/j.1462–2920.2000.00118.x

Huston, A. L., Methe, B., & Deming, J. W. (2004). Purification, characterization, and sequencing of an extracellular cold-active aminopeptidase produced by marine psychrophile *colwellia psychrerythraea* strain 34H. *Applied and Environmental Microbiology, 70* (6), 3321–3328. doi:10.1128/AEM.70.6.3321–3328.2004

Imanaka, T. (2011). Molecular bases of thermophily in hyperthermophiles. *Proceedings of the Japan Academy.Series B, Physical and Biological Sciences, 87* (9), 587–602.

Imanaka, T., Shibazaki, M., & Takagi, M. (1986). A new way of enhancing the thermostability of proteases. *Nature, 324* (6098), 695–697. doi:10.1038/324695a0

Jakubowska, A., & Korona, R. (2009). Lack of evolutionary conservation at positions important for thermal stability in the yeast ODCase protein. *Molecular Biology and Evolution, 26* (7), 1431–1434. doi:10.1093/molbev/msp066

Jencks, W. P. (1975). Binding-energy, specificity, and enzymic catalysis – circe effect. *Advances in Enzymology, 43*, 219–410.

Jones, M. E. (1980). Pyrimidine nucleotide biosynthesis in animals: Genes, enzymes, and regulation of UMP biosynthesis. *Annual Review of Biochemistry, 49*, 253–279. doi:10.1146/annurev.bi.49.070180.001345

Freed, K. F. (2011). Entropy–Enthalpy Compensation in Chemical Reactions and Adsorption: An Exactly Solvable Model. *The Journal of Physical Chemistry B, 115*, 1689–1692.

Koshland, D. E. (1958). Application of a theory of enzyme specificity to protein synthesis. *Proceedings of the National Academy of Sciences, 44* (2), 98–104.

Koshland, D. E. (1995). The key-lock theory and the induced fit theory. *Angewandte Chemie International Edition in English, 33* (23–24), 2375–2378. doi:10.1002/anie.199423751

Krug, R. R., Hunter, W. G., & Grieger, R. A. (1976). Statistical interpretation of enthalpy–entropy compensation. *Nature, 261* (5561), 566–567. Retrieved from http://dx.doi.org/10.1038/261566a0

Kumar, S., Ma, B., Tsai, C. J., Sinha, N., & Nussinov, R. (2000). Folding and binding cascades: Dynamic landscapes and population shifts. *Protein Science : A Publication of the Protein Society, 9* (1), 10–19. doi:10.1110/ps.9.1.10

Kumar, S., & Nussinov, R. (2004). Different roles of electrostatics in heat and in cold: Adaptation by citrate synthase. *Chembiochem : A European Journal of Chemical Biology, 5* (3), 280–290. doi:10.1002/cbic.200300627

Lambert, J. H. (1760). *Photometria sive de mensura et gradibus luminis, colorum et umbrae*. Augsburg, Germany: Eberhardt Klett.

Lee, J. K., & Houk, K. N., (1997). A proficient enzyme revisited: The predicted mechanism for orotidine monophosphate decarboxylase. *Science (New York, N.Y.), 276* (5314), 942–945.

Leffler, J.E. (1955) The enthalpy-entropy relationship and its implications for organic chemistry. *Journal of Organic Chemistry, 20* (9), 1202–1231. doi: 10.1021/jo01126a009

Leffler, J.E. (1963) Concerning the isokinetic relationship. *Nature, 205* (4976), 1101–1102.

Lonhienne, T., Gerday, C., & Feller, G. (2000). Psychrophilic enzymes: Revisiting the thermodynamic parameters of activation may explain local flexibility. *Biochimica et Biophysica Acta, 1543* (1), 1–10.

Lundberg, M., Blomberg, M. R., & Siegbahn, P. E. (2002). Density functional models of the mechanism for decarboxylation in orotidine decarboxylase. *Journal of Molecular Modeling, 8* (4), 119–130. doi:10.1007/s00894–002–0080–2

Ma, B., Kumar, S., Tsai, C. J., Hu, Z., & Nussinov, R. (2000). Transition–state ensemble in enzyme catalysis: Possibility, reality, or necessity? *Journal of Theoretical Biology, 203* (4), 383–397. doi:10.1006/jtbi.2000.1097

Mahon, M. M., Gramatikova, S. I., Christen, P., Fitzpatrick, T. B., & Malthouse, J. P. G. (1998). The pyridoxal–5′–phosphate–dependent catalytic antibody 15A9: Its efficiency and stereospecificity in catalysing the exchange of the α–protons of glycine. *FEBS Letters, 427* (1), 74–78. doi:10.1016/S0014–5793 (98)00397–4

Menger, F. M., & Glass, L. E. (1980). Contribution of orbital alignment to organic and enzymic reactivity. *Journal of the American Chemical Society, 102* (16), 5404–5406. doi:10.1021/ja00536a054

Methé, B. A., Nelson, K. E., Deming, J. W., Momen, B., Melamud, E., Zhang, X., *et al*. (2005). The psychrophilic lifestyle as revealed by the genome sequence of *colwellia psychrerythraea* 34H through genomic and proteomic analyses. *Proceedings of the National Academy of Sciences, 102* (31), 10913–10918. doi:10.1073/pnas.0504766102

Miller, B. G., Butterfoss, G. L., Short, S. A., & Wolfenden, R. (2001). Role of enzyme-ribofuranosyl contacts in the ground state and transition state for orotidine 5'–phosphate decarboxylase: A role for substrate destabilization? *Biochemistry, 40* (21), 6227–6232.

Miller, B. G., Snider, M. J., Short, S. A., & Wolfenden, R. (2000). Contribution of enzyme-phosphoribosyl contacts to catalysis by orotidine 5'–phosphate decarboxylase. *Biochemistry, 39* (28), 8113–8118.

Miller, B. G., Snider, M. J., Wolfenden, R., & Short, S. A. (2001). Dissecting a charged network at the active site of orotidine–5'–phosphate decarboxylase. *The Journal of Biological Chemistry, 276* (18), 15174–15176. doi:10.1074/jbc.M011429200

Miller, B. G., & Wolfenden, R. (2002). Catalytic proficiency: The unusual case of OMP decarboxylase. *Annual Review of Biochemistry, 71*, 847–885. doi:10.1146/annurev.biochem.71.110601.135446

Miller, B. G., Traut, T. W., & Wolfenden. (1998). A role for zinc in OMP decarboxylase, an unusually proficient enzyme. *Journal of the American Chemical Society, 120* (11), 2666–2667. doi:10.1021/ja980066i

Nicholas, K. M., Wentworth, P., Harwig, C. W., Wentworth, A. D., Shafton, A., & Janda, K. D. (2002). *A cofactor approach to copper-dependent catalytic antibodies* doi:10.1073/pnas.052001099

Novagen. (1997). *pET system manual* (7th ed.). Madison, WI: Novagen.

Olufsen, M., Smalas, A. O., Moe, E., & Brandsdal, B. O. (2005). Increased flexibility as a strategy for cold adaptation: A comparative molecular dynamics study of cold– and warm–active uracil DNA glycosylase. *The Journal of Biological Chemistry, 280* (18), 18042–18048. doi:10.1074/jbc.M500948200

Page, M. I., & Jencks, W. P. (1971). Entropic contributions to rate accelerations in enzymic and intramolecular reactions and the chelate effect. *Proceedings of the National Academy of Sciences, 68* (8), 1678–1683.

Pauling, L. (1946). Molecular architecture and biological reactions. *Chem. Eng. News, 24*, 1375.

Pauling, L. (1948). The nature of forces between large molecules of biological interest. *Nature, 161* (4097), 707–709.

Polanyi, M. (1921). Adsoption catalysis. *Zeitschrift Fur Elektrochemie Und Angewandte Physikalische Chemie, 27*, 142–150.

Porter, D. J. T., and Short, S.A. (2000). Yeast Orotidine-5‘-Phosphate Decarboxylase: Steady-State and Pre-Steady-State Analysis of the Kinetic Mechanism of Substrate Decarboxylation. *Biochemistry, 39*(38), 11788–11800.

Qian, H. (1998). Entropy-enthalpy compensation: Conformational fluctuation and induced-fit. *Journal of Chemical Physics*. *109* (22), 10015–10017.

Poduch, E., Wei, L., Pai, E. F., & Kotra, L. P. (2008). Structural diversity and plasticity associated with nucleotides targeting orotidine monophosphate decarboxylase. *Journal of Medicinal Chemistry, 51*(3), 432-438. doi:10.1021/jm700968x

Radzicka, A., & Wolfenden, R. (1995). A proficient enzyme. *Science (New York, N.Y.), 267* (5194), 90–93.

Rahman, R. N., Fujiwara, S., Nakamura, H., Takagi, M., & Imanaka, T. (1998). Ion pairs involved in maintaining a thermostable structure of glutamate dehydrogenase from a hyperthermophilic archaeon. *Biochemical and Biophysical Research Communications, 248* (3), 920–926. doi:10.1006/bbrc.1998.8933

Rahman, R. N., Fujiwara, S., Takagi, M., & Imanaka, T. (1998). Sequence analysis of glutamate dehydrogenase (GDH) from the hyperthermophilic archaeon pyrococcus sp. KOD1 and comparison of the enzymatic characteristics of native and recombinant GDHs. *Molecular & General Genetics : MGG, 257* (3), 338–347.

Rose, M., Grisafi, P., & Botstein, D. (1984). Structure and function of the yeast URA3 gene: Expression in escherichia coli. *Gene, 29*(1–2), 113-124. doi:10.1016/0378-1119(84)90172-0

Russell, N. J. (2000). Toward a molecular understanding of cold activity of enzymes from psychrophiles. *Extremophiles : Life Under Extreme Conditions, 4* (2), 83–90.

Salameh, M., & Wiegel, J. (2007). Lipases from extremophiles and potential for industrial applications. *Advances in applied microbiology* (pp. 253–283) Academic Press. doi:10.1016/S0065–2164 (06)61007–1

Schowen, R. L. (1978). In Gandour R. D., Schowen R. L. (Eds.), *Transition states of biochemical processes*. New York: Plenum.

Segel, I. H. (1975). *Enzyme kinetics*. New York: John Wiley & Sons, Inc.

Sellek, G. A., & Chaudhuri, J. B. (1999). Biocatalysis in organic media using enzymes from extremophiles. *Enzyme and Microbial Technology, 25* (6), 471–482. doi:10.1016/S0141–0229 (99)00075–7

Shambaugh, G. E.,3rd. (1979). Pyrimidine biosynthesis. *The American Journal of Clinical Nutrition, 32* (6), 1290–1297.

Sharp, K. (2001). Entropy-enthalpy compensation: fact or artifact? *Protein Science*, *10* (3), 661–667. doi:10.1110/ps.37801

Shostak, K., & Jones, M. E. (1992). Orotidylate decarboxylase: Insights into the catalytic mechanism from substrate specificity studies. *Biochemistry, 31* (48), 12155–12161. doi:10.1021/bi00163a026

Silverman, R. B., & Groziak, M. P. (1982). Model chemistry for a covalent mechanism of action of orotidine 5'–phosphate decarboxylase. *Journal of the American Chemical Society, 104* (23), 6434–6439. doi:10.1021/ja00387a047

Smalas, A. O., Leiros, H. K., Os, V., & Willassen, N. P. (2000). Cold adapted enzymes. *Biotechnology Annual Review, 6*, 1–57.

Smith, D. R., Doucette-Stamm, L. A., Deloughery, C., Lee, H., Dubois, J., Aldredge, T., et al. (1997). Complete genome sequence of methanobacterium thermoautotrophicum deltaH: Functional analysis and comparative genomics. *Journal of Bacteriology, 179*(22), 7135-7155.

Smiley, J. A., & Saleh, L. (1999). Active site probes for yeast OMP decarboxylase: Inhibition constants of UMP and thio-substituted UMP analogues and greatly reduced activity toward CMP–6–carboxylate. *Bioorganic Chemistry, 27* (4), 297–306. doi:10.1006/bioo.1999.1140

Sumner, J. B. (1926). The isolation and crystallization of the enzyme urease. *Journal of Biological Chemistry, 69* (2), 435–441.

Sumner, J. B. (1937; 1937). The story of urease. *Journal of Chemical Education, 14* (6), 255. Retrieved from http://dx.doi.org/10.1021/ed014p255

Suttle, D. P., Bugg, B. Y., Winkler, J. K., & Kanalas, J. J. (1988). Molecular cloning and nucleotide sequence for the complete coding region of human UMP synthase. *Proceedings of the National Academy of Sciences of the United States of America, 85*(6), 1754-1758.

Tellinghuisen, J. (2006). Van't Hoff analysis of K degrees (T): How good...or bad? *Biophysical Chemistry, 120* (2), 114–120. doi:10.1016/j.bpc.2005.10.012

Toth, K., Amyes, T. L., Wood, B. M., Chan, K. K., Gerlt, J. A., & Richard, J. P. (2009). An examination of the relationship between active site loop size and thermodynamic activation parameters for orotidine 5'–monophosphate decarboxylase from mesophilic and thermophilic organisms. *Biochemistry, 48* (33), 8006–8013. doi:10.1021/bi901064k

Traut, T. W. (1994). Physiological concentrations of purines and pyrimidines. *Molecular and Cellular Biochemistry, 140* (1), 1–22.

Tsai, C. J., Ma, B., & Nussinov, R. (1999). Folding and binding cascades: Shifts in energy landscapes. *Proceedings of the National Academy of Sciences, 96* (18), 9970–9972.

Warshel, A. (1998). Electrostatic origin of the catalytic power of enzymes and the role of preorganized active sites. *Journal of Biological Chemistry, 273* (42), 27035–27038. doi:10.1074/jbc.273.42.27035

Westheimer, F. H. (1962). Mechanisms related to enzyme catalysis. *Advances in Enzymology., 24*, 441–482.

Wiesmeyer, H., & Cohn, M. (1957). Purification and characterization of amylomaltase induced in Escherichia-coli. *Federation Proceedings, 16* (1), 270.

Turnbough, C. L., Kerr, K. H., Funderburg, W. R., Donahue, J. P., & Powell, F. E. (1987). Nucleotide sequence and characterization of the pyrF operon of escherichia coli K12. *Journal of Biological Chemistry, 262*(21), 10239-10245.

Wilfong, E. M., Kogiso, Y., Muthukrishnan, S., Kowatz, T., *et al*. (2011). A Multidisciplinary Approach to Probing Enthalpy–Entropy Compensation and the Interfacial Mobility Model. *Journal of the American Chemical Society, 133*, 11515–11523.

Williams, D. H., Stephens, E., O'Brien, D. P., & Zhou, M. (2004). Understanding noncovalent interactions: Ligand binding energy and catalytic efficiency from ligand-induced reductions in motion within receptors and enzymes. *Angewandte Chemie International Edition, 43* (48), 6596–6616. doi:10.1002/anie.200300644

Williams, D. H., Stephens, E., & Zhou, M. (2003). How can enzymes be so efficient? *Chemical Communications, (*16), 1973–1976. doi:10.1039/B305544M"

Wolfenden, R. (2003). Thermodynamic and extrathermodynamic requirements of enzyme catalysis. *Biophysical Chemistry, 105* (2–3), 559–572.

Wood, B. M., Chan, K. K., Amyes, T. L., Richard, J. P., & Gerlt, J. A. (2009). Mechanism of the Orotidine 5′-Monophosphate Decarboxylase-Catalyzed Reaction: Effect of Solvent Viscosity on Kinetic Constants. *Biochemistry, 48* (24), 5510–5517.

Wu, N., Gillon, W., & Pai, E. F. (2002). Mapping the active site-ligand interactions of orotidine 5'–monophosphate decarboxylase by crystallography. *Biochemistry, 41* (12), 4002–4011.

Xu, Y., Yamamoto, N., & Janda, K. D. (2004). Catalytic antibodies: hapten design strategies and screening methods. *Bioorganic and Medicinal Chemistry, 12*, 5247–5268. doi:10.1016/j.bmc.2004.03.077

Zeikus, J. G., & Wolfe, R. S. (1972). Methanobacterium thermoautotrophicus sp. n., an anaerobic, autotrophic, extreme thermophile. *Journal of Bacteriology, 109*(2), 707-715.

Zhang, X., & Houk, K. N., (2005). Why enzymes are proficient catalysts: beyond the pauling paradigm. *Accounts of Chemical Research, 38* (5), 379–385. doi:10.1021/ar040257s

Zhou, X., Jin, X., Medhekar, R., Chen, X., Dieckmann, T., & Toney, M. D. (2001). Rapid kinetic and isotopic studies on dialkylglycine decarboxylase. *Biochemistry, 40* (5), 1367–1377.